Peptide-Based Inhibitors of Huntingtin Exon I Aggregation

A thesis submitted in partial fulfillment of the requirements for the degree of

DOCTOR OF PHILOSOPHY

BY

VINAY KUMAR BELWAL

Department of Biosciences and Bioengineering

Indian Institute of Technology Guwahati

Guwahati – 781 039, India

October 2021

INDIAN INSTITUTE OF TECHNOLOGY GUWAHATI
DEPARTMENT OF BIOSCIENCES AND BIOENGINEERING

DECLARATION

The research work presented in this thesis is an original work carried out by me in the Department of Biosciences and Bioengineering, Indian Institute of Technology Guwahati, India, for the degree of the Doctor of Philosophy. The research work was carried out under the guidance of my supervisors Dr. Nitin Chaudhary and Dr. Sachin Kumar, and no work has been submitted, in part or whole, for any other degree to any other University/Institute. As per the standards of reporting research findings, due acknowledgements have been made wherever the work described is based on the findings of other researchers.

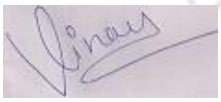

Vinay Kumar Belwal

Date: 12 October 2021

INDIAN INSTITUTE OF TECHNOLOGY GUWAHATI
DEPARTMENT OF BIOSCIENCES AND BIOENGINEERING

CERTIFICATE

This is to certify that the work incorporated in the thesis titled "**Peptide-Based Inhibitors of Huntingtin Exon I Aggregation**" submitted by Mr Vinay Kumar Belwal for the award of the degree of Doctor of Philosophy is an authentic record of the research work carried out under my guidance in the Department of Biosciences and Bioengineering, Indian Institute of Technology Guwahati, India. The work is original and has not been submitted in part or full for any other degree of any other University/Institute.

Dr. Nitin Chaudhary
(Supervisor)
Date: Nov 01, 2021

Dr. Sachin Kumar
(Co-supervisor)
Date: Nov 01, 2021

Dedicated to My Family….

Acknowledgement

Completing this thesis would not have been possible without the amazing people around me who helped me along this journey. I want to take a moment to thank them and express my sincere gratitude to all of them.

I would first and foremost like to thank my supervisor Dr. Nitin Chaudhary for making this project a reality, generating ideas, giving me support, encouragement, and scientific freedom over the course of my Ph.D. It was my privilege to work and learn under his guidance. I would always be grateful for the kindness, patience, and trust that he bestowed on me. Similar, profound gratitude goes to my co-supervisor, Dr. Sachin Kumar, for his insightful suggestion and thoughtful question regarding the work. Throughout the journey, he is always very kind enough to extend his help personally and professionally.

I am grateful to my committee chairperson Dr. Vibin Ramakrishnan, and my committee members Dr. Senthilkumar S. and Dr. Archana M Nair, for their insightful comments, guidance, and encouragement during my research period and their kind words of advice during my progress seminars. I am hugely appreciative to all faculty members of the Department of Biosciences and Bioengineering, Indian Institute of Technology, Guwahati. They have been very kind enough to extend their help at various phases of my research, and I do hereby acknowledge all of them. In addition, I would like to express my sincere gratitude to the non-teaching staff of the Department of Biosciences and Bioengineering, for their kind cooperation and support during this period.

I acknowledge the Department of Biosciences & Bioengineering, Central Instrument Facility, Indian Institute of Technology Guwahati, for providing me access to the state of the art instrumentation facilities as invaluable resources for executing my research experiments. Furthermore, I acknowledge, Ministry of Education, Government of India, for the financial assistance to carry out my research work.

My heartfelt appreciation to all my friends, past and present lab members, Karabi, Sravani, Praksh, Sajitha Gaurav J, Aparna, Gaurav P, Debika, Jahnu, Anshuman, Vivek, Shagun, Feba, Anirban, Pranav, Shubhra, Subhangini, and Aishwarya, Khyati, Gaurav K, Deep, Ram, Pankaj, Tilak, Gajendra

from the core of my heart, for their love, support and unfailing help during my research work. I will always cherish the wonderful time spent with them.

Above all, I thank my parents for their love, affection, and trust in me. I don't have enough words to express my gratitude towards my parents for giving me the freedom to chase my dreams, my best friend Rashmi, who stood by me in all my ups and downs, and my brothers Mukesh and Deepak, whose love and support was immeasurable in my journey. My research would not have been possible without their encouragement and blessings.

Table of Contents

Abbreviations

AFM	Atomic Force Microscopy
CD	Circular Dichroism
DIPEA	*N*,*N*-diisopropylethylamine
DMSO	Dimethylsulfoxide
DMF	*N*,*N*-Dimethylformamide
EDTA	Ethylenediaminetetraacetic acid
FE-TEM	Field emission transmission electron microscope transmission
Fmoc	Fluorenylmethyloxycarbonyl
HATU	1-[Bis(dimethylamino)methylene]-1*H*-1,2,3-triazolo[4,5-*b*]pyridinium 3-oxide hexafluorophosphate
HBTU	*N*,*N*,*N*′,*N*′-tetramethyl-*O*-(1*H*-benzotriazol-1-yl)uronium hexafluorophosphate
HCCA	α-Cyano-4-hydroxycinnamic acid
HD	Huntingtin Disease
HDx1	Pathogenic Huntingtin exon 1 protein
HOBt	1-hydroxybenzotriazole hydrate
HPLC	High performance liquid chromatography
Htt^{N17}	Huntingtin's N-terminal 17-residue peptide stretch
Httx1	Huntingtin exon 1 protein
MALDI-TOF	Matrix-assisted laser desorption ionization-time of flight
OD	Optical density
PolyQ	Polyglutamine
PTMs	Post-translational modifications
QBP1	Polyglutamine binding peptide 1
TFA	Trifluoroacetic acid
ThT	Thioflavin T

Thesis Synopsis

Huntington's disease (HD) is a progressive neurodegenerative disorder that becomes more severe with age. There is no specific therapeutic or treatment to date that can cure HD. However, scientists worldwide are continually working to find out effective therapies for HD. Since the identification of the HD gene, nearly 25 years ago, there has been enormous progress in understanding HD pathology's molecular features at the cellular level. These studies have led to the beginning of a systematic process of target selection and validating the potential HD therapeutic candidates.

QBP1 is a peptide that binds to the extended polyQ regions and prevent their transition from the monomeric protein to amyloid-like structures. Similarly, the role of htt^{N17} in modulating the huntingtin aggregation and pathogenicity has been investigated. In view of the above contexts, the current thesis explored the huntingtin exon 1 aggregation inhibition by the peptides derived from QBP1 and htt^{N17}.

The thesis is organized into five chapters

Chapter 1: Introduction and a Review of the Literature (Huntington Disease: an ill-effect of expansionism)

This chapter gives a brief introduction and a review of the literature of various characteristics of huntingtin and the Huntingtin disease

Chapter 2: Material and Methods

Chapter 2 describes the materials and methodologies employed to carry out the thesis research work

Chapter 3: The role of the turn-supporting motif in polyglutamine binding peptide (QBP1) in huntingtin aggregation inhibition

Using a phage screen display, Burke and coworkers identified six Trp-rich 11-residue peptides, termed polyglutamine binding peptides (QBP1-6) that bind and inhibit polyglutamine aggregation [1]. Out of these 6 peptides, peptide Ac-SNWKWWPGIFD-am, known as QBP1, inhibits polyglutamine aggregation most effectively. Subsequently, the structure-function study with the most active peptide QBP1 led to identifying a minimal 8-residue peptide (mQBP1) without any

activity loss [2]. Both peptides harbor a Pro-Gly dipeptide motif, a feature characteristic of potential β-turn regions. In this chapter, the role of the β-turn motif in huntingtin aggregation inhibition was investigated. Using single amino acid substitutions to generate analogs that could support, introduce, or eliminate the β-turn, it was shown that the turn-supporting motif is essential for QBP1-mediated inhibition of huntingtin aggregation.

Chapter 4: Inhibition of huntingtin aggregation by its N-terminal 17-residue peptide (htt^{N17}) and its analogs

The N-terminal 17-residue stretch of huntingtin (htt^{N17}) folds into an amphipathic helix. The htt^{N17}–harboring polyQ peptides form oligomers that are mediated via the assembly of the htt^{N17} α-helices. The oligomerization results in higher local concentration of the polyglutamine (polyQ) region, thereby facilitating amyloid formation. The htt^{N17} co-assembles with the htt^{N17}-harbouring polyQ peptides, thereby reducing the local polyQ concentration, and consequently inhibiting aggregation. This study presents the aggregation inhibition of the exon I region of huntingtin by htt^{N17} and its analogs. The C-terminal amidation of htt^{N17} is found to be essential for activity. The htt^{N17} peptides with free amino terminus and the acetylated amino terminus possess comparable activity. An htt^{N17} analog, wherein the Leu7 and Ala10 are substituted with Aib residues, is designed that exhibits significantly higher activity than the native htt^{N17}.

Chapter 5: Huntingtin aggregation inhibition activity of the mixtures of the most active analogs of htt^{N17} and QBP1 and the fusion peptide derived from them.

In this chapter, the aggregation inhibition potential of the fusion peptide, obtained by appending a QBP1 analog to the C-terminus of a highly active htt^{N17} analog, were investigated. Compared to the either parent peptide, the activity of the fusion peptide was severely compromised. However, when the parent peptides were mixed together, the activity was restored. This lack of activity in the fusion peptide is largely attributed to the folding of the peptide. The peptide folds into an α-helical conformation, possibly by drawing the otherwise non-helical QBP1 as well into the helical conformation.

Chapter 6: Conclusion and Future directions

The chapter concludes the thesis by discussing the highlights of results described in chapters 3-5. The results, the future possibilities, and interesting but unexplored questions are discussed.

List of Publications

Publications related to the thesis work

i. **Vinay Kumar Belwal**, Debika Datta, Nitin Chaudhary. The β-turn-supporting motif in the polyglutamine binding peptide QBP1 is essential for inhibiting huntingtin aggregation, FEBS Letters, 2020, **594**, 2894-2903.

ii. **Vinay Kumar Belwal**, Aishwarya Vijayakumar, Nitin Chaudhary. Inhibition of huntingtin aggregation by its N-terminal 17-residue peptide and its analogs, Archives of Biochemistry and Biophysics, 2021, **712**, 109033

iii. **Vinay Kumar Belwal**, Nitin Chaudhary. Investigation into the role of QBP1-htt^{N17} hybrid peptide and ^{D}mQBP1-NG in HDx1 protein aggregation. (Manuscript under preparation)

Publications from other collaborative work (Not in the thesis)

i. Karabi Saikia, **Vinay Kumar Belwal**, Debika Datta, Nitin Chaudhary "Aromatic-rich C-terminal region of LCI is a potent antimicrobial peptide in itself," Biochemical and Biophysical Research Communications, 2019, **519**, 372-377

ii. **Vinay Kumar Belwal**, Nitin Chaudhary. Amyloids and their untapped potential as hydrogelators. Soft Matter, 2020, **16**, 10013-10028.

CHAPTER 1

Introduction and a Review of the Literature

(Huntington Disease: an ill-effect of expansionism)

1.1. Introduction

Huntington's disease (HD) is an autosomal dominant neurodegenerative disorder [1]. HD is caused by the expansion of the CAG tract beyond a threshold limit (35 repeats) in the exon 1 region of the huntingtin gene. The CAG codes for glutamine and an expansion in the CAG tract results in the huntingtin protein with an expanded polyglutamine (polyQ) region. The CAG expansion, therefore, transforms the native huntingtin protein into the pathogenic one [2-4]. Huntingtin protein is involved in various functions, particularly in the neurons, and loss of its function is one of the attributes of HD. Besides, the pathogenic huntingtin misfolds and self-assembles to form cytotoxic aggregates (Fig.1.1). A person with HD suffers from a progressive movement disorder and cognitive and motor impairment due to neurons' death in different regions of the brain [5, 6]. The onset of the disease and severity of neurodegeneration correlates with the length of the polyQ stretch [3]. Pathogenic protein misfolds and forms large inclusion bodies within the cytoplasm and nucleus [7]. These large proteinaceous inclusions are found in a reasonable amount in the form of endogenous huntingtin in the subcellular fractions of neuron-like clonal striatal cells [7, 8], and the brain lipid of HD mouse models [9]. Such inclusions disrupts the endoplasmic reticulum [10], and nuclear membrane of the cells [11]. In humans, the heterozygous terminal deletion or physical disruption of the huntingtin does not lead to any disease phenotype [12]. Interestingly, however, the expression of the Httx1 with an expanded polyQ stretch is sufficient to cause HD in the mouse models [7, 13, 14]. The pathogenic huntingtin exon 1 (HDx1) forms fibrillar structures similar to those formed by the full-length pathogenic huntingtin protein [15], emphasizing the importance of the amino-terminal region in the HD pathogenicity.

The huntingtin protein's region encoded by exon 1 contains three distinct regions of very different amino acid compositions. The amino terminal region is a 17 residue stretch (htt^{N17}), which acts as a nuclear export signal [16]. The middle stretch is of variable length, and is composed exclusively of glutamine residues, forming the so called polyQ region. The polyQ region is followed by the C-terminal proline-rich domain [15]. Compared to the htt^{N17} region, the polyQ region is polymorphic [17]. The presence of polyQ inclusions strongly correlates with the disease pathology, but the underlying correlation of the polyQ repeat length with aggregation propensity remains controversial. At present, it has been agreed upon that the misfolding and aggregation of the HDx1 (HD causing exon 1) or the N-terminal huntingtin fragments that harbor the pathogenic

polyQ repeats are the main culprits of causing HD. The role of the flanking sequences surrounding the polyQ region in modulating the aggregation process is also quite influential. The C-terminal polyproline region retards the fibril formation [18, 19], whereas the htt^{N17} region enhances it [19-21].

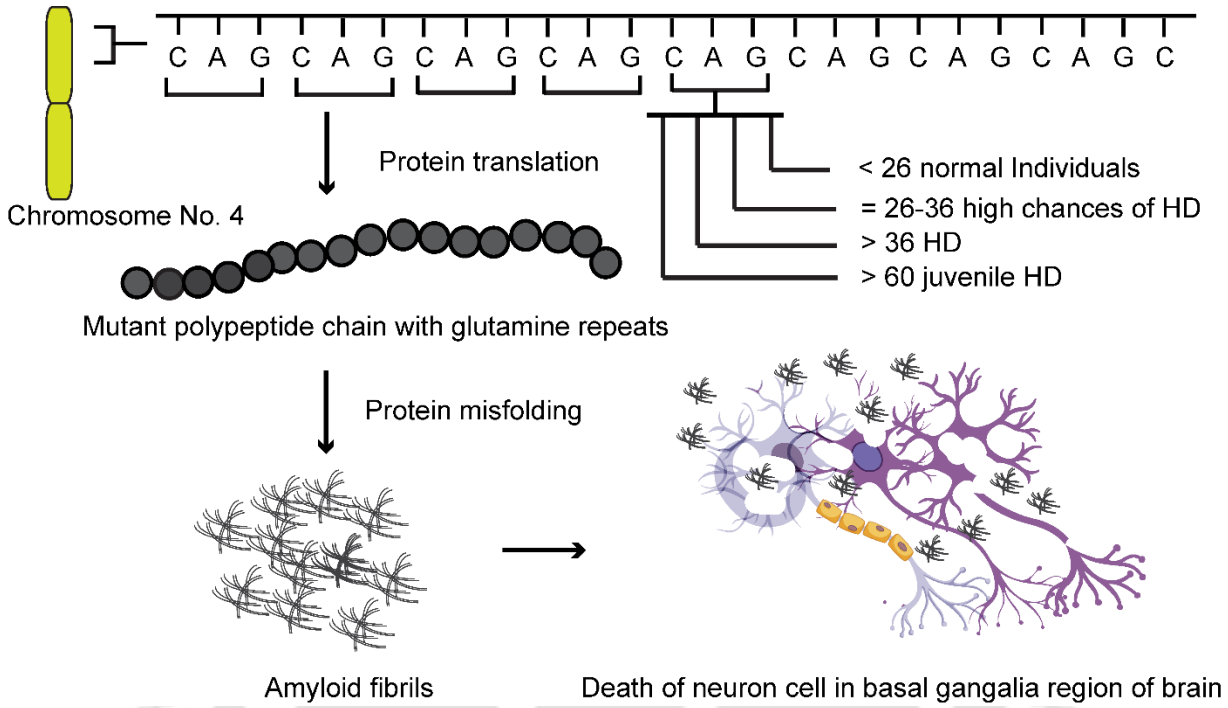

Fig. 1.1. *A diagrammatic representation of the Huntington's disease.*

Htt^{N17} region plays a crucial role in the structure and function of healthy as well as pathogenic huntingtin protein. The htt^{N17}, *per se*, is not an aggregation-prone peptide [22]. Wetzel and coworkers showed that the peptide takes up a somewhat collapsed structure that resists aggregation [19]. Tagging with polyQ causes repeat length-dependent disruption of htt^{N17} structure, wherein the htt^{N17} becomes more extended and aggregation-prone. The htt^{N17}-polyQ quickly forms oligomers that are mediated via htt^{N17} region with rather exposed polyQ stretch. In a subsequent study, Wetzel and coworkers investigated the aggregation of htt^{N17}–tagged short polyQ peptides [20]. The aggregation of these peptides proceeded via α-helical oligomers. In addition, the htt^{N17} peptide was found to form α-helical tetramers at high concentrations, suggesting that htt^{N17} exists in solution as an equilibrium mixture of unstructured monomer and an α-helical tetramer. The

htt^{N17} can adopt amphipathic helical conformation [19, 23-25] that facilitates the interaction of huntingtin with lipid membranes, functions as a membrane-targeting domain, and associates with trafficking of huntingtin to the mitochondria, Golgi, and endoplasmic reticulum. [16, 26]. The htt^{N17} harbours amino acids that can undergo post-translational modifications (PTMs) [27], which regulate various important functions like membrane binding, subcellular localizations, and also have a pronounced impact on the pathogenic huntingtin's toxicity and aggregation [28-31].

This chapter is, essentially, a review of various characteristics of huntingtin. This includes its structure, function, aggregation propensity, and the various modifications that modulate these properties.

1.2. Huntingtin structure and function

Huntingtin protein is expressed in the cytoplasm of mammalian cells, majorly in the brain and testis. It plays a crucial role in neuronal development and interacts with proteins involved in transcriptional regulation [32, 33], cell signaling and cell adhesion [34], intracellular transport [35], microtubule-mediated transport [36-38], mitotic spindle orientation [39], and neurogenesis [39-41]. Moreover, it is essential for healthy embryonic development during gastrulation as the targeted disruption of murine homologs of huntingtin gene is lethal in homozygote mice models and shows behavioral and morphological changes in heterozygote mice models [42-44]. Even though the pathological condition in HD is believed to be largely due to the toxic "gain of function" of the pathogenic huntingtin [7], the "loss of function" of pathogenic protein is also reported to contribute to the HD pathology [45, 46]. Loss of huntingtin function disrupts the neuronal subtypes and promotes the HD-associated characteristics [47]. Similarly, early embryonic deletion of huntingtin from pyramidal neurons affects the development and survival of neurons [48], which leads to progressive neurodegeneration and sterility in mouse models [48-50]. Huntingtin is also essential for the mitochondrial structure and function, as the loss of its function displays early embryonic lethality and metabolic aberrations [51]. Huntingtin has a neuroprotective role and protects the neurons from NMDA receptor-mediated excitotoxicity [52]. It is required for synaptic development and connectivity in the cortex [49]. Recently, Burrus *et al*. reported that the loss of huntingtin in striatal projection neurons affects motor regulation synaptic connectivity, cell health, and survival during aging [53].

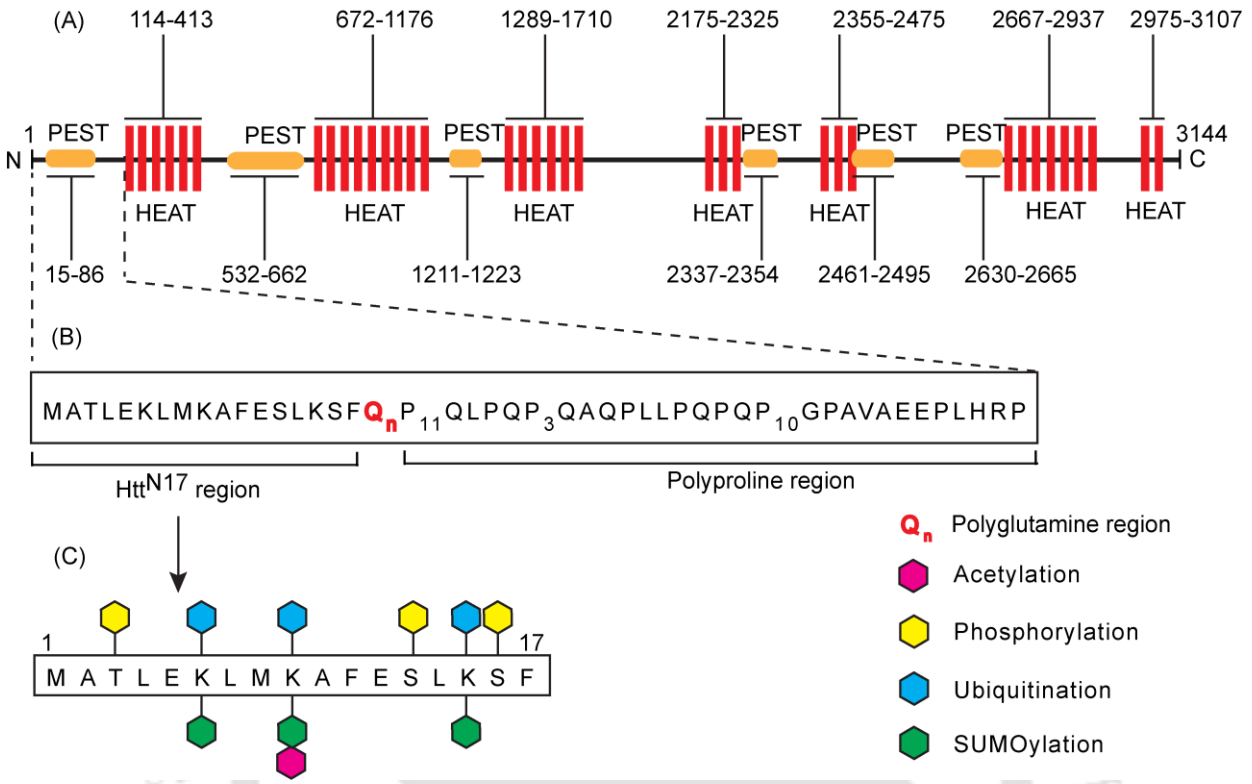

Fig. 1.2. *A schematic representation of the various features of huntingtin. (A) Full-length huntingtin protein with HEAT repeat sites and PEST domains. (B) Huntingtin exon 1 with three distinct regions. (C) Htt^{N17} sequence with different sites of posttranslational modifications.*

Despite the role of huntingtin protein in the vital cellular and molecular process, the precise structural and functional role of the protein is not well-defined. As far as HD is concerned, most studies have focused on the exon 1 region as polyQ tract lies in this region (Fig 1.2B). Full-length human huntingtin is a large protein of around 348 kDa, having 3144 amino acids (Fig. 1.2A) [17]. The exact number of amino acids and the mass of the protein may vary depending upon the number of glutamine residues in the polyQ stretch of the exon I region. Huntingtin acts as a scaffold protein in intracellular trafficking and cellular pathways. The current structural model of huntingtin protein is of a flexible, superhelical solenoid structure with a hydrophobic core having an array of several repeats called HEAT repeats (Fig. 1.2A) [54-57]. These HEAT repeats are important for protein-protein interactions [58], and are clustered into four major domains: HTT, elongation factor 3, protein phosphatase 2A, and TOR1 (HEAT is the combined term for these four domains) [59]. Apart from HEAT repeats, huntingtin protein also contains several PEST domains, the domains

rich in proline (P), glutamic acid (E), serine (S), and threonine (T). PEST domains are the signal sequences for proteolytic degradation and are majorly found in the disordered regions. These domains are the home of most reported post-translational modifications like phosphorylation, SUMOylation, ubiquitination, acetylation, and proteolytic cleavage site in huntingtin protein. [27, 57, 60].

1.3. Huntingtin exon 1 (Httx1) and its aggregation

It has been found that the aggregates formed in HD mostly consist of N-terminal fragments that are largely ubiquitinated and are supposed to be the main component involved in HD pathology [14, 61]. The fragments are generated from the protein via proteolytic cleavage after translation or via alternate splicing after transcription [62]. *In vitro* studies as well as the high-resolution electron micrographs of brain slices of HD patients show well-defined fibrillar or filamentous structures [63]. Aggregates purified from HD patients' brains bind to congo red with green birefringence, indicating an amyloid-like structure [64]. *In vivo* aggregates are often associated with other cellular proteins, including proteins involved in misfolding or aggregation and other polyQ containing proteins. They are also found to sequester vital cellular proteins like transcription factors, suggesting how these aggregates exhibit toxicity [63]. It is well known that the polyQ-containing aggregates are always found in all nine CAG expansion diseases that include HD, spinal and bulbar muscular atrophy (SBMA), dentatorubral-pallidoluysian atrophy (DRPLA), and spinocerebellar ataxia (SCA type-1,2,3,6,7, and 17)[65]. The aggregation rate increases with polyQ repeat length, reflecting correlations between repeat length, disease risk, and age of onset [66]. These observations led to the theory that repeat length-dependent aggregation of polyQ is the causing event of expanded CAG repeat diseases [19]. Therefore, several studies have been conducted on artificially synthesized polyQ peptides (e.g., $K_2Q_nK_2$) of variable length. These model peptides can adopt multiple conformations including α-helix, random-coil, and extended loop in solution. Their self-assembly, however, results in β-sheet-rich fibrillar aggregates [67, 68]. Amyloidogenic proteins are commonly observed to be conformationally flexible [69]. Kim et al. proposed that the polyQ expansion in the huntingtin protein increases the length of the random coil region, promoting aggregation, and facilitating abnormal interaction with other proteins in the cells [69].

Out of 67 exons in full-length huntingtin, the exon 1 has been relatively poorly conserved compared to the other huntingtin exons during evolution [57]. It is located in the PEST1 domain of the full-length huntingtin and translated as an N- terminal part of the full huntingtin protein [60]. Httx1 contains 17 amino acids region (htt^{N17}), followed by a variable length polyQ region which could impart pathogenicity, and a C-terminal polyproline region (Fig 1B). Httx1 with 35 or more glutamines in the polyQ stretch becomes pathogenic that misfolds and forms inclusion bodies. HDx1, *i.e.* the httx1 having pathogenic polyQ repeats, is sufficient to induce the disease phenotype in animal models [8]; and forms fibrils very similar to those formed by the full-length pathogenic protein. Therefore, most huntingtin aggregation studies have been carried out with the HDx1 or its truncated fragments. The polyQ stretch is longer and polymorphic in humans as compared to other species, and its size increased during evolution [17, 70]. As far as vertebrates are concerned, a tetraglutamine stretch is found in the fish, amphiphians, and birds. In humans, the polyQ stretch is highly variable with up to 35 Qs in the non-pathogenic huntingtin [70, 71]. Interestingly, the rodents have 7-8 Qs in the polyQ tract. The role of polyQ tract in the huntingtin is not known clearly. Still, surprisingly, the polyQ stretch's deletion seems to be a potentially beneficial mutation that increases neuronal autophagy and longevity in mice [70]. Similarly, the polyproline region is only found in mammals and is polymorphic in the human population, which shows a recent evolution of the huntingtin protein [57]. It is believed that this region evolved as a defense system against the aggregation and toxicity of pathogenic huntingtin protein by affecting the N-terminus structure [18, 72, 73]. This region was found to suppress the HDx1 aggregation [74] and is a binding site for several interacting proteins [35]. Studies showed that polyproline sequence in chemically synthesized polyQ peptides suppresses the tendency of polyQ to adopt a β-sheet structure [18, 75] and suppresses the aggregation kinetics [19, 72]. Although this region appears to be functionally important and beneficial for the HD pathogenicity, its deletion does not significantly affect the normal function of full-length huntingtin in mice models [76]. However, the htt^{N17} region's role is quite significant in the huntingtin structure and function, which is discussed next.

1.4. The structural and functional roles of htt^{N17} region in monomeric and aggregated huntingtin

The htt^{N17} region plays an important role in the structure and function of huntingtin protein, as well as in the development of HD. The htt^{N17} stretch is conserved among the vertebrates [17]. This region is associated with a number of membrane-associated cellular processes like intracellular vesicle trafficking [77, 78] and subcellular localization [30]. The role of htt^{N17} in cellular localization to the endoplasmic reticulum (ER), golgi apparatus, endosomal vacuoles, and the nucleus is reported via different methods in drosophila and mice HD models [79-81]. The htt^{N17} is also subjected to multiple post-translational modifications (Fig 1C) like phosphorylation [82-86], SUMOylation [28, 87-89], ubiquitination [87, 90-92], and acetylation [82, 93-95], which not only regulate the structure and function of full length huntingtin, but also have a significant impact on its aggregation and toxicity [27]. Htt^{N17} has a cytoplasmic retention signal that can retain the pathogenic huntingtin in the cytoplasm and modulate its aggregation, nuclear entry, and toxicity. Htt^{N17} leads the protein to ER and other vesicles. It can translocate huntingtin to the nucleus and vice versa, that is affected by the response to ER stress conditions [30]. Htt^{N17} region also has a leucine-rich nuclear export signal (NES), which regulates Httx1 subcellular localization and aggregation [16]. Mutation in the NES region increases the huntingtin nuclear accumulation and cellular toxicity [16, 30, 96]. An additional NES has been reported near the protein's C-terminus as well that regulate the huntingtin's subcellular localization [97, 98]. Htt^{N17} also modulates the calcium homeostasis by promoting aggregation and disrupting Ca^{2+} levels in glutamate-challenged PC12 cells [31]. Huntingtin localization is affected by reactive oxygen species (ROS) stress where htt^{N17} domain acts as a reactive oxygen species sensor for huntingtin. It is reported that the oxidation at Met8 regulates huntingtin phosphorylation and nuclear localization [99].

NMR studies suggest that, under physiological conditions, monomeric htt^{N17} has no stable secondary structure in solution and forms a compact coil that resists aggregation and shows some degree of helicity in CD spectra [19, 24, 30]**.** It forms an amphipathic helix when interacting with membranes but unfolds in the aqueous solution [23, 100]. This amphipathic nature of htt^{N17} helix acts as a lipid-binding domain and facilitates the interaction of polyQ with lipid monolayers and bilayers [23, 26, 101], and plays a critical role in huntingtin aggregation on lipid membranes. The

amphipathic helix formed by htt^{N17} is a curvature-sensing segment that displays enhanced binding to the highly curved membranes [25, 102]. Bechinger and coworkers investigated the structure and topology of the synthetic htt^{N17} in the membranes using solution and solid-state NMR spectroscopy [23]. The peptide takes up an α-helical conformation from Lys6 to Phe17 in the dodecyl phosphocholine micelles and acts as a reversible membrane anchor for huntingtin [23]. Côté and coworkers, using all atom simulation, refined the htt^{N17} α-helical structure in the POPC bilayer [103]. They further showed that the peptide perturbs the membrane in a manner that favors dimerization. A number of computational studies have been carried out either with htt^{N17}, or the htt^{N17}-Q_m-P_n to probe the secondary structure of the htt^{N17}. Most of them predict the htt^{N17} to be unstructured in the aqueous solution [24, 73, 104-106]. Some studies, however, predict it to adopt an α-helical conformation [103, 107, 108]. Therefore, htt^{N17} has been proposed to take up multiple conformations. Such variation, to some extent, could be due to the variation in the experimental and computational methods employed to determine the structure. For example, Wetzel and coworkers reported concentration-dependent oligomerization of the htt^{N17}(F17W)-Q in aqueous solution at physiological pH [20] . The peptide formed α-helical oligomers at concentation ≥ 0.67 mM. It has also been largely agreed upon that the htt^{N17} takes up the α-helical structure in the fibrils as well [20, 21, 109, 110]. FTIR analysis shows the stabilization of the helical conformation of htt^{N17} during oligomerization. It is believed that the amphipathicity of htt^{N17} confers it the self-assembling property, allowing oligomerization. When tagged with the polyQ stretch, such htt^{N17} oligomerization would increase the local concentration of the polyQ stretches, thereby facilitating amyloid formation [109].

To understand the mechanisms behind HDx1 aggregation as well as to come up with the therapeutics, it is imperative to have the structural information of the aggregates formed by HDx1. A number of studies have attempted to unravel the structure of these aggregates. PolyQ peptides, designed models of Httx1, and the HDx1 have been investigated using spectroscopic and microscopic methods. FTIR and X-ray diffraction studies on HDx1 fibrils have confirmed the amyloid fibrils' characteristic cross-β structure [111, 112]. The amyloid-like nature of the HDx1 aggregates, therefore, has been established beyond doubt. Like all amyloid fibrils, it is challenging to study the HDx1 fibril structure using traditional techniques such as X-ray crystallography and solution NMR. However, the structures of htt^{N17}, polyQ peptides, and the Httx1-like peptides with different polyQ lengths have been determined and deposited in the Protein Data Bank (PDB)

repository (Table 1.1). All reported structures and the modeled polyQ regions are nonpathogenic, conformationally flexible, and get affected by the nearby residues' conformation. The structure of the httx1 with non-pathogenic polyQ repeat (17 Qs) has been determined using X-ray crystallography [69]. The structure comprises the amino-terminal htt^{N17} as an α-helix, a flexible Q_{17} region, and a polyproline helix formed by the proline-rich C-terminal region. The Q_{17} region adopts multiple conformations that include α-helix, random coil, and extended loop [69].

Table 1.1. *Structures of the different regions, fragments, or models of httx1*

Structure	PDB ID	Method	Reference	Remarks
Crystal Structure of MBP-A3-httN17-Q17-polyP-mixed P/Q (C^{95})	3IOR	XRD: 3.6 Å	[69]	MBP is the maltose binding domain, A3 acts as a small linker. C indicates the crystal name. The crystals are sorted by β angle of unit cell. The values of β angles are assigned to each crystal by numbers. For the same β angles, letters of the alphabet note crystals. The mercury socked crystal is indicated by Hg in subscript
Crystal Structure of MBP-A3-httN17-Q17-polyP-mixed P/Q (C_b^{92})	3IOT	XRD: 3.5 Å		
Crystal Structure of MBP-A3-httN17-Q17-polyP-mixed P/Q (C^{94})	3IOU	XRD: 3.7 Å		
Crystal Structure of MBP-A3-httN17-Q17-polyP-mixed P/Q (C^{99})	3IOV	XRD: 3.7 Å		
Crystal Structure of MBP-A3-httN17-Q17-polyP-mixed P/Q (C_{Hg}^{99})	3IOW	XRD: 3.5 Å		
Crystal Structure of MBP-A3-httN17-Q17-polyP-mixed P/Q (C^{90})	3IO4	XRD: 3.63 Å		
Crystal Structure of MBP-A3-httN17-Q17-polyP-mixed P/Q (C_a^{92})	3IO6	XRD: 3.7 Å		
Structure of anti-huntingtin VL domain in complex with huntingtin peptide htt^{N17}**(5-18)** (EKLMKAFESLKSFQ)	3LRH	XRD: 2.6 Å	[113]	Htt^{N17}(5-18) indicates the N-terminal residues 5–18 of Htt and including the first residue of the poly-Gln stretch
Solution structure of the N-terminal domain of huntingtin (htt^{N17}) in 50 % TFE	2LD0	Solution NMR	[23]	
Solution structure of the N-terminal domain of	2LD2	Solution NMR		

huntingtin (htt^{N17}) in presence of DPC micelles				
Crystal Structure of MBP-A_3-htt^{N17}-Q_7HQHQHQ27-polyP-mixed P/Q (X1C1: alpha)	4FE8	XRD: 3 Å	[114]	MBP is the maltose binding domain, A_3 acts as a small linker. The X1C1 indicates one of the two conformations observed for X1 crystal type. The conformation was termed alpha. The X1C2 indicates one of the two conformations observed for X1 crystal type. The conformation was termed beta. The X2C1 indicates one of the two conformations observed for X2 crystal type. The conformation was termed loop. The X2C2 indicates one of the two conformations observed for X2 crystal type. The conformation was termed beta.
Crystal Structure of MBP-A3-htt^{N17}-Q7HQHQHQ27-polyP-mixed P/Q (X1C2: Beta)	4FEB	XRD: 2.8 Å		
Crystal Structure of MBP-A3-htt^{N17}-Q7HQHQHQ27-polyP-mixedP/Q (X2C1: Beta)	4FEC	XRD: 3 Å		
Crystal Structure of MBP-A3-htt^{N17}-Q7HQHQHQ27-polyP-mixedP/Q (X2C2: Beta)	4FED	XRD: 2.81 Å		
Crystal structure of scFvC4:Htt^{N17} complex	4RAV	XRD: 2.5 Å	[115]	scFvC4 stands for C4 single-chain Fv antibody
Htt46Q-HAP40 complex structure	6EZ8	Cryo-EM: 4 Å	[116]	Htt46Q indicates the full-length human huntingtin protein with 46Q at exon1 region. HAP40 indicates huntingtin-associated protein 40
Structure of the htt^{N17}Q7 (tetramer/dimer mixture)	6N8C	Solution NMR	[117]	

1.5. Role of htt^{N17} in huntingtin exon 1 (HDx1) aggregation

PolyQ aggregation occurs via nucleation growth polymerization mechanism [118, 119]. Wetzel and coworkers, using $K_2Q_{36}K_2$ showed that the aggregation nucleus is a monomer and corresponds to an unfavorable protein folding reaction. The rate-limiting nucleation events did not involve monomers' condensation into oligomers, as there is no significant development of β-structure within the polyQ peptide before its aggregation. It starts with the monomer's folding, which means either that individual peptide molecules undergo aggregation rapidly after they acquire β-sheet structure, or that aggregation and β-sheet acquisition are concerted events [119].

The structures of fibrils formed by proteins/peptides involved in Alzheimer's disease (β-amyloid), Parkinson's disease (α-synuclein), tauopathies (tau), hemodialysis related amyloidosis (β_2-microglobulin) have been revealed by electron paramagnetic resonance and solid-state nuclear magnetic resonance spectroscopy. Interestingly, despite considerable variations in their sequences and native structures, the fibrils of all these proteins exhibit common structural features; they all take up a parallel in-register cross-β structure [120]. The cross-β structure observed for polyQ fibrils [121, 122], however, is different. They form antiparallel β-sheets [19, 109, 123-125]. Langen and coworkers investigated the structural organization of the HDx1 (46Q) fibrils using EPR spectroscopy of the spin labeled HDx1 [126]. Their data clearly ruled out the in-register fibrillar structure for HDx1. They found that the polyQ region becomes highly immobile in the fibrillar form, an observation consistent with the polyQ region forming the fibrillar core. Besides, the htt^{N17} was found to be involved in the tertiary or quaternary interactions. The C- terminal domain, on the other hand, adopts a polyproline II structure and remains highly dynamic without any significant packing interactions.

Mutations that reduce the α-helical propensity of htt^{N17}, not only affect the huntingtin's functions inside the cell [127], but also reduce the overall aggregation propensity of the HDx1 [127]. Designed polyQ peptides have been reported in the literature to form amyloid fibrils without significantly populating the oligomeric species [22, 128]. Tagging with htt^{N17} or polyP stretch, however, strongly modulates the aggregation [19, 73]. These polyQ flanking stretches have contrasting roles to play as far as polyQ aggregation is concerned. Whereas, htt^{N17} enhances the aggregation, the polyP stretch reduces it. Htt^{N17}, by itself, does not form amyloid-like structures. In fact, it takes up a somewhat collapsed conformation that resists aggregation. However, when

fused with the polyQ peptides, the htt^{N17} conformation gets disrupted rendering it aggregation-prone. The htt^{N17}-polyQ peptides from htt^{N17}-mediated oligomers with polyQ stretch exposed [19, 129]. The aggregation of htt^{N17}-polyQ peptides is initiated *via* the homotypic interaction between htt^{N17}. The peptides oligomerize through intermolecular self-association of the htt^{N17} stretches. The oligomerization brings the polQ stretches in close proximity, and is followed by the nucleation event to form an amyloid-like aggregate with a highly rigid and dehydrated amyloid core composed of htt^{N17} and polyQ . In contrast, the highly mobile and solvated polyproline C-terminal tail lacks pronounced packing and protrudes outward from the amyloid core. Frydman and coworkers investigated the importance of htt^{N17} helix amphipathicity on HDx1 (51Q) aggregation. Ala substitution of the polar residues diminished the aggregation propensity to ~50%, whereas Ala substitution of the non-polar residues on the hydrophobic face completely abolished the aggregation. It is interesting to note that the htt^{N17}-lacking HDx1, however, shows complete aggregation on the same time scale, albeit with slower kinetics [127].

1.6. Htt^{N17} as a potential therapeutic target

There is no specific therapy or treatment to date that can cure HD. However, scientists worldwide are continually working to find out effective therapies for HD. Many potential therapeutic agents that include riluzole, memantine, tetrabenazine, minocycline, caspase-6 inhibitors, C2-8, trehalose, creatine, coenzyme Q10, cysteamine, and epigallocatechin-gallate have shown improvement in motor and cognitive dysfunction in different mice lines, and are in different stages of the drug development process [130]. Drugs like deuterabenazine or SD-809, tetrabenazine, and dalbenazine are the only FDA approved medications available in the United States for the treatment of chorea in HD. These drugs are vesicular monoamine transporter type-2 (VMAT2) inhibitors that act on the neuroactive peptides and neurotransmitters like dopamine in the nerve terminals. These drugs do not cure HD, but are essentially used for the management of chorea linked with HD.

Apart from this, several compounds have been isolated from animal models, which can detect the aggregate formation or act as anti-aggregation agents to inhibit or suppress the huntingtin aggregation. They include molecular tweezers [131], intracellular antibodies for polyQ sequences [132], molecular chaperons, protease enzymes caspase 3, calpain, peptides [133-137] and other small chemical compounds [138].

1.6.1. Huntingtin modifying enzymes and interacting proteins

The huntingtin undergoes various post-translational modifications that modulate its structure, function and the aggregation propensity [27] . In Httx1, several residues in the htt^{N17} stretch undergo post-translational modifications. Phosphorylation is one of the most versatile post-translation modification that regulates a variety of cellular functions such as cell signaling, protein-protein interactions, protein degradation, cellular translocations, and many more [57]. The htt^{N17} region harbors three residues *viz.* T3, S13, and S16 that undergo phosphorylation [27, 82-84]. Phosphorylation of T3 modulates the HDx1 conformation and reduces its aggregation propensity. It stabilizes the α-helical conformation of the htt^{N17}, thereby diminishing the HDx1 aggregation [82]. Lower T3 phosphorylation has been observed in the HD mice models and clinical samples of HD patients [83]. Like T3, S13 and S16 are also hypo-phosphorylated in HD [99, 139], and hyper-phosphorylation of these residues protects the mouse models from HD pathogenicity [99]. In contrast to T3 phosphorylation that stabilizes the htt^{N17} helix, however, the S13 and S16 phosphorylations disrupt the amphipathic α-helix at the N-terminus [139]. Yang and coworkers investigated the role of htt^{N17} Ser phosphorylation on the full-length huntingtin-induced HD pathogenesis. They showed that the double phosphomimetic mutations S13D/S16D inhibit the aggregation, while the double phosphoresistant mutations S13A/S16A do not [86]. Wetzel and coworkers studied the role of htt^{N17} phosphorylation in the model HDx1 peptide (37 Qs). Single substitution S13D or S16D as well as the double substitution S13D/S16D within htt^{N17} were found to suppress the htt^{N17} oligomerization, thereby inhibiting the aggregation [85]. Even though single site phosphorylation and phosphomimetic mutations inhibit the fibril formation, they fail to inhibit oligomerization [85]. Double phosphorylation S13pS/S16pS is less abundant than single-site phosphorylation [140], but prevents oligomerization as well both *in vitro* and *in vivo* [141, 142].

The htt^{N17} also undergoes ubiquitination and SUMOylation. Ubiquitination and SUMOylation are biochemically similar, but the consequences of these modifications are very different. Whereas the ubiquitination marks a protein for degradation by proteasomes or lysosomes [143-145]. SUMOylation is associated with protein stabilization, nuclear-cytosolic transport, and transcriptional regulation [146]. SUMOylation and ubiquitination mostly compete for identical residues and act antagonistically. In Htt^{N17}, there are 3 lysine residues K6, K9, and K15 that can undergo SUMOylation and ubiquitination. Marsh and coworkers showed that the SUMOylation

of HDx1 exacerbates neurodegeneration in HD drosophila models, whereas ubiquitination abrogates it. They found that SUMOylation of HDx1 leads to its increased accumulation, but reduced amount of large aggregates. The HD pathology, therefore, could be due to the accumulation of soluble toxic oligomers [28].

The three lysine residues in the htt^{N17} region also happen to be the candidates for acetylation. Besides, the N-terminal acetylation of the httx1 has been reported to be acetylated, wherein the N-terminal methionine is cleaved and the Ala2 is acetylated [84]. Interestingly, the pathogenic huntingtin protein is poorly acetylated compared to the wild-type protein, which shows that decreased acetylation is associated with HD pathogenesis [93]. The acetylation of lysine residues in the htt^{N17} region inhibits fibril formation, promotes larger globular aggregates, and reduces toxicity. It also lowers the binding affinity of htt^{N17} to the lipid membranes, which prevents membrane damage due to the fibril formation [93]. Lashuel and coworkers demonstrated that single residue acetylation, K6, K9, or K15 within htt^{N17} of HDx1 did not affect the protein's structural properties and aggregation kinetics. However, acetylation on K6 reversed the aggregation inhibitory effect of T3 phosphorylation [82]. The enzymes involved in these post-translational modifications happen to be potential therapeutic targets.

Proteins and molecular chaperones that bind to the htt^{N17} region and suppress the huntingtin aggregation can also be used for therapeutic interventions. There are several proteins and molecular chaperones that have been shown to interact with the htt^{N17}. They include the heat shock protein 70 (Hsp70) [147], C-terminus of Hsp70-interacting protein (CHIP) [90], TCP-1 ring complex (Tric) [148], translocated promoter region (TPR) [96], huntingtin-interacting protein K (HYPK) [149], nuclear export factor chromosome region maintenance-1 (CRM1) or Exportin1 [98], protein kinase C and casein kinase 2 substrates in neurons (PACSIN1) [150].

1.6.2. Molecular tweezers

CLR01, a molecular tweezer, binds specifically with the lysine residues in the htt^{N17} region and inhibits the HDx1 aggregation *in vitro* and living cells. In HDx1, CLR01 disrupts the amphipathic helical nature of htt^{N17} and prevents the htt^{N17} self-association [131]. As discussed above, htt^{N17}, when fused with polyQ, self-associates to form α-helical oligomers before the nucleation event

[19]. Notably, CLR01 is a lysine-specific molecular tweezer known to inhibit several amyloidogenic proteins' self-assembly and toxicity by binding to the lysine residues [151]. Identification and screening of molecules that can interact with htt^{N17} amino acids and modulate its structure could turn out to be potential therapeutic candidates to counter huntingtin aggregation.

1.6.3. Intrabodies

Intrabodies are the antibody fragments that are intracellularly expressed to bind the intracellular proteins [152]. As the target specificity resides in the Fv variable region alone, they can be expressed intracellularly without affecting their substrate-recognition. The first anti-huntingtin intrabody scFvC4 was selected from the naive human spleen ScFv phage display library through iterative panning against htt^{N17} [153]. The scFvC4 binds with the initial 15 residues of HDx1 [115]. Another anti-N terminus intrabody $V_L12.3$ was selected from a non-immune human yeast surface display library. The htt^{1-20} was used as the target to select $V_L12.3$ [154]. The crystal structure of ScFvC4 with htt^{N17} has been determined (PDB ID: 4RAV). The htt^{N17} binds to the intrabody in an α-helical conformation such that the residues 3-11 of the peptide make contact with the intrabody. The binding shields the hydrophobic face of the amphipathic helix from the solvent. The X-ray structure of the $V_L12.3$ bound to its epitope htt_{5-18} has also been determined (PDB ID: 3LRH) [113]. Several other intrabodies have been identified using different regions of HDx1 as the target sequences. These intrabodies have recently been reviewed by Messer and Butler [152].

1.6.4. Peptide-based inhibition

Peptides is another interesting class of molecules that have been explored as inhibitors of amyloid formation. From the HD aggregation point of view, some peptide-based inhibitor molecules specifically bind with the different huntingtin regions and counter the protein aggregation process [135, 137]. Burke and coworkers, using phage display screening, identified six 11-residue Trp-rich peptides that displayed preferential binding to the pathogenic polyQ repeats [135]. One of these peptides QBP1 (SNWKWWPGIFD) displayed far better discrimination between the pathogenic and non-pathogenic glutamine repeats. QBP1 binds to the pathogenic polyQ and prevents its aggregation from forming amyloid-like structures [135]. Molecular dynamics simulations suggested that the QBP1 folds into a so-called α-hairpin conformation, that binds with

the β-hairpin conformation adopted by the polyQ peptides [155]. Laurents and coworkers, using the NMR spectroscopy, showed that the Pro5-Gly6 forms a type II β-turn, whereas the other residues participate to form a hydrophobic cluster [156]. As the htt^{N17} oligomerization is known to catalyze the aggregation of HDx1, possibly by increasing the local concentration of the polyQ regions in the htt^{N17}–mediated oligomers, the role of htt^{N17} in HDx1 aggregation inhibition has also been explored [21, 137].

This thesis is concerned with the huntingtin aggregation inhibition by the QBP1 and the htt^{N17} derivatives. The relevant literature on these peptides is discussed in the respective chapters.

CHAPTER 2

Material and Methods

2.1. Materials

Rink amide resin, Fmoc-Phe-Wang resin, *N*,*N*-diisopropylethylamine (DIPEA), piperidine, trifluoroacetic acid (TFA), 1,2-ethanedithiol, thioanisole, acetic anhydride, 1,1,1,3,3,3-hexafluoro-2-propanol (HFIP), α-cyano-4-hydroxycinnamic acid (HCCA), and dimethyl sulfoxide (DMSO) were purchased from Sigma-Aldrich Chemicals Pvt. Ltd. All fluorenylmethyloxycarbonyl (Fmoc)-protected amino acids, *N*,*N*,*N*′,*N*′-tetramethyl-*O*-(1*H*-benzotriazol-1-yl)uranium hexafluorophosphate (HBTU), and 1-[Bis(dimethylamino)methylene]-1*H*-1,2,3-triazolo[4,5-*b*]pyridinium 3-oxide hexafluorophosphate (HATU) were purchased from Novabiochem (Darmstadt, Germany). *N*,*N*-dimethylformamide, diethyl ether, and *m*-cresol were obtained from Merck, India. 1-hydroxybenzotriazole hydrate (HOBt), sodium dihydrogen phosphate (NaH_2PO_4), Tris(hydroxymethyl)aminomethane (Tris base), and other routine chemicals was purchased from Sisco Research Laboratory India, Merck India, and HiMedia. Luria-Bertani medium for bacterial culture were procured from HiMedia. Ni-NTA beads were obtained from Qiagen. The pET32a-HD46Q plasmid was a gift from Pamela Bjorkman (Addgene plasmid#11515;http://n2t.net/addgene:11515; RRID: Addgene_11515). The source of other specialized materials is mentioned wherever their use is mentioned.

2.2. Experimental Methods

2.2.1. Protein Expression and Purification

The thioredoxin-HDx1 (Trx-HDx1) fusion construct (Fig 2.1) cloned in pET32a vector (pET32a-HD46Q) in *E. coli* DH5α cells was procured from Addgene [157]. The plasmid was isolated, and the *E. coli* BL21-DE3 cells were transformed. The overnight grown primary culture of the transformed cells was diluted 100-fold in LB medium (secondary culture). The secondary culture was grown to mid-log phase (OD_{600} = 0.6). The protein expression was subsequently induced with 1 mM IPTG at 18 ºC. The overnight grown cells were centrifuged at 5000 rpm for 15 min and the supernatant discarded. The pellet was suspended in the lysis buffer (20 mM Tris-HCl buffer, pH 8.0 containing 300 mM NaCl, 10 mM imidazole, 1 mM PMSF, and 1% Triton X-100). Following

20 min of lysis at room temperature, the lysates were centrifuged at 20,000×g for 45 minutes at 4 ºC and the supernatant collected. Ni-NTA beads (Qiagen) were equilibrated with the lysis buffer. The cell lysate was subsequently added to the beads and incubated overnight at 4°C with gentle shaking. The Ni-NTA beads were then transferred into a 10 ml gravity column (Pierce™ Centrifuge Columns), washed with several volumes of wash buffer (20 mM Tris-HCl, pH 8.0, 300 mM NaCl, 20 mM imidazole). The Trx-HDx1 was then eluted with the elution buffer (20 mM Tris-HCl, pH 8.0, 300 mM NaCl, 300 mM imidazole) and analyzed by SDS-PAGE. The eluted protein was concentrated using Vivaspin Turbo 15 3000 MWCO centrifugal concentrator (Sartorius). The Trx-HDx1 was further purified by FPLC on a Superdex-75 and HiLoad™ 16/600 Superdex ™ 75 pg gel-filtration column (GE Healthcare) using 10 mM phosphate buffer, pH 7.4.

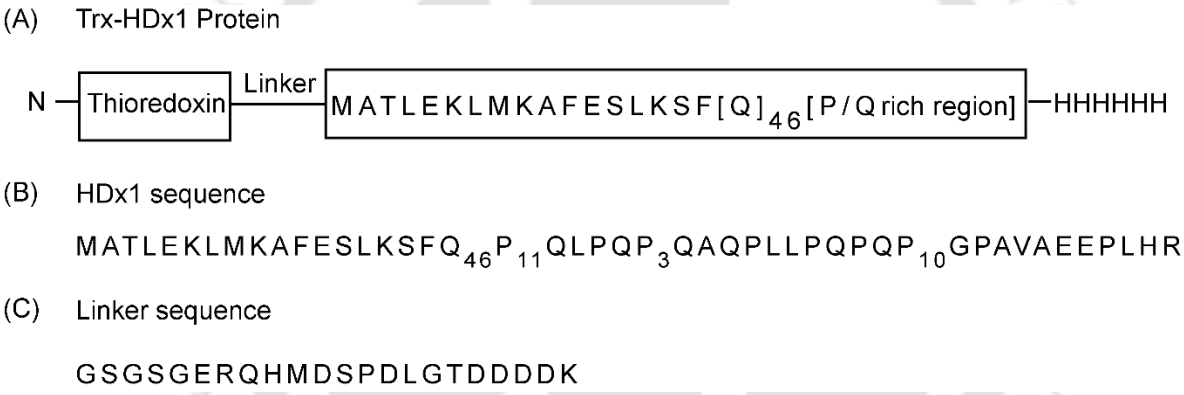

Fig. 2.1. *The thioredoxin-fused HDx1 used for the study (panel A), the sequence of the HDx1 with 46 glutamines in the polyQ tract (panel B) and the linker sequence (panel C).*

2.2.2. Protein solution and concentration

The concentration of the protein was estimated using a molar absorption coefficient of 13,940 $M^{-1}cm^{-1}$ in 10 mM phosphate buffer pH 7.4 [158]. Freshly prepared Trx-HDx1 protein was used for all the assays without removing the thioredoxin tag. The presence of the thioredoxin tag ensures reproducible monomeric protein preparations, a prerequisite to carry out the aggregation inhibition assay.

2.2.3. Peptide synthesis

The peptides with C-terminal amidation were synthesized manually on Rink amide resin using Fmoc chemistry by employing HBTU (or HATU)/HOBt/DIPEA activation (Fig. 2.2). The peptide acid (the only peptide acid used in this study) was synthesized on the Wang resin pre-loaded with the C-terminal amino acid, which was Phe in this case. The peptides lacking Aib residues were synthesized using HBTU activation, while those harboring Aib were synthesized using HATU activation. DMF was used as the solvent for synthesis. Each amino acid was coupled twice wherein first coupling was carried out with 3 equivalents (3X) and second coupling carried out with 2 equivalents (2X) of amino acids with respect to the resin substitution value (X). Protected amino acids were activated using equimolar HBTU (or HATU), equimolar HOBt, and 2-fold molar excess of DIPEA. First coupling was carried out for minimum 1 hour while second coupling was carried out for at least 30 minutes. Fmoc removal after amino acid attachments to the resin was carried out using 20% piperidine in DMF. The resin was washed scrupulously after each Fmoc removal step to ensure complete removal of piperidine. The N-terminal acetylation of peptides, wherever applicable, was carried out on-resin using 10 equivalents of acetic anhydride and 5 equivalents of DIPEA. The synthesized peptides were cleaved from the resin using a cocktail containing TFA, thioanisole, *m*-cresol, and 1,2-ethanedithiol in a ratio of 20:2:2:1. Cleaved peptides were filtered through glass wool and precipitated in ice-cold diethyl ether. The precipitated peptides were subsequently washed several times using diethyl ether to ensure the complete removal of chemical scavengers. The crude peptides were air-dried and stored at -20 $^{\circ}$C

2.2.4. Peptide Purification and characterization

Peptides were purified on a reversed-phase C-18 column using a linear gradient of water and acetonitrile (10-100%) containing 0.1% TFA on a Shimadzu Prominence Modular HPLC instrument (Shimadzu, Kyoto, Japan). A small amount of collected peptide fractions were mixed with HCCA matrix in the volume ratio of 1:1 and characterized by matrix-assisted laser desorption/ionization-time of flight (MALDI-TOF) mass spectrometry (Bruker Autoflex Speed MALDI-TOF/TOF, USA).

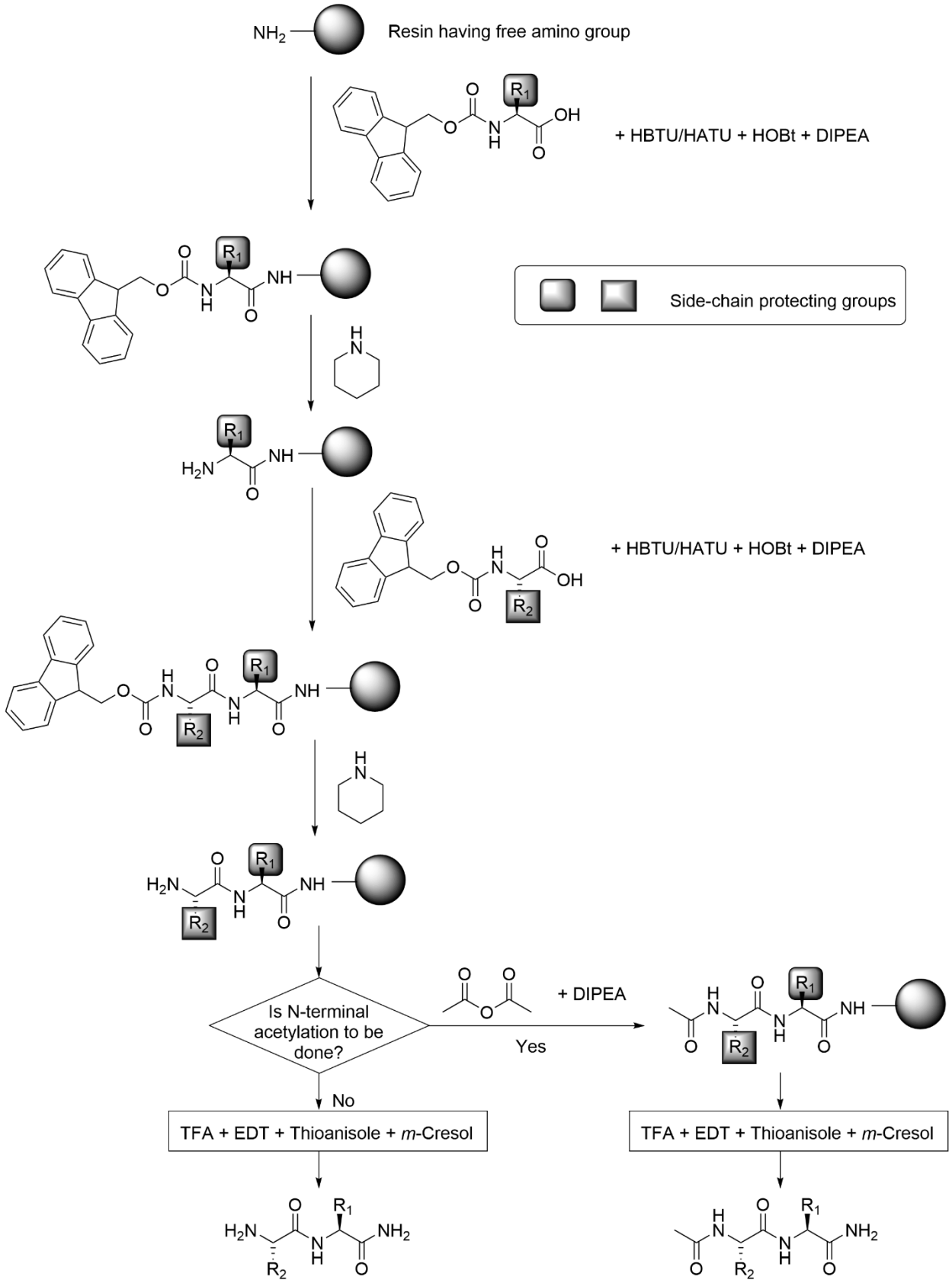

Fig.2.2. *The scheme of peptide synthesis. For clarity, the synthesis of dipeptides with free and acetylated amino terminus is shown.*

2.2.5. Peptide solutions and concentration estimation

Peptide stocks solutions were prepared in water. However, the peptides with low water solubility were dissolved in DMSO. The concentrations of peptides were determined by measuring the absorbance at 280 nm and using Trp absorption coefficient of 5690 $M^{-1}cm^{-1}$. The solutions of the Trp-lacking peptides were prepared by carefully weighing the peptides.

2.2.6. Disaggregation of peptides

To ensure that the htt^{N17}-derived peptides were free from aggregates, they were treated with TFA/HFIP as described by Chen and Wetzel [17]. Briefly, the peptides were weighed and dissolved in TFA/HFIP (1:1) at a concentration of 0.5 mg/mL. After 5 h of incubation at room temperature, the peptides were dried using N_2 gas and further subjected to N_2 purging for 1 hour to ensure complete solvent removal. The dried peptides were immediately resuspended in water, the pH of which was pre-adjusted to 3.0 using TFA. After complete dissolution, the peptide solutions were centrifuged for one hour at 50,000×g at 4 $^{\circ}$C. The clear supernatants were collected, and validated by 90° scattering at 450 nm using a spectroflourometer (Jasco FP 8500). The slit widths were set at 2.5 nm. All the solutions caused scattering comparable to that of the solvent. The freshly prepared peptide stock solutions (2 mM) in TFA/water (pH 3.0) were used for the assays.

2.2.7. Molecular dynamics simulations

Molecular dynamics simulations of the QBP1 and its analogs were carried out at the CDAC-IIT Guwahati Supercomputing facility, using the Gromacs software package (v 5.0.4) [159]. The peptides were built in the fully extended conformation using Ribosome software [160]. The φ and ψ dihedrals for ^{D}Pro were specified as 70° and 45°, respectively. GROMOS96 54a7 forcefield

[161] was employed and Aib parameters were incorporated in the Gromacs package as described by Castro and Micaêlo [162]. Energy minimization and 100 ns MD run were performed as described previously [163]. Dihedral angle analysis was done using the Gromacs built-in utilities and visualization was carried out with Discovery Studio Visualizer [6].

2.2.8. Trx-HDx1 aggregation assay using turbidimetry

The aggregation of the fusion protein Trx-HDx1 was assayed in 10 mM phosphate buffer, pH 7.4, by monitoring the turbidity at 405 nm as previously described [135]. Briefly, the turbidity was measured at 24 h interval at 405 nm using Cary 60 UV-Vis spectrophotometer (Agilent Technologies).

For chapter 3, freshly prepared 2.5 mm peptide solutions in DMSO were used for each aggregation inhibition assay. The freshly prepared protein solutions (13 µM concentration) were incubated with 2-fold molar excess (26 µM) of peptides at 37 °C for 7 days (168 h).

For chapters 4, the aggregation of 15 µM Trx-HDx1 was assayed in the presence of equimolar peptide concentration. Briefly, 6 µl of the peptide stock solutions (2 mM in TFA/water, pH 3.0) was added to 800 µl of 15 µM Trx-HDx1 solution in 10 mM phosphate buffer, pH 7.4, and incubated at 37 °C for ten days (240 h).

For chapters 5, the aggregation of 15 µM Trx-HDx1 was assayed in the presence of equimolar peptide concentration. Briefly, 6 µl of the peptide stock solutions (2 mM in deionized water) was added to 800 µl of 15 µM Trx-HDx1 solution in 10 mM phosphate buffer, pH 7.4, and incubated at 37 °C for ten days (240 h).

2.2.9. Trx-HDx1 aggregation assay using Thioflavin T (ThT) fluorescence

For chapter 3, the Trx-HDx1 protein was incubated at 13 µM concentration in 10 mM phosphate buffer, pH 7.4 for 168 h at 37 °C with 2 molar equivalents of the peptides. The 100 µl aliquots from the sample were taken out at 0^{th} hour (freshly prepared reaction mixture) and 168^{th} hour, and mixed with 1.3 µl of 1 mM ThT stock solution, prepared in deionized water.

For chapter 4 and 5, the Thioflavin T (ThT) fluorescence assay was carried out with 15 µM of protein in 10 mM phosphate buffer, pH 7.4 for 240 h at 37 °C incubated with equimolar amount of peptides, as in turbidity assay. The 50 µl aliquots from the incubated protein samples were taken out at every 24 h and mixed with 2 µl of 1 mM ThT stock solution, prepared in deionized water. ThT fluorescence emission was recorded on the Jasco FP8500 spectrofluorometer with 450 nm excitation, slit width 2.5 nm. The fluorescence emission intensity was monitored at 485 nm for 60 seconds, slit width 5 nm. The data is presented by taking the average fluorescence intensity of the 60 seconds scan.

2.2.10. Circular dichroism (CD) spectroscopy

All CD spectra were recorded on a Jasco J-1500 CD spectropolarimeter with a 1 nm slit width, and a 0.1 nm step size. The spectra were recorded in a 1 mm path length quartz cell with 8 accumulations. Each spectrum was corrected by subtracting the solvent (blank) spectrum. The corrected data were converted to mean residue ellipticity ($[\theta]_{MRE}$) using the formula:

$$[\theta]_{MRE} = \frac{M_r \times \theta_{obs}}{100 \times l \times c}$$

Here, M_r is the mean residue weight (peptide molecular weight /number of amino acid residues), θ_{obs} is the observed ellipticity in millidegrees, l is the pathlength in decimeters, c is the peptide concentration in mg/ml [163].

The CD spectra for QBP1 peptides were recorded at 30 µM concentration in deionized water. CD spectra for Trx-HDx1 protein were recorded in 10 mM phosphate buffer, pH 7.4. For QBP1 peptides, the 13 µM protein was incubated in 10 mM phosphate buffer, pH 7.4 without or with 26 µM peptides. CD spectra for the freshly-prepared samples and the 168 h old samples were recorded by taking out 20 µl aliquots. The 20 µl aliquots were diluted 10-fold with 10 mM phosphate buffer, pH 7.4.

For chapters 4 and 5, the CD spectra of peptides were recorded at 50 µM concentration in 10 mM phosphate buffer, pH 7.4. To investigate the protein aggregation inhibition, the CD spectra of 15 µM Trx-HDx1 protein samples, incubated with or without 15 µM peptide, were recorded in 10 mM phosphate buffer, pH 7.4. Briefly, the 15 µM protein was incubated in 10 mM phosphate

buffer, pH 7.4, with or without 15 µM of each peptide. The spectra for the freshly prepared (0 h), the 168 h-old, and 240 h-old samples were recorded by taking out 20 µl aliquots from the incubated reaction and diluting them 10-fold in 10 mM phosphate buffer, pH 7.4. As the peptides are very small than the Trx-HDx1, the contribution of the peptides in the CD spectra of peptide-incubated Trx-HDx1 was ignored.

2.2.11. Atomic force microscopy (AFM)

AFM images for the 168 h incubated Trx-HDx1 were recorded on Asylum MFP-3D Origin atomic force microscope (Oxford Instruments). The samples (40 µl) were deposited on clean glass slides. After an hour, the slides were washed 3 times with deionized water and air-dried. The images were acquired in non-contact mode using a silicon probe at 1 Hz scan rate. The images presented were 1^{st} order flattened.

2.2.12. Transmission electron microscopy (TEM)

TEM images were recorded using a JEOL FE-TEM (Model: 2100F) operating at 200 kV. The samples (10 µl) were placed on fresh carbon-coated grids and incubated for 5 min. The excess sample was wicked away with a lint-free tissue paper and further washed two times with deionized water. Afterward, the sample grids were stained with 2% uranyl acetate (w/v) solution and vacuum dried.

CHAPTER 3

The role of the turn-supporting motif in polyglutamine binding peptide QBP1 in huntingtin aggregation inhibition

The 11-residue polyglutamine binding peptide Ac-SNWKWWPGIFD-am, known as QBP1, inhibits the polyglutamine aggregation. In addition, a minimal 8-residue stretch in the QBP1 peptide (Ac-WKWWPGIF-am) is reported in the literature to possess the activity comparable to that of full-length QBP1. Both the peptides harbor a Pro-Gly dipeptide motif, a feature diagnostic of potential β-turn regions. In this chapter, we investigated if the presence of a β-turn motif is important for the huntingtin aggregation inhibition. Using single amino acid substitutions to generate analogs that could support, introduce, or eliminate the β-turn formation; we show that the turn-supporting motif is essential for the QBP1-mediated huntingtin aggregation inhibition.

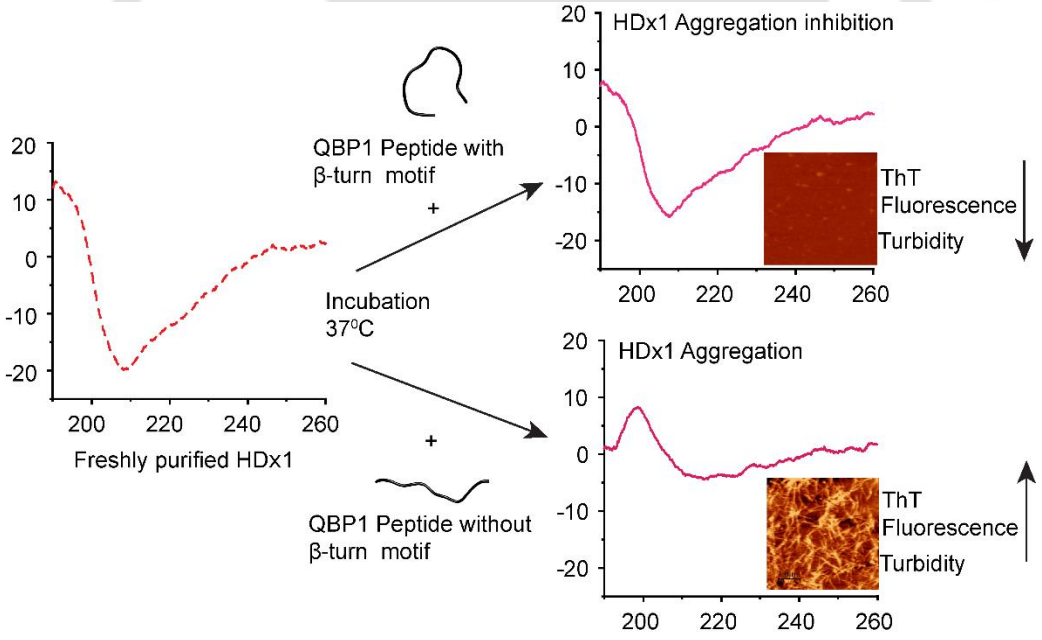

3.1. Introduction

Protein misfolding and aggregation into amyloid fibrils is associated with the pathogenesis of many diseases [164], and affects millions of people worldwide [165]. Out of at least nine neurodegenerative diseases that are characterized by the polyglutamine (polyQ) expansion, Huntington's disease (HD) is one of the most extensively studied [166]. The protein huntingtin harbors a polyQ stretch in its first exon. The occurrence of the disease and the age of onset strongly depends on the length of the polyQ region. A stretch of up to 35 glutamines is considered to be non-pathological. The polyQ stretch length of 40 or more, as a result of the expansion of CAG codon repeat in the first exon region of the gene, almost always results in HD [167]. A long polyQ stretch (>35Q) makes the protein unstable and misfolded, causing it to accumulate in the cells as amyloid-like aggregates, ultimately resulting in cell death [2, 3].

The exon 1 region of the pathogenic huntingtin (HDx1) is sufficient to form fibrils and induce the disease phenotype in mice [13]. The exon 1 region, therefore, happens to be an appropriate model system for understanding huntingtin aggregation. The HDx1 aggregation is characterized by a lag phase, a short extension phase, and a stationary phase. The HDx1 has a 17 residue N-terminal region, followed by a polyQ middle region, and a C-terminal proline-rich region. All three regions play defined roles in HDx1 aggregation [168]. The N-terminal region is known to accelerate the self-assembly and is believed to be in the α-helical conformation in the fibrillar structures [126, 169]. The polyQ region forms the β-sheet rich fibrillar core, whereas the C-terminal region lies outside the fibrillar core [126]. The C-terminal region adopts a type II polyproline structure and is known to retard the fibril formation. The N17 stretch has also been shown to play a critical role in the membrane-mediated HDx1 aggregation [170].

It is imperative to devise strategies that could inhibit huntingtin aggregation. Peptides have proven to be excellent models for deciphering the principles underlying amyloid formation [171]. Besides, peptides and peptide-based molecules hold great promise to inhibit the amyloid formation [172-174]. Peptides are recognized as highly selective, relatively safe, and well-tolerated drug candidates [171]. Using a phage screen display, Burke and coworkers identified six Trp-rich 11-residue peptides, termed polyglutamine binding peptides (QBP1-6), that bind and inhibit polyglutamine aggregation [175]. Subsequently, the structure-function study with the most active

peptide QBP1 led to the identification of a minimal 8-residue peptide (mQBP1) without any loss of activity [176].

As both the QBP1 and the mQBP1 harbor the turn-supporting Pro-Gly motif, we investigated if the turn-supporting dipeptide motif is essential for the HDx1 aggregation inhibition activity. Using the peptide analogs wherein the type I′ and II′ turn-supporting motifs were incorporated through single amino acid substitutions, we show that the turn-supporting motif is necessary for the peptide's activity.

3.2. Hypothesis

Tomita et al. carried out the structure-activity relationship analysis of QBP1 [176]. Alanine scanning of the peptide shows that all the hydrophobic residues other than Pro *viz.* Trp3, Trp5, Trp6, Ile9, and Phe10 are required for the activity. It is noteworthy that the Pro7Ala analog retains around 76% activity compared to the wild-type sequence. Proline, owing to its side chain bonded to the peptide backbone, shows high conformational rigidity. It is, therefore, surprising that the Pro7Ala substitution is well tolerated in QBP1. Similarly, the Gly8Ala analog is shown to have retained around 85% activity. A closer look suggests that the Pro7Ala and Gly8Ala substitutions do not significantly compromise the β-turn propensity in this region, like Pro-Gly, both the Ala-Gly and Pro-Ala can mediate a β-turn. An obligatory turn-inhibiting motif could be ^{L}Pro-^{L}Pro.

The D-amino acid scanning of the peptide sequence shows that these amino acids are well-tolerated near the peptide termini, but the activity is severely compromised when they are incorporated near the middle region. The D-amino acid analogs wherein the 4th and 5th residues are changed to D-stereoisomers retain around 13% and 8% activity. The Gly and Pro residues make the 4th and 5th residues, respectively, from the C-terminus. Interestingly, however, the analogs wherein the Pro-Gly motif is modified to ^{D}Pro-Gly and Pro-^{D}Ala, retain around 33% and 21% activity, respectively. ^{D}Pro-Gly is a well-established type II′ β-turn inducing motif [177]. Pro-^{D}Ala is shown to mediate the type II β-turn in the crystal structure of a model peptide. The CD spectra in methanol and water/methanol (9:1) also suggested a type II β-turn [178]. Tomita et al. showed that the two N-terminal residues, as well as the C-terminal Asp residue, are dispensable without any compromise in the activity, thereby identifying a minimal QBP1 peptide. A previous study has shown that the repeats of the Trp-rich stretch *i.e.*, WKWW separated by Val or Pro as the spacer residue, can also

efficiently inhibit polyglutamine aggregation [175]. The spacer residue was found to be necessary for the activity. It was proposed that the WKWW domain might bind the polyglutamine domain. At the same time, the adjacent proline interferes with beta-sheet formation by introducing a kink, preventing the binding of additional polyglutamine protein required to form aggregate. Laurents and coworkers subsequently determined the structure of the mQBP1 using solution NMR. The Pro-Gly motif was found to be mediating a type II β-turn while Trp 4 and Ile 7, together with Lys 2, Trp 3, and Phe 8, form a hydrophobic cluster [156]. As the structure of mQBP1 is known in isolation, it is unclear if a Pro-Gly mediated β-turn is necessary for its activity. The functional role of the Pro-Gly dipeptide motif in QBP1 and mQBP1, therefore, remains unclear. We set-out to test if the β-turn supporting motif is necessary for the peptides activity or not.

3.3 Results and Discussion

3.3.1. Purification and Characterization of Trx-HDx1 Protein

The study was carried out using HDx1 (46Qs) that carries an N-terminal thioredoxin tag. The rationale behind using the fused protein was to attain a monomeric protein that displays a reproducible and slow aggregation kinetics. As a delay in aggregation kinetics is the standard assay for the aggregation-inhibition activity of a compound, a highly reproducible kinetics with a lag phase is highly desirable. The free (untagged) HDx1, unfortunately, displays a rapid aggregation without a lag-phase, making it unsuitable for an aggregation-inhibition assay [170]. The Trx-HDx1 protein was purified on a Superdex-75 (10/300 GL) gel filtration column (GE Healthcare) using GE Healthcare AKTA purifier 100 FPLC system. The 10 mM phosphate buffer, pH 7.4 was used at a flow rate of 0.4 ml per minute, and protein elution monitored by the UV absorption at 280 nm. Trx-HDx1 protein eluted as a single peak but collected in 0.4 ml fractions (Fig. 3.1A). After the gel filtration, each fraction was characterized by SDS-PAGE electrophoresis (Fig. 3.1B). Trx-HDx1 (46Q) shows anomalous migration in gel filtration chromatography and SDS–PAGE [157]. The apparent molecular mass, therefore, differs from the theoretical mass.

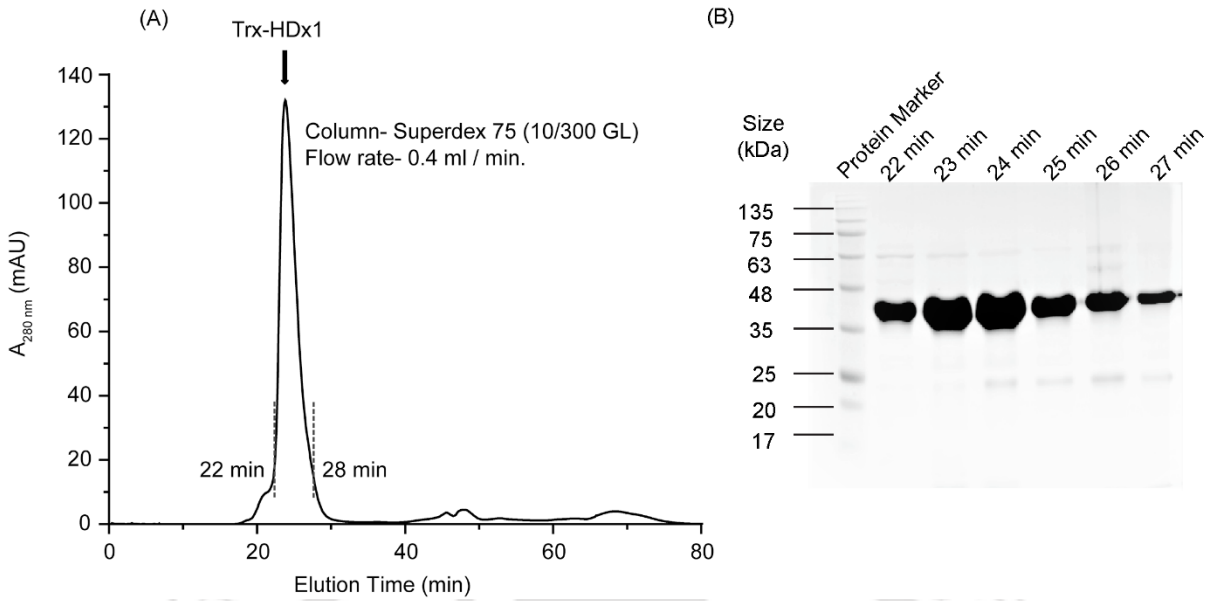

Fig. 3.1. *Characterization of the purified Trx-HDx1. (A) The gel filtration chromatogram of Trx-HDx1. The major peak was collected from 22-28 min elution time as 6 different fractions (1 minute per fraction i.e., 0.4 ml/fraction). (B) The SDS-PAGE of all the fractions. Each well was loaded with 20 µl of the eluted fraction. Fractions corresponding to 23-26 min were pooled and used for the subsequent experiments.*

3.3.2 Peptide design strategy

To investigate if the β-turn is essential for the activity, we designed the QBP1 and mQBP1 analogs wherein exactly one amino acid was replaced so as to incorporate the type I′ and II′ β-turn-supporting motifs. The Gly8Pro analog was used as the negative control for turn formation. The sequences and their IDs are shown in Table 3.1. The summary of the MALDI-TOF mass spectrometric data for these peptides is shown in Table 3.2

Table 3.1. *The IDs and the sequences of the peptides employed in this study.*

Peptide ID*	Sequence*,§	Remarks
QBP1	Ac-SNWKWWPGIFD-am	PG is considered a diagnostic of β-turns in proteins and often found in type I β-turns.
mQBP1	Ac-WKWWPGIF-am	
QBP1-pG	Ac-SNWKWW**p**GIFD-am	In designed peptides, pG preferentially folds into type II′ β-turn [177].
mQBP1-pG	Ac-WKWW**p**GIF-am	

QBP1-UG	Ac-SNWKWW**U**GIFD-am	UG in designed peptides is reported to mediate a type I′ β-turn in hydrogen-bonding organic solvents [179].
mQBP1-UG	Ac-WKWW**U**GIF-am	
QBP1-NG	Ac-SNWKWW**N**GIFD-am	NG is known to mediate β-turns with a preference for the type I′ turn [180].
mQBP1-NG	Ac-WKWW**N**GIF-am	
QBP1-PP	Ac-SNWKWWP**P**IFD-am	PP cannot mediate a turn and is used in this study as a negative control for the turn.
mQBP1-PP	Ac-WKWWP**P**IF-am	

*The lower case 'p' represents ^{D}Pro, and 'U' represents 2-aminoisobutyric acid (Aib).
§ 'Ac' at N-terminus indicates N-terminal acetylation, 'am' at C-terminus indicates peptide amide.

Table 3.2. *The summary of the MALDI-TOF mass spectrometric analysis of the peptides listed in Table 3.1.*

Peptide ID	Calculated monoisotopic mass (Da)	Expected MH^+ mass (Da)	Observed MH^+ mass (Da)	Percent mass error
QBP1	1475.688	1476.696	1477.067	0.025
mQBP1	1159.586	1160.594	1159.762	0.072
QBP1-pG	1475.688	1476.696	1477.172	0.032
mQBP1-pG	1159.586	1160.594	1159.811	0.067
QBP1-UG	1463.755	1464.763	1466.07	0.089
mQBP1-UG	1147.653	1148.661	1149.264	0.053
QBP1-NG	1492.678	1493.686	1493.148	0.036
mQBP1-NG	1176.576	1177.584	1177.53	0.005
QBP1-PP	1515.719	1516.727	1516.259	0.031
mQBP1-PP	1199.617	1200.625	1199.92	0.059

3.3.3. Secondary structure of the peptides

The structure of the peptides in deionized water was investigated using CD spectroscopy (Fig. 3.2). The QBP1 peptide shows a minimum around 202 nm with a shallower band around 214 nm, and a positive band observed around 229 nm. The 214 and 229 nm bands are the exciton-coupled bands, indicating an interaction between the aromatic side-chains suggesting a distinct aromatic cluster [181, 182]. QBP1-pG displays a broad negative band with a minimum around 204 nm and a shoulder around 214 nm. The spectrum also shows a crossover around 192 nm and the 229 nm band characteristic of the aromatic interactions. The spectrum is suggestive of a folded peptide

conformation. QBP1-UG shows two distinct negative bands around 202 and 215 nm suggesting a mixture of the random coil and β-sheet structures. The positive band around 228 nm is absent for QBP1-UG, suggesting a different arrangement of the aromatic residues. The QBP1-NG displays negative bands around 202 and 221 nm. The 221 nm band indicates the presence of some helical content. The spectrum of QBP1-PP is very similar to that of the QBP1. As Pro-Pro cannot mediate a turn, the aromatic CD signature is somewhat surprising. However, any other conformation that fixes the aromatic residues close to each other could contribute to such an aromatic CD band.

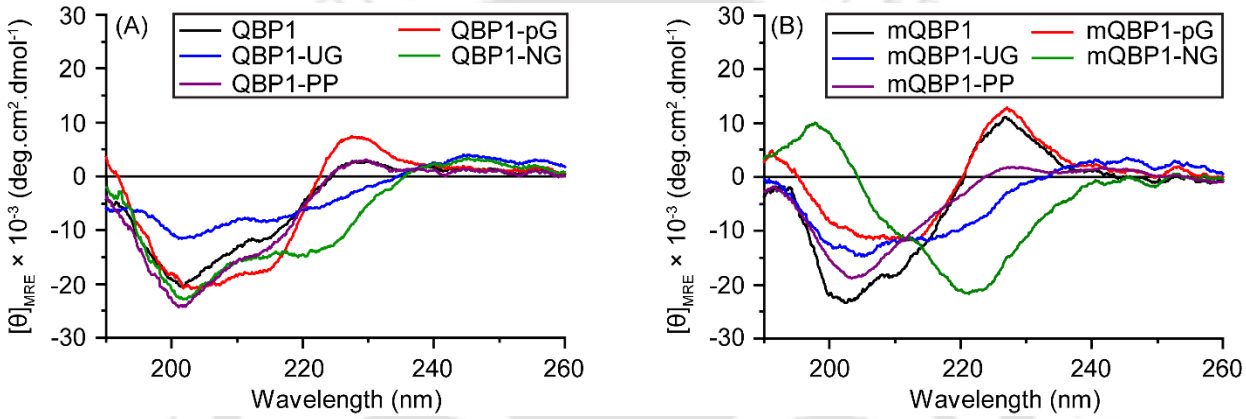

Fig. 3.2. *CD spectra of QBP1 (A) and mQBP1 (B) analogs in water.*

The CD spectra of the mQBP1 and its analogs are shown in Fig. 3.2B. The spectrum for mQBP1 shows a negative band around 203 nm with a shoulder around 210 nm and a moderately intense positive band around 227 nm. Laurents and coworkers have reported the CD spectrum for mQBP1 with very similar spectral features. They assigned the 210 and 227 nm bands to the well-ordered Trp residues, which was validated by the NMR structure [156]. The mQBP1-PP shows a spectrum with a minimum around 204 nm and a rather weak 227 nm positive band. The spectrum is suggestive of largely unordered conformation. The spectrum of mQBP1-pG shows a broad minimum from ~200-215 nm, a crossover around 195 nm, and a moderately intense positive band around 227 nm suggesting a folded peptide. The spectrum of mQBP1-UG is very similar to that of QBP1-UG. The spectrum of mQBP1-NG suggests distinct folding; the spectrum shows a negative band around 222 nm with a hump around 209 nm and a positive band around 198 nm. Such spectra have been assigned to the type I β-turn in the literature [183].

3.3.4. Molecular dynamics simulation of peptides

The folding of the QBP1 and its analogs in water was also investigated using molecular dynamics (MD) simulations (Fig. 3.3-3.7). In QBP1, the Pro residue takes up the dihedral angles characteristic of type II β-turn. Gly, on the other hand, is more flexible (Fig. 3.3). The ϕ, however, lies largely between 60-120° after around 70 ns of simulation whereas the ψ lies largely between -30 to -90°. A classical type II turn is characterized by the $(\phi,\psi)_{i+1}$ of -60° and 120° and $(\phi,\psi)_{i+2}$ of 80° and 0° [184]. The Pro-Gly motif in QBP1 simulation, therefore, does not seem to result in a typical type II turn, possibly due to steric clashes between the bulkier *i* (Trp) and *i+3* (Ile) residues. ^{D}Pro-Gly has been reported as the mirror-image turn-nucleating dipeptide motif. It preferentially nucleates the type II′ β-turn but can support type I′ turn as well. MD simulation with QBP1-pG shows that that the peptide folds into a β-hairpin structure within 20 ns (Fig 3.4). An ideal type II′ turn is characterized by the $(\phi,\psi)_{i+1}$ of 60° and -120° and $(\phi,\psi)_{i+2}$ of -80° and 0° [184]. In QBP1-pG MD simulation, ^{D}Pro takes up the ϕ and ψ values around 60° and around -100° while Gly takes up the ϕ and ψ values around -120° and 0°. The ^{D}Pro-Gly motif, therefore, induces a type II′ in the QBP1-pG. Similarly, Aib-Gly motif in QBP1-UG (Fig. 3.5) and Asn-Gly in QBP1-NG mediate β-turns (Fig. 3.6). The QBP1-PP remains rather extended throughout the simulation (Fig. 3.7). The MD simulations of the minimal QBP1 peptides did not result in stable β-turns. However, their folding with β-turn while interacting with the polyQ region cannot be ruled out.

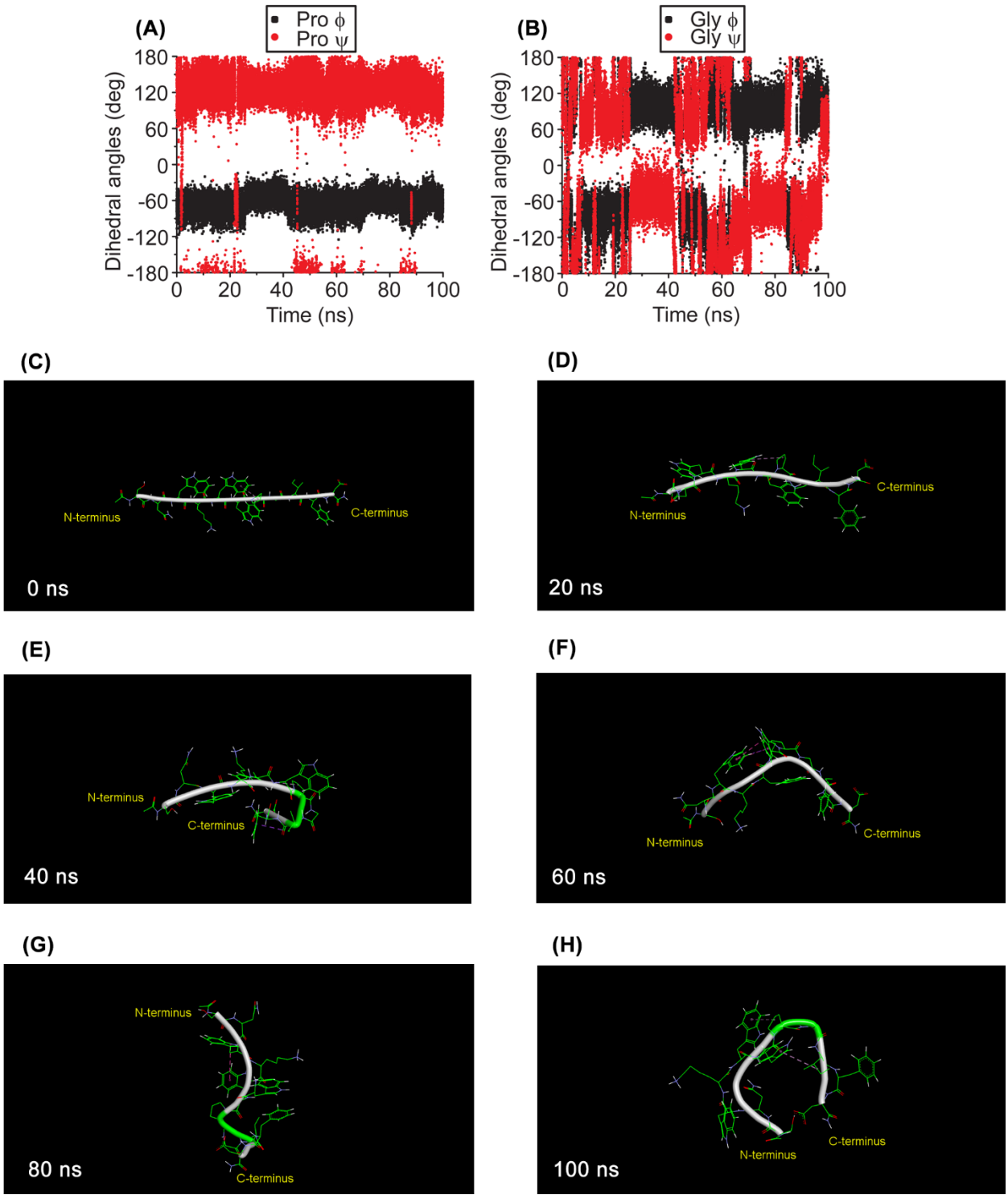

Fig. 3.3. *MD simulation of QBP1. The dihedral angles of Pro7 (A) and Gly8 (B). The snapshots of the peptide trajectory at 20 ns interval (C-H).*

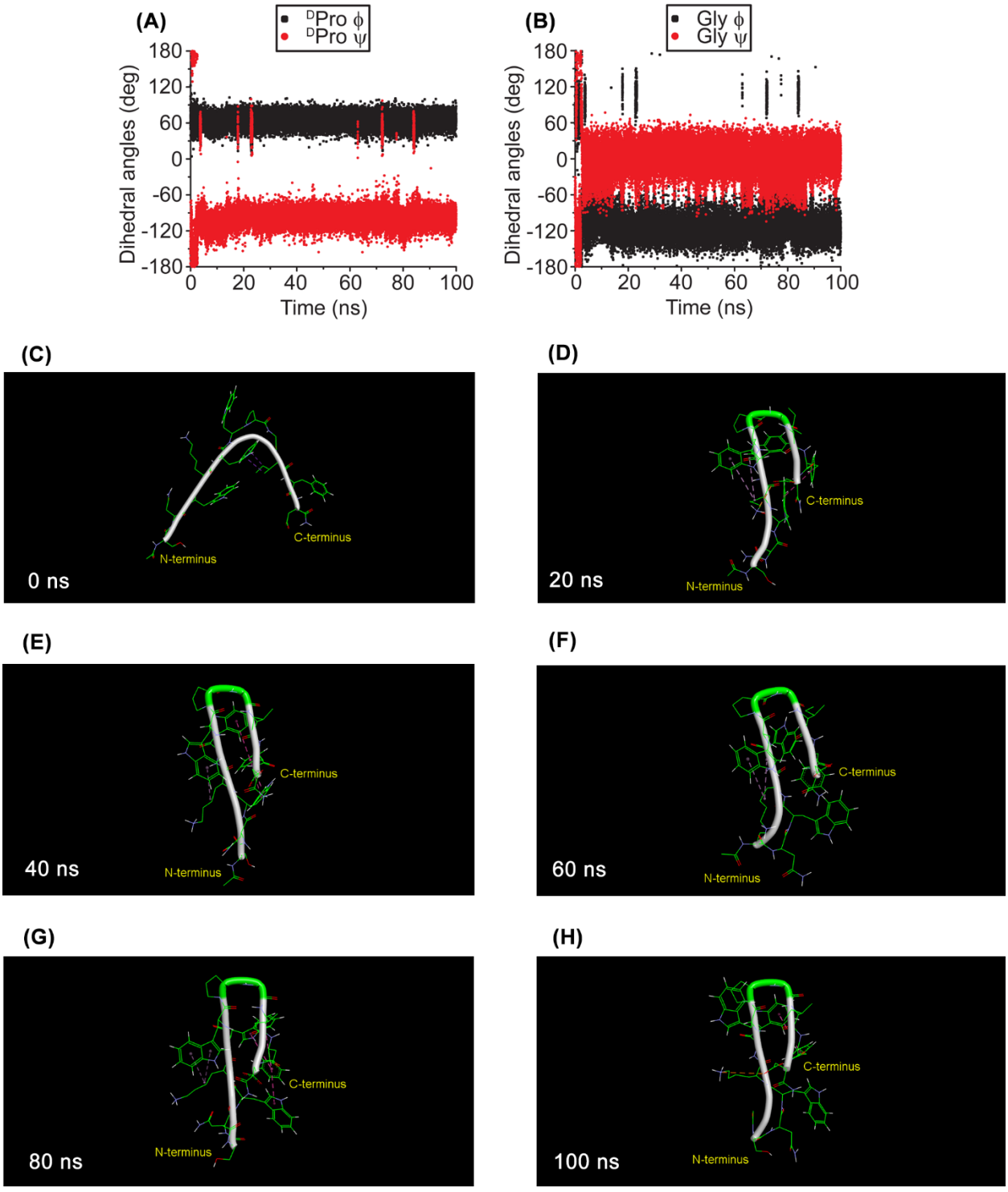

Fig. 3.4. *MD simulation of QBP1-pG. The dihedral angles of* ^{D}*Pro7 (A) and Gly8 (B). The snapshots of the peptide trajectory at 20 ns interval (C-H).*

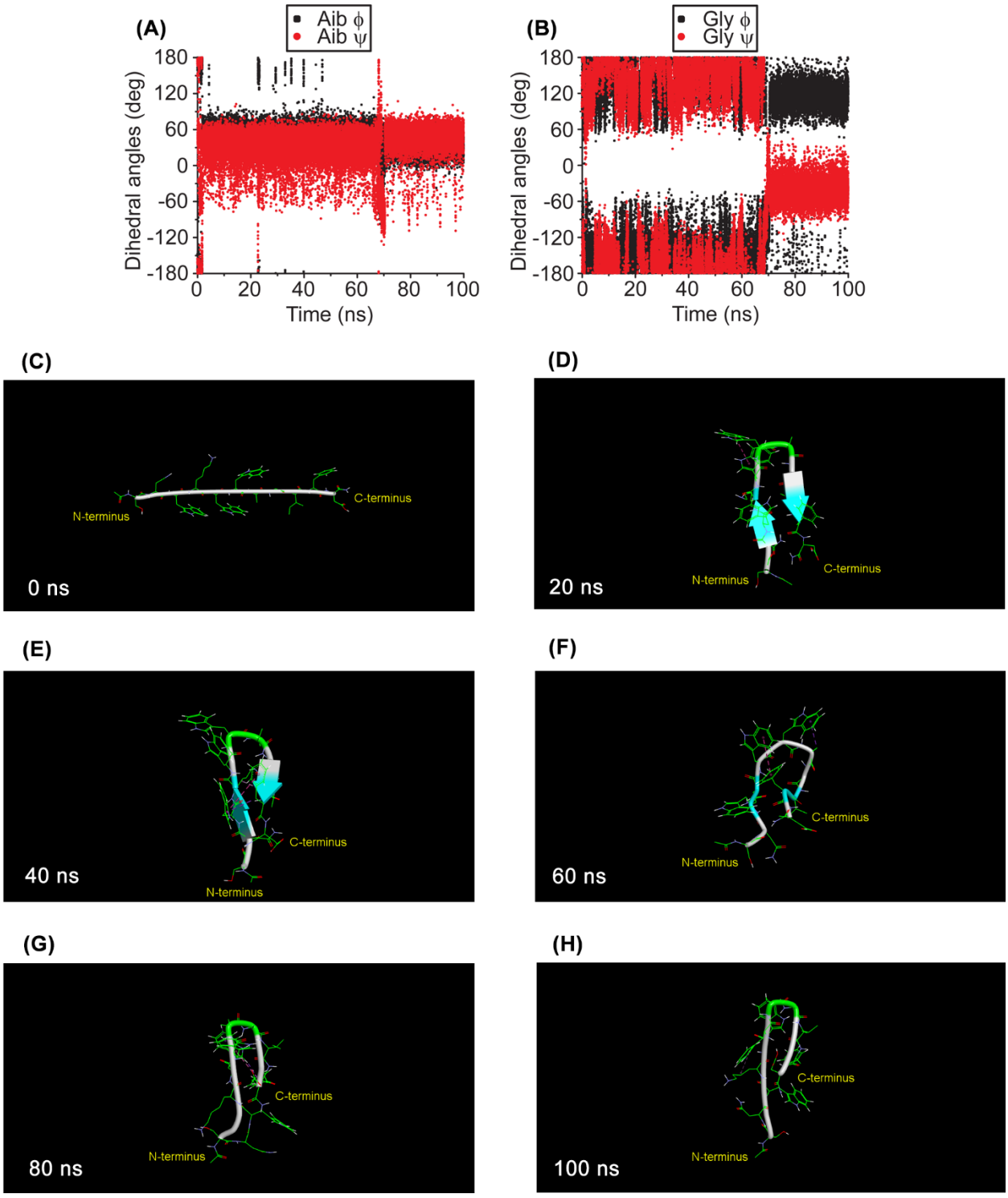

Fig. 3.5*. MD simulation of QBP1-UG. The dihedral angles of Aib7 (A) and Gly8 (B). The snapshots of the peptide trajectory at 20 ns interval (C-H).*

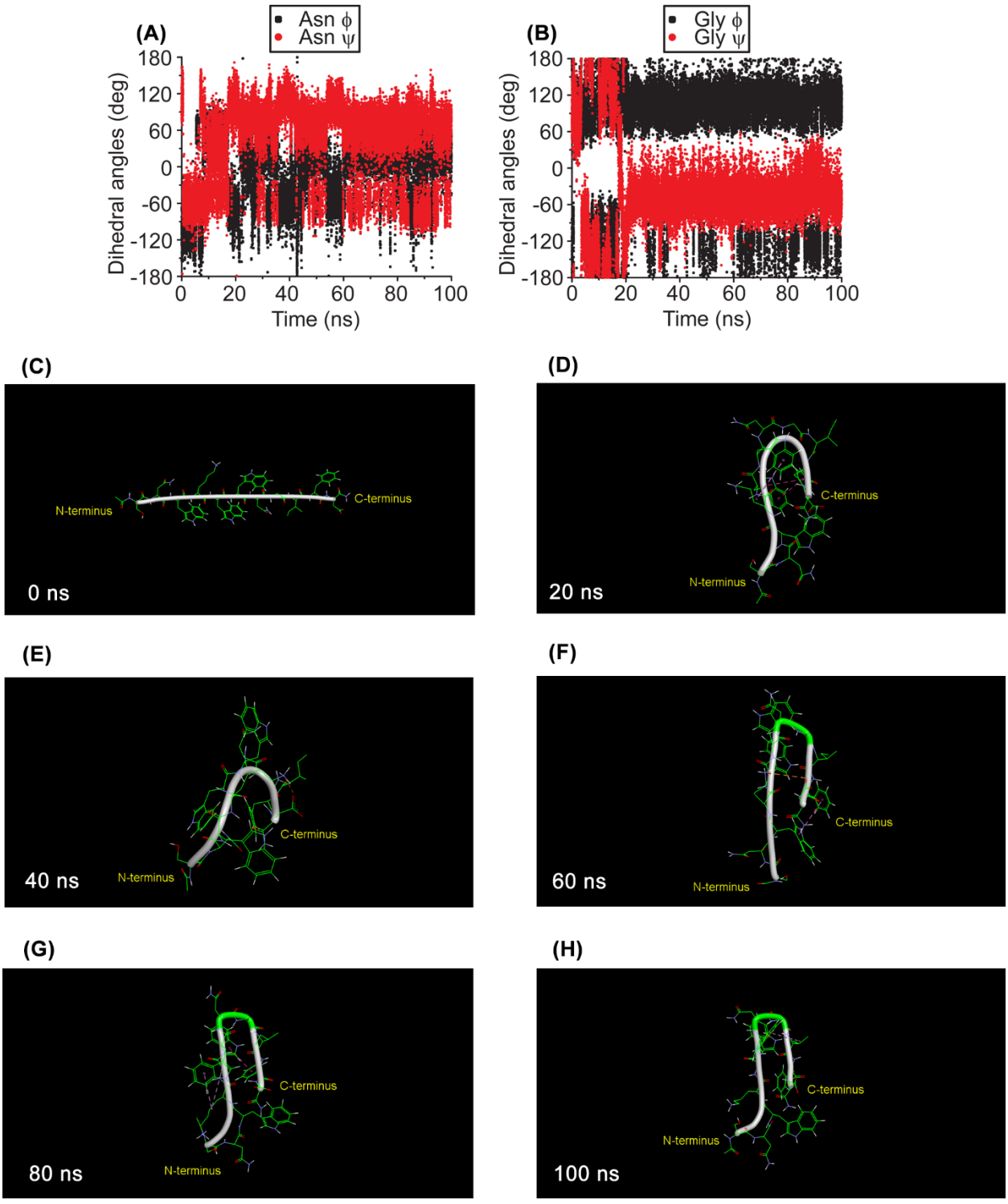

Fig. 3.6. *MD simulation of QBP1-NG. The dihedral angles of Asn7 (A) and Gly8 (B). The snapshots of the peptide trajectory at 20 ns interval (C-H).*

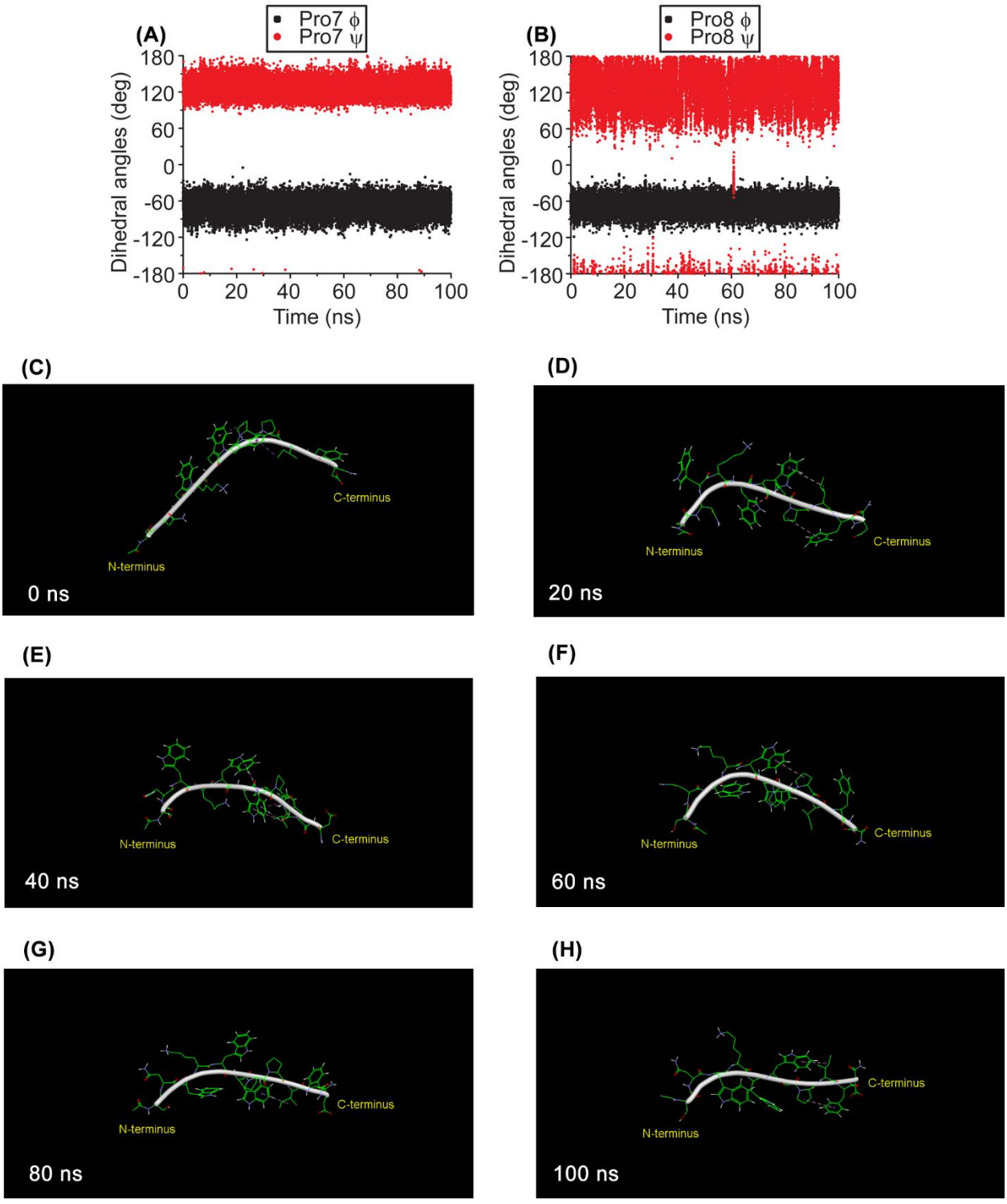

Fig. 3.7. *MD simulation of QBP1-PP. The dihedral angles of Pro7 (A) and Pro8 (B). The snapshots of the peptide trajectory at 20 ns interval (C-H).*

3.3.6. Trx-HDx1 aggregation inhibition

The aggregation of Trx-HDx1 was monitored through the time-course measurement of turbidimetry for one week, as described by Burke and coworkers [135]. The 13 µM Trx-HDx1 protein was found to aggregate in 10 mM phosphate buffer, pH 7.4 with a lag phase of around 2 days, and reached saturation after about 5 days (Fig. 3.8). Aggregation inhibition by the peptides was assayed at twice the molar concentration *i.e.*, at 26 µM peptide concentration. No appreciable aggregation was observed in the presence of QBP1 (Fig. 3.8A). In the presence of QBP1-pG, QBP1-UG, and QBP1-NG, the turbidity is comparable to that in the presence of QBP1, suggesting that all three β-turn-supporting motif-harboring peptides inhibit Trx-HDx1 aggregation. The peptide harboring the ^{L}Pro-^{L}Pro motif *i.e.*, QBP1-PP, on the other hand, failed to inhibit aggregation. However, the peptide caused a little extension of the lag phase, suggesting that the peptide does interact with HDx1 but cannot inhibit the aggregation as efficiently as the peptides harboring turn-supporting dipeptide motifs. Similar results were obtained with the minimal peptides as well; wherein all three turn-supporting motif-harboring peptides inhibit HDx1 aggregation. In contrast, the ^{L}Pro-^{L}Pro motif-harboring peptide only delays the aggregation by around 24 h (Fig. 3.8B). These data suggest that the turn-supporting motif is required for the QBP1-mediated Trx-HDx1 aggregation inhibition.

3.3.7. ThT fluorescence spectroscopy

Aggregation of Trx-HDx1 was also monitored by ThT fluorescence assay. Protein, with or without peptides, was incubated at 37 $^{\circ}$C and analyzed after 168 h of incubation using ThT fluorescence spectroscopy (Fig. 3.9). The Trx-HDx1 protein, in the absence of peptides, shows around 10-fold enhancement in ThT fluorescence, suggesting amyloid formation. Trx-HDx1 incubated with QBP1-PP (Fig. 3.9A) and mQBP1-PP (Fig. 3.9B) show 10-fold and 8-fold ThT fluorescence enhancement, respectively. On the other hand, the Trx-HDx1 incubated with the turn-supporting motif-harboring peptides, cause only ~2-3-fold ThT fluorescence enhancement. These data are in agreement with the turbidimetric data, supporting the requirement of the turn-supporting motif in aggregation inhibition.

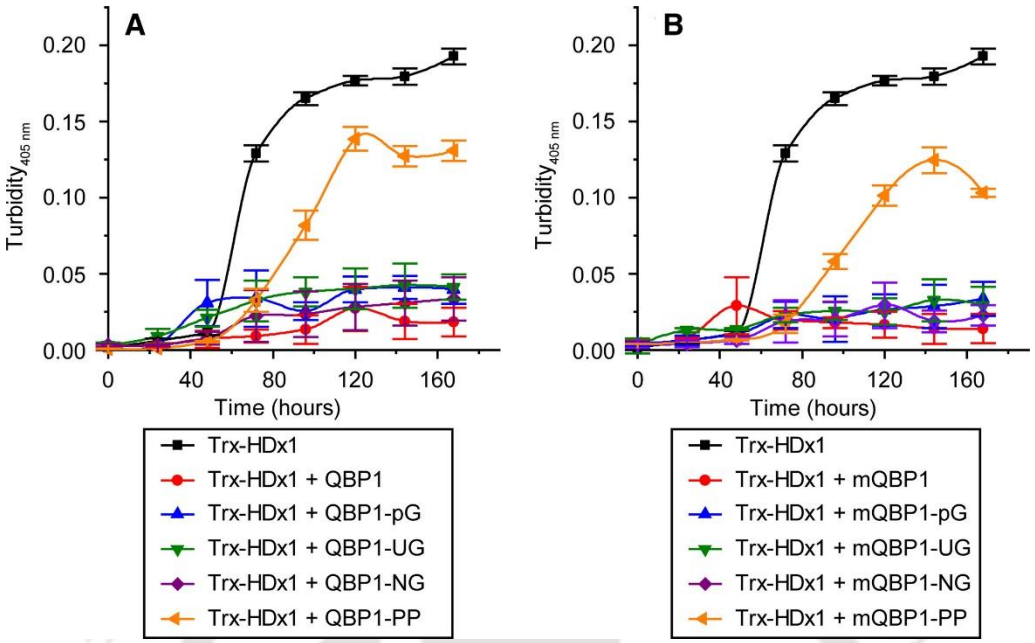

Fig. 3.8. *Aggregation kinetics of Trx-HDx1 in the presence of QBP1 (A) and mQBP1 (B) analogs. The error bars represent the standard deviation.*

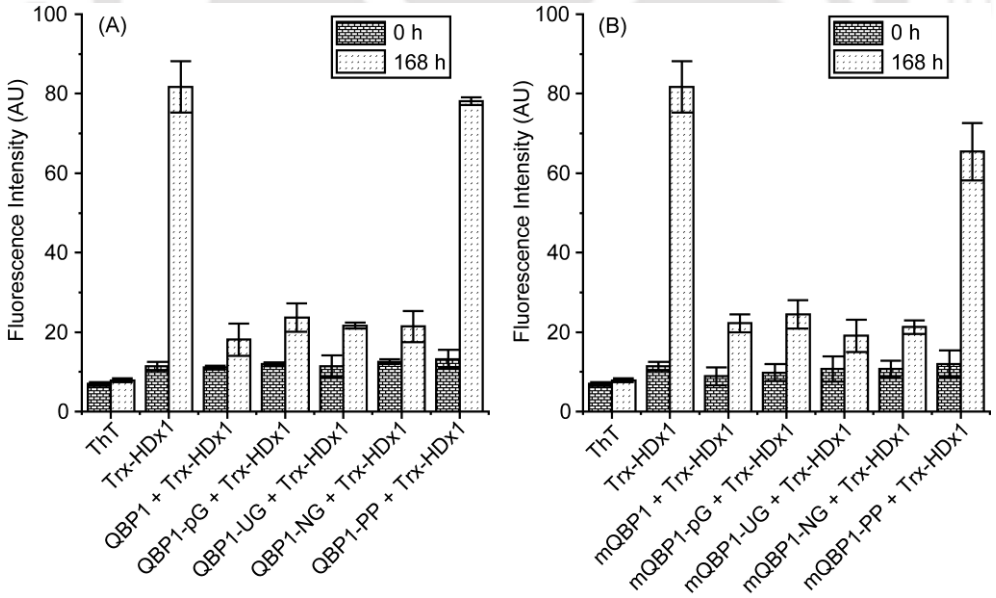

Fig. 3.9*. ThT fluorescence assay for the Trx-HDx1 protein in the presence of QBP1 (A) and mQBP1 (B) peptides. The error bars represent the standard deviation.*

3.3.8. CD spectroscopic analysis of Trx-HDx1 aggregation

The aggregation of Trx-HDx1 and its inhibition by the peptides was further investigated using CD spectroscopy (Fig. 3.10). As the size of the Trx-HDx1 protein is very large compared to that of the peptides, the contribution of the peptides to CD spectra was ignored. The freshly prepared Trx-HDx1 shows a negative band around 208 nm and a positive band around 193 nm (Fig. 3.10A). The spectrum is very similar to those reported in the literature for Trx-HDx1 [185, 186]. The CD spectrum of 168 h-incubated Trx-HDx1 is distinctly different, with a broad negative band around 218 nm and a weak positive band around 200 nm. The spectra were deconvoluted using the SELCON 3 and CONTIN-LL algorithms on DichroWeb online server using SP175 reference set [187]. The data are shown in Table 3.3.

Table 3.3. *Percentage secondary structure components for the freshly purified (0 h) and 168 h-incubated Trx-HDx1. The standard deviations were calculated from the three independent CD experiments.*

Trx-HDx1 incubation period	Conformation	SELCON 3	CONTIN-LL
0 h	α-helix	36 ± 1	36 ± 2
	β-sheet	13 ± 3	13 ± 1
	turns	16 ± 1	13 ± 1
	unordered	35 ± 2	38 ± 2
168 h	α-helix	13 ± 3	15 ± 3
	β-sheet	36 ± 2	34 ± 3
	turns	13 ± 1	12 ± 1
	unordered	38 ± 3	39 ± 2

The freshly prepared (0 h) Trx-HDx1 shows 36% helicity and 13% β-sheet content. The 168 h-old Trx-HDx1 shows around 13-15% helicity and a rather enhanced β-sheet content (~34-36%), suggesting amyloid formation. It is important to note that the protein undergoes aggregation upon incubation. The aggregation would contribute to the loss in the CD signal. The errors reported for the secondary structure content in the 168 h-old Trx-HDx1, therefore, are underestimated. When Trx-HDx1 is incubated with the QBP1 (Fig. 3.10B) or mQBP1 (Fig. 3.10C), no appreciable change

in the CD spectrum is observed after 168 h of incubation, suggesting aggregation inhibition. Similarly, there is little change in the CD spectra of Trx-HDx1 after 168 h incubation with QBP1-pG (Fig. 3.10D), mQBP1-pG (Fig. 3.10E), QBP1-UG (Fig. 3.10F), mQBP1-UG (Fig. 3.10G), and QBP1-NG (Fig. 3.10H), suggesting aggregation inhibition. The CD spectra of the 168 h-old Trx-HDx1 protein incubated with the ^{L}Pro-^{L}Pro motif-harboring peptides QBP1-PP and mQBP1-PP show CD spectra similar to that of aggregated Trx-HDx1 (Fig. 4J and 4K). The turn-lacking QBP1, therefore, fails to inhibit the Trx-HDx1 aggregation. These data are in line with those obtained from the turbidimetry assay.

The CD spectra of Trx-HDx1 with mQBP1-NG are quite exciting (Fig. 3.10I). The freshly-prepared as well as the 168 h-old protein display spectra with negative bands around 208 and 222 nm, a signature characteristic of classical α-helical conformation. The lower intensity of the positive band, however, is suggestive of some contribution from random coil/polyproline II conformation as well [188]. As the protein has 56-amino acid long proline-rich C-terminal domain, we assign this contribution to the polyproline II helix. The proline-rich C-terminal domain is reported to take the polyproline II conformation even in the fibrillar HDx1 [189]. The CD spectrum of the mQBP1-NG shown in Fig. 1 shows a distinct folded structure with a negative band around 222 nm. The peptide mQBP1, therefore, induces an α-helical conformation in the Trx-HDx1 protein. This is an interesting piece of data as the folding of an amyloidogenic protein into an α-helical conformation could diminish its aggregation propensity.

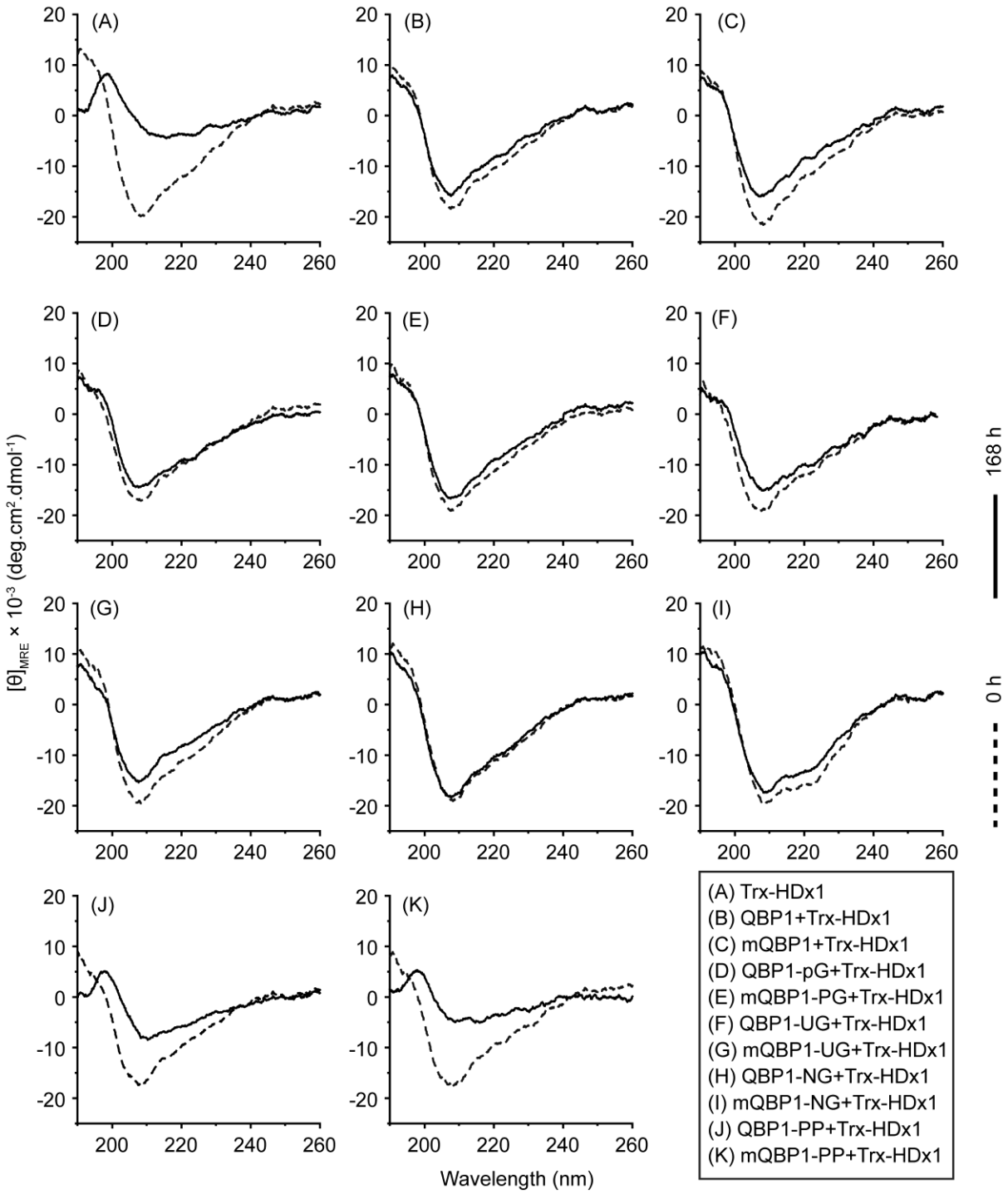

Fig. 3.10. *CD spectra of the Trx-HDx1 protein in the presence of QBP1 and mQBP1-derived peptides.*

3.3.9 AFM imaging

The formation of amyloid fibrils was investigated using AFM imaging of the 168 h-old Trx-HDx1 samples (Fig. 3.11). The Trx-HDx1, when incubated without any peptide, formed distinct fibrillar structures (Fig. 3.11A). A small amount of short fibrils was observed for the Trx-HDx1 incubated with QBP1-pG (Fig. 3.11D) and mQBP1-pG (Fig. 3.11E). No distinct fibrils could be observed for the protein incubated with Aib-Gly and Asn-Gly analogs. The protein incubated with QBP1-PP (Fig. 3.11J) and mQBP1-PP (Fig. 3.11K), as anticipated, shows distinct fibrils

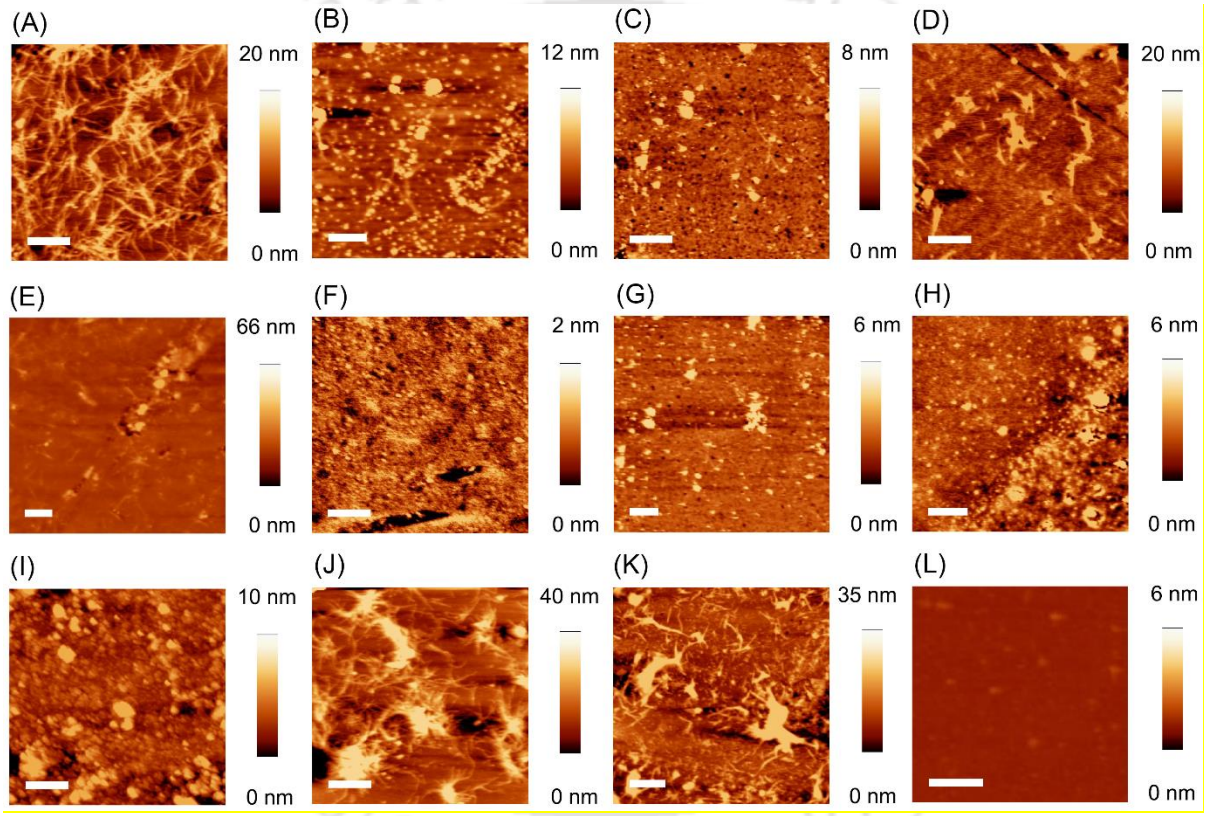

Fig. 3.11*. AFM images of Trx-HDx1 samples incubated with peptides for 168 h in 10 mM phosphate buffer, pH 7.4. (A) Trx-HDx1, (B) Trx-HDx1 + QBP1, (C) Trx-HDx1 + mQBP1, (D) Trx-HDx1 + QBP1-pG, (E) Trx-HDx1 + mQBP1-pG, (F) Trx-HDx1 + QBP1-UG, (G) Trx-HDx1 + mQBP1-UG, (H) Trx-HDx1 + QBP1-NG, (I) Trx-HDx1 + mQBP1-NG, (J) Trx-HDx1 + QBP1-PP, (K) Trx-HDx1 + mQBP1-PP. (L) Freshly-prepared (0 h) Trx-HDx1. The scale bars represent 1 µm.*

These data suggest that the Pro-Gly motif in the QBP1 and mQBP1 peptides takes a turn conformation, which is important for its polyglutamine aggregation inhibition activity. Laurents and coworkers recently reported the inhibition of TDP-43 aggregation by mQBP1 [190]. TDP-43 is a protein that contains a Q/N-rich segment, and gets deposited as amyloid aggregates in amyotrophic lateral sclerosis and frontotemporal dementia. The mQBP1 binds to the Q/N-rich region, thereby inhibiting the TDP-43 aggregation. Interestingly, a scrambled sequence of mQBP1, Ac-WPIWKGWF-am, was found to possess the aggregation inhibition activity comparable to that of mQBP1, indicating that the composition of the peptide could be sufficient for the activity. The mQBP1 has been reported to inhibit the aggregation of yet another protein having a Q/N-rich region, the Orb2A [191]. Interestingly, however, the scrambled Ac-WPIWKGWF-am peptide was found to be inactive, and in fact, used as a negative-control for mQBP1-mediated aggregation inhibition. The NMR structure of mQBP1 reveals an ordered Trp-rich hydrophobic cluster and a Pro-Gly-mediated type II β-turn [192]. The structure of the scrambled Ac-WPIWKGWF-am peptide, however, is not reported in the literature. It is worth noticing that the position of Glycine residue in the mQBP1 and the scrambled peptide is invariant. A Lys-Gly motif can very much support the type-II β-turn [193]. Laurents and coworkers have reported the CD spectrum of the scrambled Ac-WPIWKGWF-am peptide as well [192]. The peptide shows a moderate intensity positive band around 208 nm with a minimum around 190, a CD signature characteristic of type II β-turn [194]. It is important to note that such spectra have been obtained using short model peptides wherein the signal is largely dominated by the turn. As mQBP1 or the scrambled mQBP1 are merely 8-residue long, the spectral features observed in the scrambled mQBP1 CD spectrum could indeed be arising from the turn. Owing to the smaller size of the turn, compared to the other secondary structures, their contribution to the CD spectra of longer peptides and proteins is very small.

3.4. Conclusions

The Pro-Gly dipeptide motif is often used to predict turns in the protein backbone. The polyglutamine binding peptide QBP1 harbors the Pro-Gly motif. This study investigated if the Pro-Gly motif in QBP1 plays a structural role in its activity. Using various analogs of the ‘Pro-Gly’ motif that can support β-turn and the Pro-Pro analog that eliminates the possibility of β-turn, we conclude, based on the aggregation inhibition assays, that the turn formation is critical for the

peptide's aggregation inhibition activity. Even though the complete backbone conformation of the peptides is not experimentally determined, the MD simulations show distinct hairpin-like structures. Besides, the conclusions made comply well with the mQBP1 structure reported in the literature. In addition, this study identified, somewhat serendipitously, a minimal QBP1 analog that induces an α-helical conformation in the Trx-HDx1 protein. The folding of an amyloidogenic protein into an α-helical conformation could have interesting implications on the amyloidogenicity and the aggregation pathway.

QBP1 inhibits early steps in huntingtin aggregation, and addition of QBP1 after aggregation does not reverse the process. QBP1 peptides with β-turn appears to inhibit aggregation by binding to the expanded polyQ region in the monomeric protein. Binding to the monomers could fix the conformation of huntingtin exon 1 region disabling it from forming the monomeric nucleus. Alternatively, it could bind to the monomeric nucleus and affecting monomer recruitment to the nucleus. A scheme indicating HDx1 aggregation and its inhibition by QBP1-based peptides is shown in Fig. 3.12

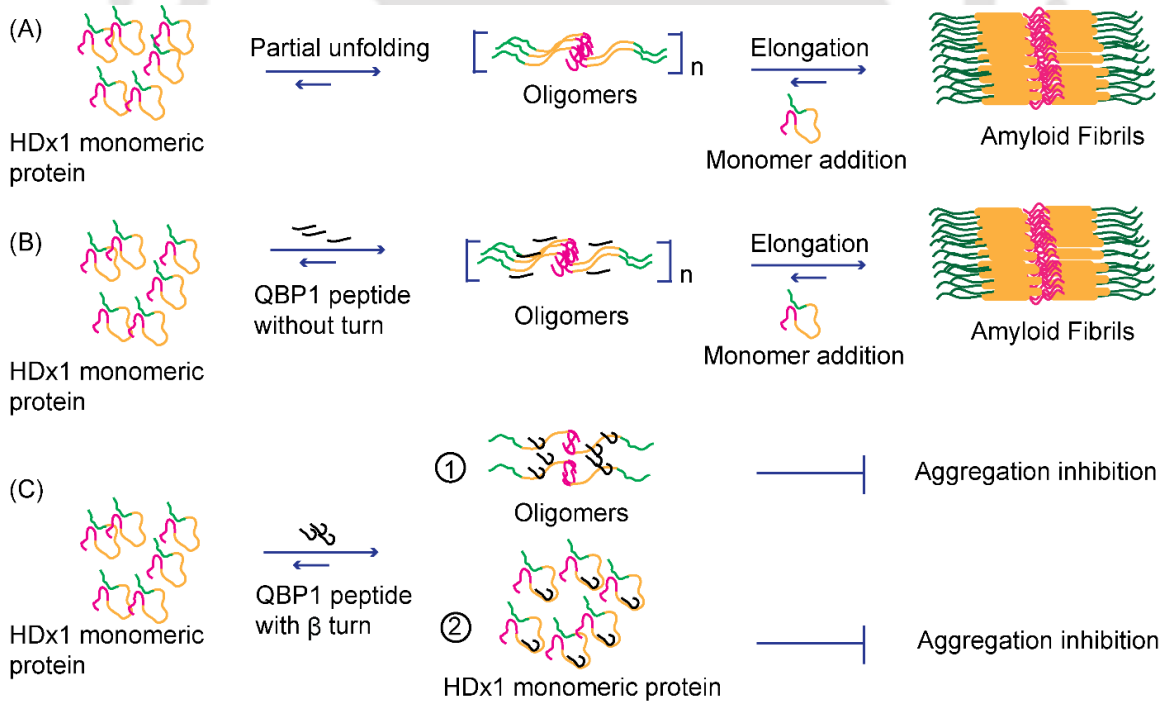

***Fig.3.12**. Schematic representation of aggregation of HDx1 protein (panel A). Failure to inhibit aggregation by a turn-lacking QBP1 analog (panel B), and aggregation inhibition by the turn-harboring QBP1 (panel C).*

CHAPTER 4

Inhibition of huntingtin aggregation by its N-terminal 17-residue peptide (htt^{N17}) and its analogs

The N-terminal 17-residue stretch of huntingtin (htt^{N17}) folds into an amphipathic helix. The htt^{N17}–harboring polyQ peptides form oligomers that are mediated via the assembly of the htt^{N17} α-helices. The oligomerization results in higher local concentration of the polyglutamine (polyQ) region, thereby facilitating amyloid formation. The htt^{N17} co-assembles with the htt^{N17}-harbouring polyQ peptides, thereby reducing the local polyQ concentration, and consequently inhibiting aggregation. This study presents the aggregation inhibition of the exon I region of huntingtin by htt^{N17} and its analogs. The C-terminal amidation of htt^{N17} is found to be essential for activity. The htt^{N17} peptides with free amino terminus and the acetylated amino terminus possess comparable activity. The htt^{N17} analog, wherein the Leu7 and Ala10 are substituted with Aib residues, exhibits significantly higher activity than the native htt^{N17}.

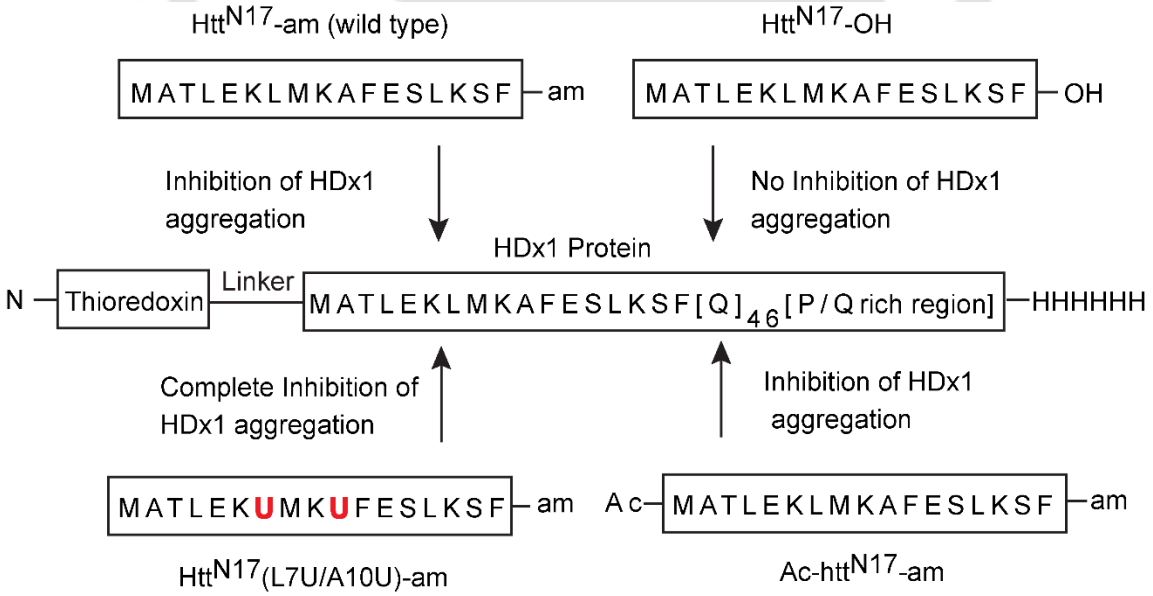

4.1. Introduction

The expanded polyQ tract in proteins is associated with several neurodegenerative diseases [166, 195]. The aggregation of the polyQ peptides, therefore, has been investigated in considerable detail [128, 196-198]. The polyQ peptides form amyloid fibrils, wherein the aggregation propensity increases with the polyQ length. Wetzel and coworkers reported that the polyQ peptides self-assemble via nucleated growth polymerization, where the critical aggregation nucleus was found to be the monomer itself [22]. Nagai and coworkers subsequently reported that the monomeric expanded polyQ stretch undergoes a conformation transition from random coil to β-sheet before assembling into amyloid fibrils [199]

The expanded polyQ peptides form fibrillar aggregates without populating the pre-fibrillar oligomers [22, 128]. The fusion of flanking sequences (htt^{N17} or polyproline) with polyQ region has strong effects on the aggregation [168]. The C-terminal polyproline suppresses the aggregation, whereas the N-terminal htt^{N17} enhances it. Besides, the position of the htt^{N17} is irrelevant. Comparable aggregation kinetics was observed for htt^{N17}-Q_{35} and Q_{35}-htt^{N17}. Compared to the polyQ peptides that self-assemble to form fibrillar aggregates, the htt^{N17}-tagged peptides resulted in the oligomers as well, alongside the fibrillar aggregates. Tagging with htt^{N17}, therefore, leads to a rather complex aggregation pathway wherein pre-fibrillar structures are also populated. The htt^{N17}, *per se*, is not an aggregation-prone peptide [22]. The peptide takes up a somewhat collapsed structure that resists aggregation. Tagging with polyQ causes repeat length-dependent disruption of htt^{N17} structure, wherein the htt^{N17} becomes more extended and aggregation-prone. The htt^{N17}-polyQ quickly forms oligomers that are mediated via htt^{N17} region with rather exposed polyQ stretch. In a subsequent study, Wetzel and coworkers investigated the aggregation of htt^{N17}–tagged short polyQ peptides [20]. The aggregation of these peptides proceeded via α-helical oligomers. In addition, they found that the htt^{N17} peptide can form α-helical tetramers at high concentrations, suggesting that htt^{N17} exists in solution as an equilibrium mixture of unstructured monomer and an α-helical tetramer. The enhanced aggregation kinetics observed for htt^{N17}-polyQ, therefore, could be due to higher local concentration of the polyQ stretches within the htt^{N17}-induced oligomers. Van der Wel and coworkers reported that the htt^{N17} takes up an α-helical conformation in the fibrils formed by the peptide htt^{N17}-$Q_{30}P_{10}K_2$ [200]. The polyQ region

constituted the rigid β-sheet core, whereas htt^{N17} was found to be much more mobile. Langen and coworkers reported the structural organization of HDx1 fibrils [126]. The polyQ stretch was found to be highly immobile, whereas the C-terminal domain was dynamic. Interestingly, the htt^{N17} was also found to be involved in tertiary and quaternary interactions. Siemer and coworkers also found similar dynamics of the three domains and proposed a bottlebrush model for the HDx1 fibrils, wherein both polyQ region and htt^{N17} constitute the center of the fibrils, whereas the C-terminal polyproline region protrudes outside the fibrils [201].

Considering that the htt^{N17} can form α-helical oligomers that lead to faster amyloid formation, the potential of htt^{N17} as an inhibitor of htt^{N17}-harbouring polyQ peptides was explored. Wetzel and coworkers reported that htt^{N17} co-assembles with htt^{N17}-$Q_{30}P_{10}K_2$, causing aggregation inhibition [21]. The inhibition is attributed to the lower local-concentration of the polyQ region in these mixed oligomers, compared to that in the pure htt^{N17}-$Q_{30}P_{10}K_2$ oligomers. Interestingly, the all D and the retro-inverso versions of htt^{N17} were found to be equally efficient in aggregation inhibition. The inhibition activity, therefore, resides in the propensity of the peptide to fold into amphipathic helices. Burra and Thakur investigated the activity of htt^{N17} variants from evolutionary distant organisms and found that the Fugu and Xenopus htt^{N17} variants inhibit the aggregation of htt^{N17}-$Q_{30}P_{10}K_2$ whereas Drosophila htt^{N17} does not [137]. The lower hydrophobicity and α-helical propensity of Drosophila htt^{N17}, compared to the other three variants could be responsible for the loss of activity. Besides, they investigated the activity of a human htt^{N17} variant, wherein 2-aminoisobutyric acid (Aib) residues were incorporated, one between 10^{th} and 11^{th} htt^{N17} residues, and the other at the N-terminus. The CD spectrum of the Aib variant was very similar to that of wild-type $htt^{N17,}$ and its aggregation inhibition activity was no better than the wild-type peptide. In fact, the activity of the Aib variant was found to be somewhat compromised. In this study, we designed several human htt^{N17} analogs and investigated their aggregation inhibition activity against the full huntingtin exon 1 (HDx1) protein having 46 glutamines.

4.2. Hypothesis

Investigations into the htt^{N17}-$Q_{35}P_{10}K_2$ aggregation inhibition by htt^{N17}, its all-D variant, its retro-inverso variant, and the scrambled htt^{N17} sequences suggested that the activity depended on the hydrophobicity and the amphipathicity of the peptides[21]. Even though the huntingtin

aggregation activity seems to reside in the amphipathicity and hydrophobicity of the peptide, irrespective of the sequence, it would be imperative to use native or native-like amphipathic peptides with similar physicochemical properties. Such sequences would prove to be non-immunogenic. Our objective was to engineer, through minimal perturbations, the native htt^{N17} sequence that could favor the α-helical conformation without compromising the hydrophobicity and hydrophobic moment.

4.3. Results and Discussion

4.3.1. Peptide design

The peptides were designed with an aim to support α-helical conformation without significantly compromising the hydrophobicity and the amphipathicity of the peptides. The physicochemical properties of the peptides are shown in Table 4.1 and the MALDI-TOF mass spectrometric data is shown in Table 4.2. As one of the designed peptides contains the non-proteinogenic amino acid 2-aminoisobutyric acid (Aib), the hydrophobicity (<H>) and the hydrophobic moment (<μH>) of the peptides were determined by using the combined consensus hydrophobicity scales (CCS) proposed by Tossi and coworkers [202].

Htt^{N17}-am, htt^{N17}-OH, and Ac-htt^{N17}-am have an identical amino acid sequence but different termini chemistry. Therefore, they have identical side-chain hydrophobicity and amphipathicity. Htt^{N17}(K6Q)-am was designed with an aim to abolish the electrostatic repulsion, if any, between Lys6 and Lys9 in the α-helical conformation. Lys6 was preferred over Lys9 for substitution as Lys9 could have favorable interaction with Glu12. Htt^{N17}(L7U/A10U)-am was designed by substituting Lue7 and Ala10 residues with Aib. As the two Aib residues reside near the middle of the peptide with 2-residues separation, a higher helicity was expected. All the peptides shown in Table 4.1 show comparable hydrophobicity. The Tossi's CCS ranges from -10 to +10 [202].

All the peptides have hydrophobicity within ±0.55. The <μH> for the native htt^{N17} was found to be 3.46. Compared to the native htt^{N17}-am, the htt^{N17}(K6Q)-am and htt^{N17}(L7U/A10U)-am show ~5% and ~13% decrease in the amphipathicity, respectively. The amphipathicity of the htt^{N17}-Q_7-am, however, is reduced to 2.45, an approximately 29% reduction in <μH>.

Table 4.1. *The IDs, sequence, and the physicochemical properties of the peptides used in this study.*

Peptide ID[a][b]	**Sequence**[b]	**<H>**[c]	**<μH>**[c]	**z**[d]
Htt^{N17}-am	MATLEKLMKAFESLKSF-NH_2	-0.15	3.46	+2
Htt^{N17}-OH	MATLEKLMKAFESLKSF-OH	-0.15	3.46	+1
Ac-htt^{N17}-am	CH_3CO-MATLEKLMKAFESLKSF-NH_2	-0.15	3.46	+1
Htt^{N17}(K6Q)-am	MATLEQLMKAFESLKSF-NH_2	+0.41	3.28	0
Htt^{N17}(L7U/A10U)-am	MATLEKUMKUFESLKSF-NH_2	-0.53	3.00	+2
Htt^{N17}-Q_7-am	MATLEKLMKAFESLKSFQQQQQQQ-NH_2	-0.17	2.45	+2

[a]The 'Ac' at N-terminus indicates acetyl group, while 'am' at C-terminus indicates C-terminal amide.

[b]U in the peptide ID and the sequence indicates 2-aminoisobutyric acid (Aib).

[c]<H> and <μH> were determined by using the CCS proposed by Tossi and coworkers **[202]**.

[d]Net charge at neutral pH

Table 4.2. *The summary of the MALDI-TOF mass spectrometric analysis of the peptides listed in Table 4.1.*

Peptide ID	**Calculated monoisotopic mass (Da)**	**Expected MH^+ mass (Da)**	**Observed MH^+ mass (Da)**	**Percent mass error**
Htt^{N17}-am	1973.042	1974.05	1973.526	0.027
Htt^{N17}-OH	1973.026	1974.034	1974.738	0.036
Ac-htt^{N17}-am	2014.052	2015.06	2016.132	0.053
Htt^{N17}(K6Q)-am	1972.005	1973.013	1973.693	0.034
Htt^{N17}(L7U/A10U)-am	1958.161	1959.169	1959.637	0.024
Htt^{N17}-Q_7-am	2868.452	2869.46	2870.907	0.050

4.3.2. Secondary structure of the peptides

The secondary structures of the peptides in 10 mM phosphate buffer, pH 7.4 were investigated using far-UV CD spectroscopy (Fig. 4.1). The CD spectra of native htt^{N17} are shown in Fig. 4.1A, and are characterized by an intense negative band around 200 nm and a weak and broad negative band around 215-230 nm. The spectral features are in agreement with those reported in the literature for htt^{N17} [203]. The spectra for htt^{N17} variants and htt^{N17}-Q_7 are shown in Fig. 4.1B. The spectra are similar to that observed for $httN^{17}$-am. However, the spectrum of htt^{N17}-Q7-am displays higher ellipticity, suggesting a more structured peptide.

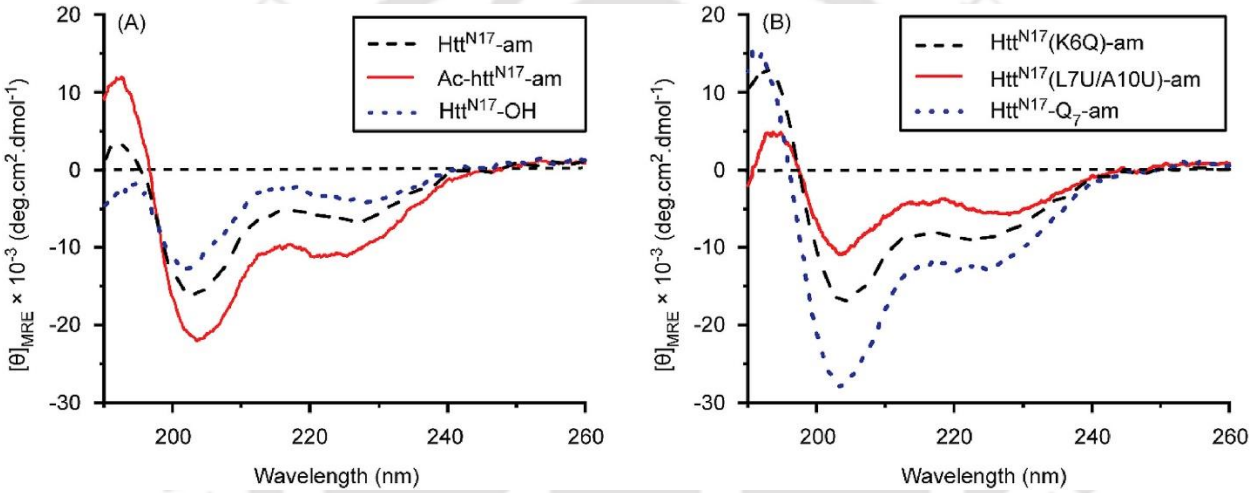

Fig. 4.1. *The far-UV CD spectra of peptides (50 µM concentration) recorded in 10 mM phosphate buffer, pH 7.4. Each spectrum is an average of 8 scans.*

4.3.3. Aggregation inhibition assays

The aggregation inhibition was assayed by measuring the aggregation kinetics of Trx-HDx1 in the presence of an equimolar amount of peptides. The aggregation kinetics was monitored through the time-course measurement of ThT fluorescence (Fig. 4.2A) as well as turbidimetry (Fig. 4.2B) for 240 hours. Trx-HDx1 (15 µM), with or without peptides in 10 mM phosphate buffer, pH 7.4, was incubated at 37 ˚C and analyzed every 24 hours up to 240 hours. Both ThT fluorescence and turbidimetry show aggregation of Trx-HDx1 (in the absence of peptides) with a lag phase of around 48 h.

The ThT fluorescence, as well as the turbidimetry, reach saturation after six days (144 h) of incubation. In the presence of htt^{N17}-am, the Trx-HDx1 aggregation is strongly inhibited. The N-acetylated version, Ac-htt^{N17}-am, is also equally effective. The activity of htt^{N17}-OH, however, is severely compromised. These data suggest that the C-terminal amidation of htt^{N17} is essential for the HDx1 aggregation inhibition. The htt^{N17}(L7U,10AU) shows better activity than htt^{N17}-am (p-value < 0.05). The htt^{N17}(K6Q) shows activity comparable to that of htt^{N17}-am. The htt^{N17}-Q_7-am displays poor activity. This could be due to the lower amphipathicity of the peptide (Table 4.1).

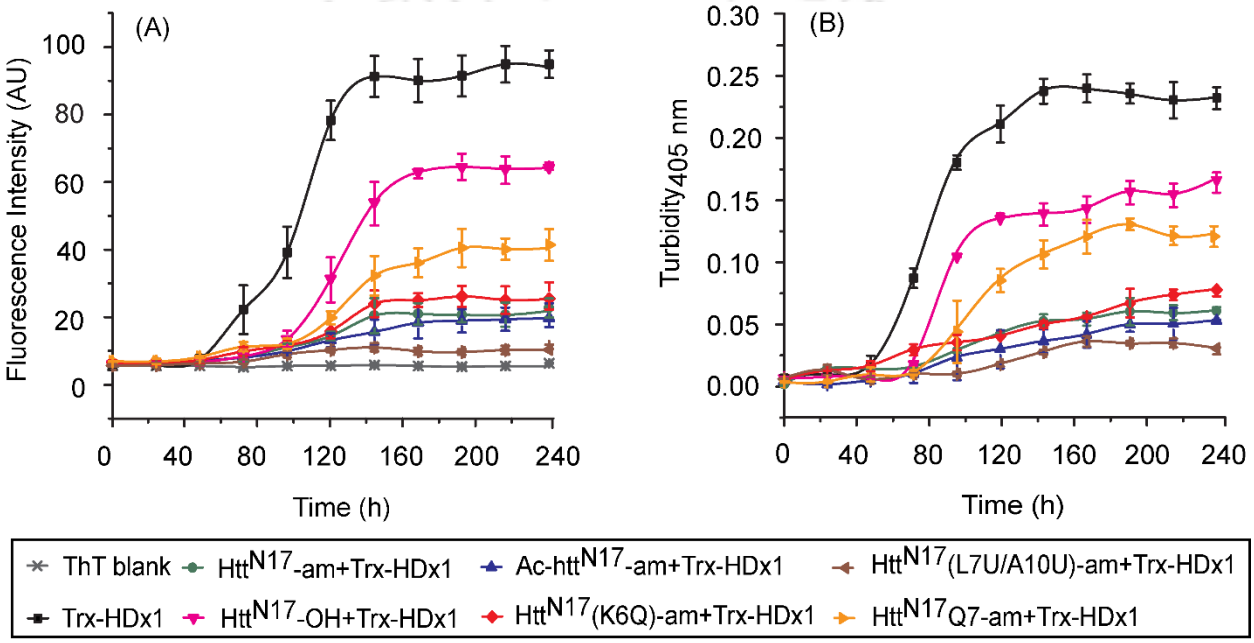

Fig. 4.2. *Aggregation kinetics of Trx-HDx1 in the presence of peptide. (A) ThT fluorescence assay (B) Turbidity assay. The error bars represent standard deviations.*

4.3.4. CD spectroscopic analysis of Trx-HDx1 aggregation

The aggregation of Trx-HDx1 and its inhibition by the peptides were further investigated using CD spectroscopy. The freshly prepared Trx-HDx1 shows a negative band around 208 nm and a positive band around 193 nm (short dash, Fig. 4.3A). The spectrum is very similar to those reported in the literature for Trx-HDx1 [185, 186, 204]. The CD spectra after 168 h (long dash) and 240 h

(solid line) incubation are distinctly different. The 240 h incubated Trx-HDx1 displays a broad negative band from ~210-235 nm and a weak positive band around 200 nm. The spectra are similar to those reported in the literature [204].

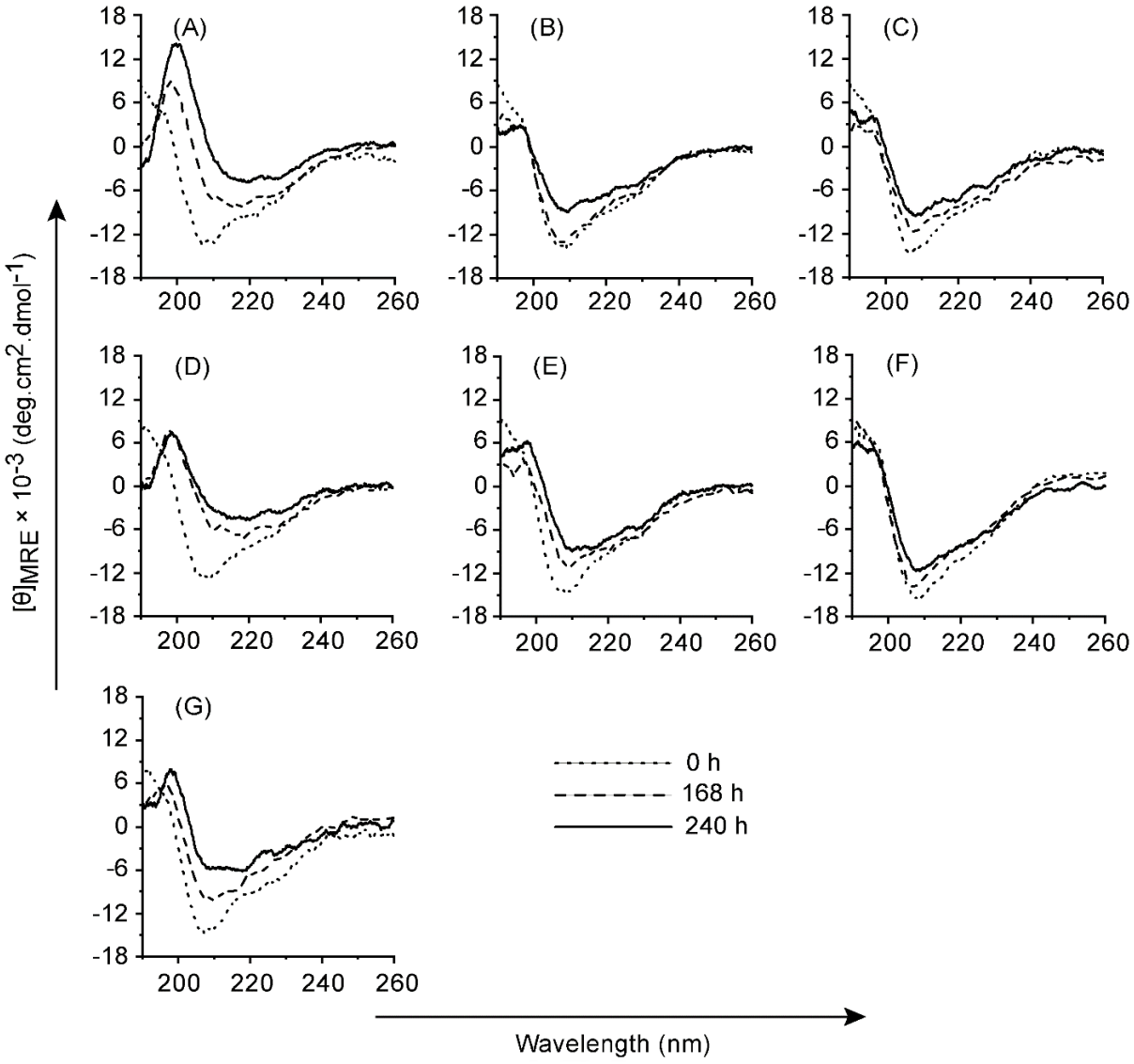

Fig.4.3. *CD spectra of the Trx-HDx1 in the presence of peptides. A) Trx-HDx1 (B) Htt^{N17}-am +Trx-HDx1 (C) Ac-htt^{N17}-am+Trx-HDx1 (D) Htt^{N17}-OH +Trx-HDx1 (E) Htt^{N17}(K6Q)-am +Trx-HDx1 (F) Htt^{N17}(L7U/A10U)-am +Trx-HDx1 (G) Htt^{N17}Q7-am +Trx-HDx1*

The spectra essentially have contribution from the peptides as well. However, as the peptides are considerably smaller than the Trx-HDx1 (250 amino acids), we ignored the contribution of peptides to these spectra. This happens to be a very good approximation as there is no appreciable difference in the 0 h spectra of Trx-HDx1 (Fig. 4.3A) and Trx-HDx1 + peptide (Fig. 4.3B-G).

The CD spectra recorded in the presence of htt^{N17}-am (Fig. 4.3B) and Ac-htt^{N17}-am (Fig. 4.3C) lack the spectral features of the aggregated Trx-HDx1. The CD spectra obtained in the presence of htt^{N17}-OH shows the broad negative band from ~205-235 nm as well as the positive band ~200 nm, indicating that the peptide fails to inhibit Trx-HDx1 aggregation (Fig. 4.3D). The spectra in the presence of htt^{N17}(K6Q)-am also support aggregation inhibition (Fig. 4.3E). The 240 h spectrum, however, shows the appearance of the spectral signatures of the aggregated Trx-HDx1. The 240 h spectrum shows shifting of the negative band to the higher wavelength along with broadening. A very weak 200 nm positive band also starts appearing. The spectra obtained in the presence of htt^{N17}(L7U/A10U)-am are shown in Fig. 4.3F. The spectra are indicative of efficient aggregation inhibition. Fig. 4.3G shows spectra recorded in the presence of $htt^{N17}Q_7$-am. The spectra suggest a loss of aggregation inhibition activity. The CD data are in excellent correlation with the ThT fluorescence and turbidimetry aggregation data.

4.3.5. TEM imaging

The Trx-HDx1 aggregation was further investigated using TEM imaging (Fig. 4.4). The freshly-prepared Trx-HDx1 sample did not reveal any aggregate (Fig. 4.4A), whereas fibrillar structures appear upon 240 h incubation (Fig. 4.4B). The micrographs of the Trx-HDx1 that was incubated with peptides for 240 h are shown in Fig. 4.4B-H. Few fibrillar aggregates were observed when the Trx-HDx1 was co-incubated with htt^{N17}-am (Fig. 4.4C). No fibrillar aggregates were observed for the Trx-HDx1 incubated with Ac-htt^{N17}-am (Fig. 4.4D). The protein incubated with htt^{N17}-OH shows fibrillar aggregates (Fig. 4.4E). The Trx-HDx1 incubated with htt^{N17}(K6Q)-am shows small aggregates; no distinct fibrils were observed (Fig. 4.4F). Htt^{N17}(L7U/A10U)-am incubated protein did not show any discernible aggregates, indicating that the peptide is the most efficient inhibitor among all the peptides studied (Fig. 4.4G). In the presence of $htt^{N17}Q_7$-am, the Trx-HDx1 formed distinct fibrillar aggregates (Fig. 4.4H).

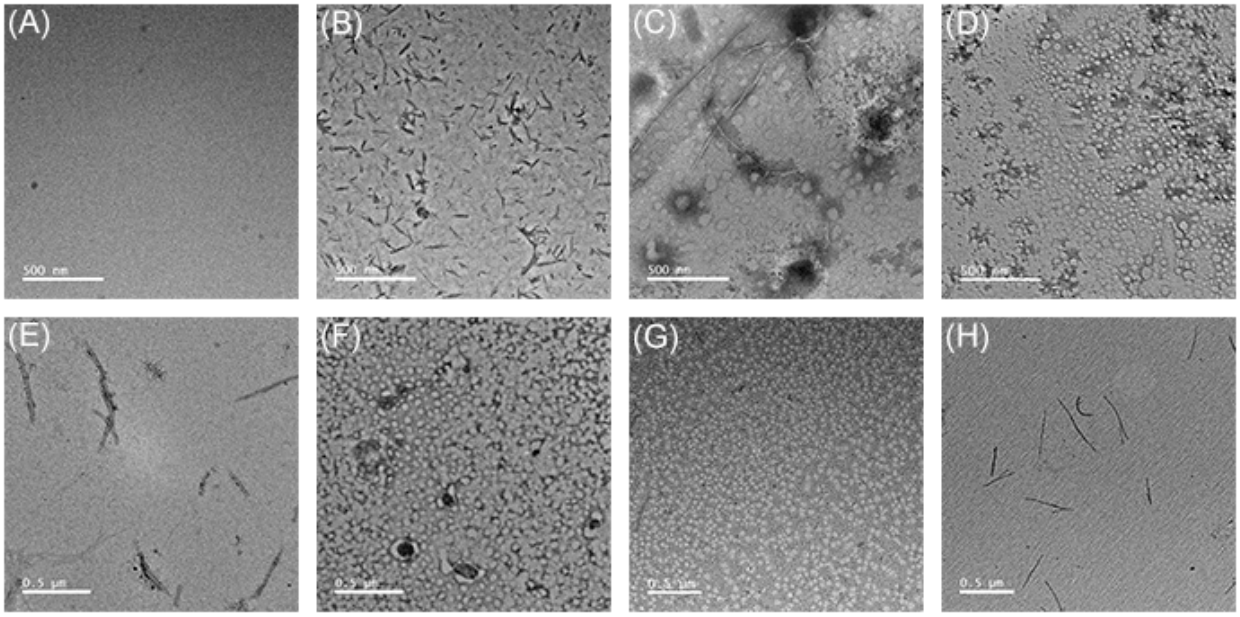

Fig. 4.4. *TEM images of Trx-HDx1 samples incubated with peptides in 10 mM phosphate buffer, pH 7.4. (A) freshly prepared Trx-HDx1 (0 h), (B) Trx-HDx1 (240 h), (C) Trx-HDx1 + htt^{N17}-am (240 h), (D) Trx-HDx1 + Ac-htt^{N17}-am (240 h), (E) Trx-HDx1 + htt^{N17}-OH (240 h) (F) Trx-HDx1 + htt^{N17}(K6Q)-am (240 h), (G) Trx-HDx1 + htt^{N17}(L7U/A10U)-am (240 h), (H) Trx-HDx1 + htt^{N17}Q$_7$-am (240 h). The scale bars represent 500 nm.*

4.4. Conclusions

The N-terminal 17-residue stretch of human huntingtin, htt^{N17} facilitates its aggregation into amyloid fibrils. The amyloid nucleation has been proposed to be mediated via oligomerization of the htt^{N17} region. The oligomers are rich in α-helical conformation. The htt^{N17}, *per se*, is not aggregation-prone but can form α-helical oligomers at high concentrations. The faster aggregation kinetics observed for polyglutamine peptides tagged with htt^{N17} is believed to be caused by an increase in the local concentration of the polyglutamine regions. The htt^{N17}, therefore, could coassemble with the htt^{N17}-harbouring polyQ peptides, thereby diluting the local polyQ concentration and consequently diminishing aggregation (Fig. 4.5).

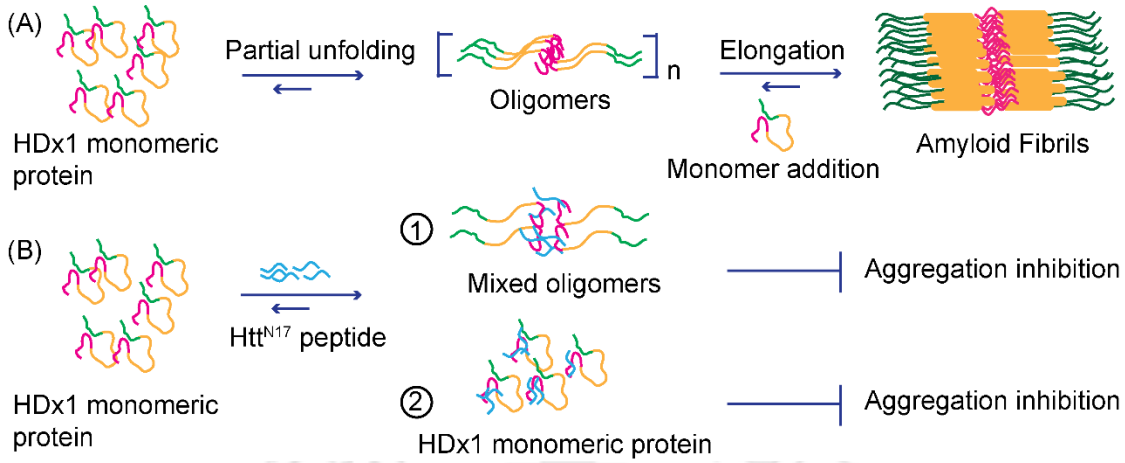

Fig.4.5. *A plausible mechanism of HDx1 aggregation and its inhibition in the presence of htt^{N17} peptides. (A) The htt^{N17} region (pink) of HDx1 binds with similar htt^{N17} regions and forms an α-helix rich oligomer core that nucleates the formation of amyloid-like structures with polyQ regions (orange). (B) Inhibition of aggregation includes the formation of mixed-oligomer core through the binding of inhibitors (blue) with the htt^{NT17} segments of HDx1 protein. The local concentration of the polyQ region in mixed oligomers is lower than that in the pure HDx1 oligomers. A decreased intermolecular interaction between polyQ stretches is believed to underlie the htt^{N17}'s activity.*

The htt^{N17} region from human, Fugu, and Xenopus have been reported to diminish the htt^{N17}–tagged polyQ peptides. We designed htt^{N17} analogs that could facilitate α-helical conformation. In addition, native htt^{N17} with different end-modifications was also investigated. We demonstrate that the C-terminal amidation of htt^{N17} is critical for its aggregation inhibition activity. The activity of peptide acid, *i.e.*, htt^{N17}-OH, is severely compromised. Tagging a small stretch of glutamines with htt^{N17} also compromises the activity. Besides, the double Aib variant, htt^{N17} (L7U/A10U)-am was found to be the best-performing peptide. Burra and Thakur have previously investigated a double Aib variant of htt^{N17}. The peptide (UMATLEKLMKUAFESLKSF), reported in the literature as Aib-NT17, was designed by tagging an Aib residue at the N-terminus and inserting the second Aib residue between Lys9 and Ala10. An insertion of Aib residue could affect the amphipathicity of the peptide. The hydrophobic moment of the peptide, using Tossi's CCS, was found to be 2.25. This large decrease in the hydrophobic moment could be the reason behind the lower activity observed for Aib-NT17 compared to that of htt^{N17}. The aggregation inhibition assays were

attempted with the free HDx1 (without Trx tag) as well. The HDx1 was pre-treated with 1:1 HFIP/TFA for several hours, dried under N_2 stream, and finally dissolved in TFA/water (pH 3.0). The dilution to a 5 μM concentration in 10 mM phosphate buffer, pH 7.4 (HFIP concentration <2%) resulted in instant aggregation, indicating that the HFIP/TFA pre-treatment is insufficient to generate oligomer/seed-free HDx1.

CHAPTER 5

Huntingtin aggregation inhibition activity of the mixtures of the most active analogs of htt^{N17} and QBP1 and the fusion peptide derived from them

Here, we investigated the aggregation inhibition potential of the fusion peptide, obtained by appending the mQBP1 analog (mQBP1-NG) to the C-terminus of a highly active htt^{N17} analog (Htt^{N17}(L7U/A10U). Compared to the either parent peptide, the activity of the fusion peptide was severely compromised. However, when the parent peptides were mixed together, the activity was restored. This lack of activity in the fusion peptide is largely attributed to the folding of the peptide. The peptide folds into an α-helical conformation that could possibly draw the otherwise non-helical QBP1 also into an α-helical conformation.

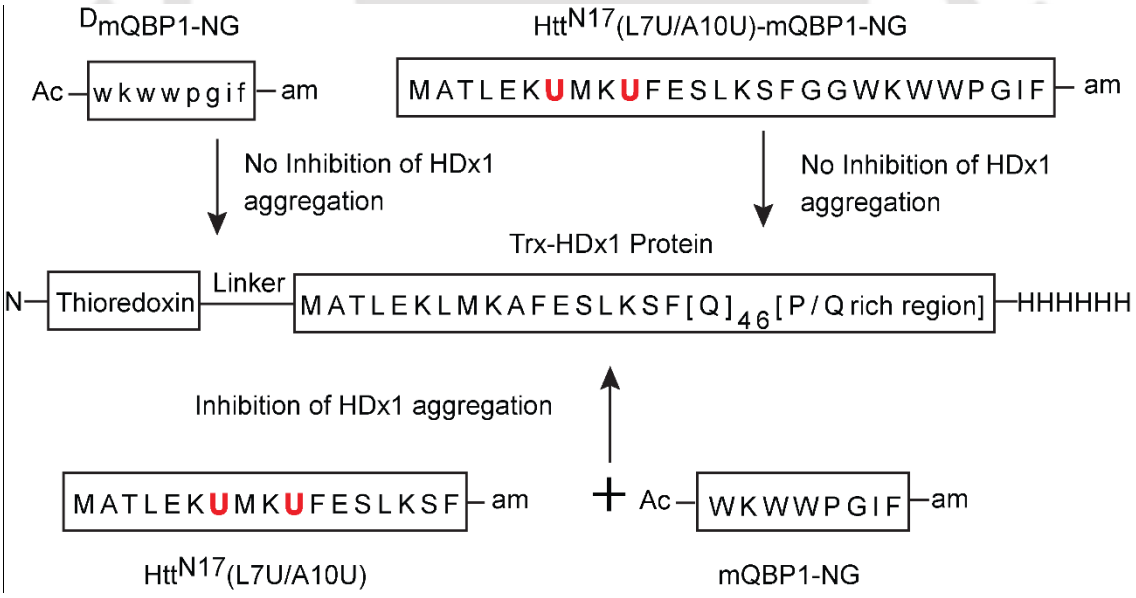

5.1. Introduction

The data in the chapter 3 concluded that the Pro-Gly motif in QBP1 plays a structural role in its activity. Even though the peptides' complete backbone conformation was not experimentally determined, the MD simulations show distinct hairpin-like structures in QBP1 and its analogs. Laurents and coworkers have previously shown that the Pro-Gly dipeptide motif in mQBP1 mediates a type II turn while Trp4 and Ile7, together with Lys2, Trp3 and Phe8, form a hydrophobic cluster [156]. The QBP1 binds to the monomeric expanded polyQ repeats and blocks the initial critical transition to the β-sheet conformation, thereby suppressing their subsequent oligomerization and fibrillogenesis, and consequently, the associated cytotoxicity and neurodegeneration [135, 205]. Overall, the conclusions made are well supported by the mQBP1 structure reported in the literature.

In chapter 4, we investigated the HDx1 aggregation inhibition by the htt^{N17} and its analogs. The data showed that the C-terminal capping was critical for the htt^{N17}'s aggregation inhibition activity. Besides, one of the analogs, the double Aib variant htt^{N17}(L7U/A10U)-am was found to exhibit significantly higher activity than the native htt^{N17}. It is believed that the htt^{N17} diminishes the HDx1 aggregation by co-assembling with the htt^{N17}-harbouring polyQ peptides, thereby diluting the local polyQ concentration in the initial htt^{N17}-mediated oligomers [21]. The results obtained in chapters 3 and 4 prompted us to investigate the activity of the fusion peptide, where the best-performing candidates from the htt^{N17} and QBP1 series of peptides are fused together.

5.2. Hypothesis

As htt^{N17} self-assembles with the N17 stretch of huntingtin while QBP1 is a polyQ-binding peptide, we hypothesized that the fusion peptide with N-terminal htt^{N17} or its active analog and the C-terminal mQBP1 or its analog separated by an oligoglycine linker could be a promising huntingtin aggregation inhibition peptide. The htt^{N17}(L7U/A10U)-am is the most active candidate in the htt^{N17} analogs investigated in chapter 4. No significant difference in activity was observed in the QBP1 series of peptides. An interesting outcome of chapter 3 was the huntingtin aggregation inhibition by the analog mQBP1-NG. The peptide induced an α-helical conformation in HDx1. The folding

of an amyloidogenic protein into an α-helical conformation could have interesting implications on the amyloidogenicity and the aggregation pathway. Therefore, mQBP1-NG was chosen for constructing the fusion peptide. Therefore, the peptide was designed to harbor the htt^{N17}(L7U/A10U) at the N-terminus, followed by a diglycine linker, and the C-terminal mQBP1-NG. Besides, the activity of the htt^{N17}(L7U/A10U)-am and mQBP1-NG mixtures was investigated by incubating the Trx-HDx1 with different molar ratios of these two peptides. Finally, the all D-variant of mQBP1-NG was also studied to explore the importance of the peptide's stereochemistry in the Trx-HDx1 aggregation inhibition. The peptides containing D-amino acids can mimic naturally occurring peptides, but they are more protease resistant, which makes them more suitable for therapeutics [206, 207].

5.3. Results and Discussion

5.3.1. Peptides

The peptides studied in this chapter are listed in Table 5.1. The peptides mQBP1-NG and htt^{N17}(L7U/A10U)-am were used as controls for Trx-HDx1 aggregation inhibition, whereas mQBP1-PP was incorporated as the negative control. As we did not find any report in the literature on the role of stereochemistry of the QBP1 peptides in huntingtin aggregation inhibition, we included the D-isomer of the mQBP1-NG as well in this study.

Table 5.1. *The IDs and the sequences of the peptides employed in this study*

Peptide ID[a]	**Sequence[a][b]**	**Remarks**
mQBP1-NG	CH_3CO-WKWWNGIF-NH_2	The mQBP1 analog wherein Pro is substituted by Asn (positive control)
^{D}mQBP1-NG	CH_3CO-wkwwngif-NH_2	D-isomer of mQBP1-NG
mQBP1-PP	CH_3CO-WKWWPPIF-NH_2	The mQBP1 analog wherein Gly is substituted by Pro (negative control)
Htt^{N17}(L7U/A10U)-am	MATLEKUMKUFESLKSF-NH_2	Trx-HDx1 aggregation inhibiting htt^{N17} analog (positive control)
Htt^{N17}(L7U/A10U)-mQBP1-NG	MATLEKUMKUFESLKSFGG WKWWNGIF-NH_2	Htt^{N17}(L7U/A10U) fused with mQBP1-NG via a diglycine liker

[a]U in the peptide ID and the sequence indicates 2-aminoisobutyric acid (Aib).

[b] Lower-case letters in the sequence represent the D-amino acids

Table 5.2. *The summary of the MALDI-TOF mass spectrometric analysis of the peptides listed in Table 5.1.*

Peptide ID	Calculated monoisotopic mass (Da)	Expected MH^+ mass (Da)	Observed MH^+ mass (Da)	Percent mass error
mQBP1-NG	1176.576	1177.584	1177.53	0.005
^{D}mQBP1-NG	1176.576	1177.584	1,178.36	0.066
mQBP1-PP	1199.617	1200.625	1199.92	0.059
Htt^{N17}(L7U/A10U)-am	1958.161	1959.169	1959.637	0.024
Htt^{N17}(L7U/A10U)-mQBP1-NG	3189.753	3190.761	3194.812	0.127

5.3.2. Secondary structures of the peptides

The secondary structures of the peptides were investigated in 10 mM phosphate buffer pH 7.4, using far-UV CD spectroscopy (Fig. 5.1).

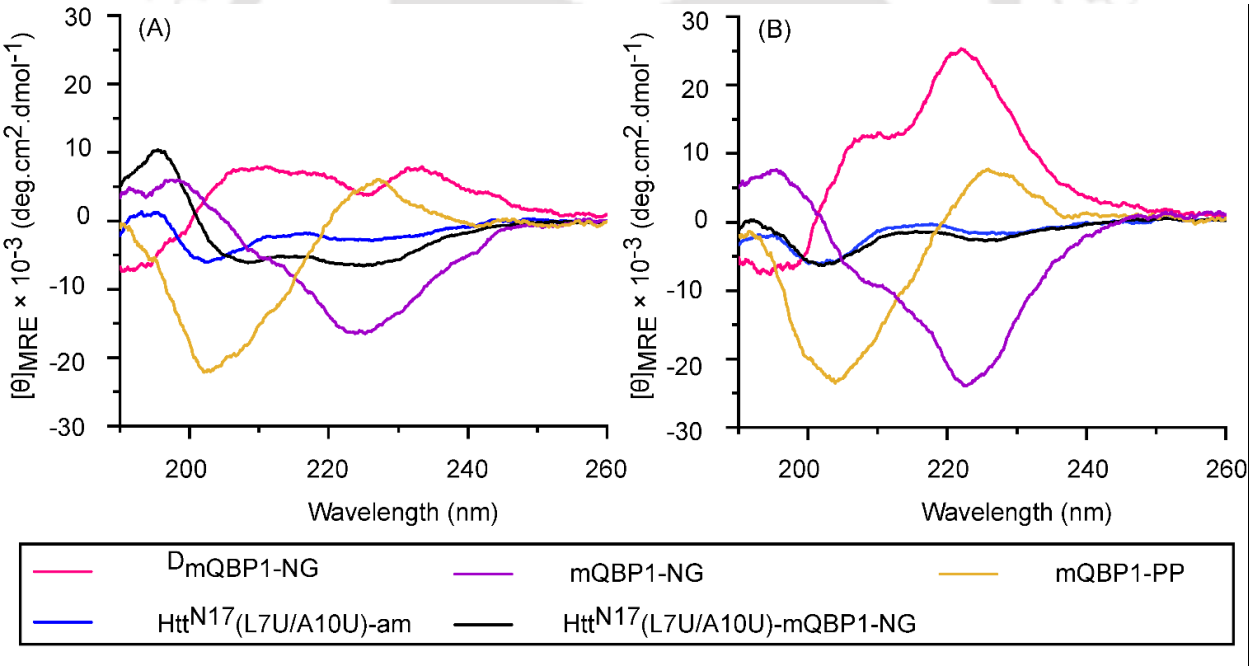

Fig. 5.1. *The far-UV CD spectra of peptides (50 µM concentration) recorded in (A) 10 mM phosphate buffer, pH 7.4 (B) in MQ (not discussed in chapter).*

The CD spectrum of mQBP1-NG is characterized by a negative band around 221 nm, a shallower band around 208 nm, and a very weak positive band around 198 nm. The all D-version of the peptide shows a somewhat mirror image of the spectrum, as expected from the D-stereoisomer of

a peptide. The CD spectrum of negative control peptide (mQBP1-PP) shows a spectrum with a minimum around 204 nm and a weak 227 nm positive band similar to that previously reported in the literature [204]. The spectrum of htt^{N17}(L7U/A10U) shows a weak broad band centered around 230 nm and an intense negative band around 201 nm, the spectral signature similar to that previously reported . The CD spectrum of htt^{N17}(L7U/A10U)-mQBP1-NG is characterized by two intense negative bands around 206 nm and 225 nm and a positive band around 194 nm indicating an α-helical conformation. The spectra, except for the ^{D}mQBP1-NG, were deconvoluted using the CONTIN-LL algorithm on Dichroweb online server using the SP175 reference set [187]. The secondary structural components obtained are shown in Table 5.2. The fusion peptide htt^{N17}(L7U/A10U)-mQBP1-NG is predominantly α-helical.

Table 5.3. *The secondary structural components obtained via CD spectral deconvolution using CONTINLL algorithm on the DICHROWEB online server [187].*

Peptides	α-helix	β-sheet	turns	unordered
mQBP1-NG	35.8	26.2	11.7	26.3
mQBP1-PP	13.6	26	14.8	45.6
Htt^{N17}(L7U/A10U)-mQBP1-NG	61.3	3.1	10.1	25.5
Htt^{N17}(L7U/A10U)-am	23.4	16.9	17.3	42.3

5.3.3. Aggregation inhibition assays

The aggregation inhibition was assayed by measuring the aggregation kinetics of Trx-HDx1 in the presence of an equimolar amount of peptides. The aggregation kinetics was monitored through the time-course measurement of ThT fluorescence (Fig. 5.2A) as well as turbidimetry (Fig. 5.2B). Trx-HDx1 (15 μM), with or without peptides in 10 mM phosphate buffer, pH 7.4, was incubated at 37 $^{\circ}$C and analyzed every 24 h up to 240 h. Both ThT fluorescence and turbidimetry showed aggregation of Trx-HDx1 (in the absence of peptides) with a lag phase of around 48 h. The ThT fluorescence, as well as the turbidity, reach saturation after six days (144 h) of incubation. The control peptides htt^{N17}(L7U/A10U) and mQBP1-NG inhibited the Trd-HDx1 aggregation. The htt^{N17}(L7U/A10U) was found to have higher aggregation inhibition activity than the mQBP1-NG.

When the two peptides were simultaneously added to HDx1 (equimolar total peptide concentration), the activity depended on their relative amounts. The activity was assayed using the htt^{N17}(L7U/A10U) to mQBP1-NG ratios of 1:3, 1:1, and 3:1. The htt^{N17}(L7U/A10U):mQBP1-NG (3:1) displayed the highest activity among the combinations, followed by the 1:1, and the 1:3 combinations. These data are consistent with the fact that htt^{N17}(L7U/A10U) is more active compared to mQBP1. Surprisingly, however, the activity of the fusion peptide htt^{N17}(L7U/A10U)-mQBP1-NG is severely compromised. The D-stereoisomer of mQBP1-NG fails to inhibit aggregation. The chirality, therefore, is essential for the activity of the peptide. The htt^{N17}(L7U/A10U) peptide alone shows the highest activity among all the peptides and peptide combinations studied.

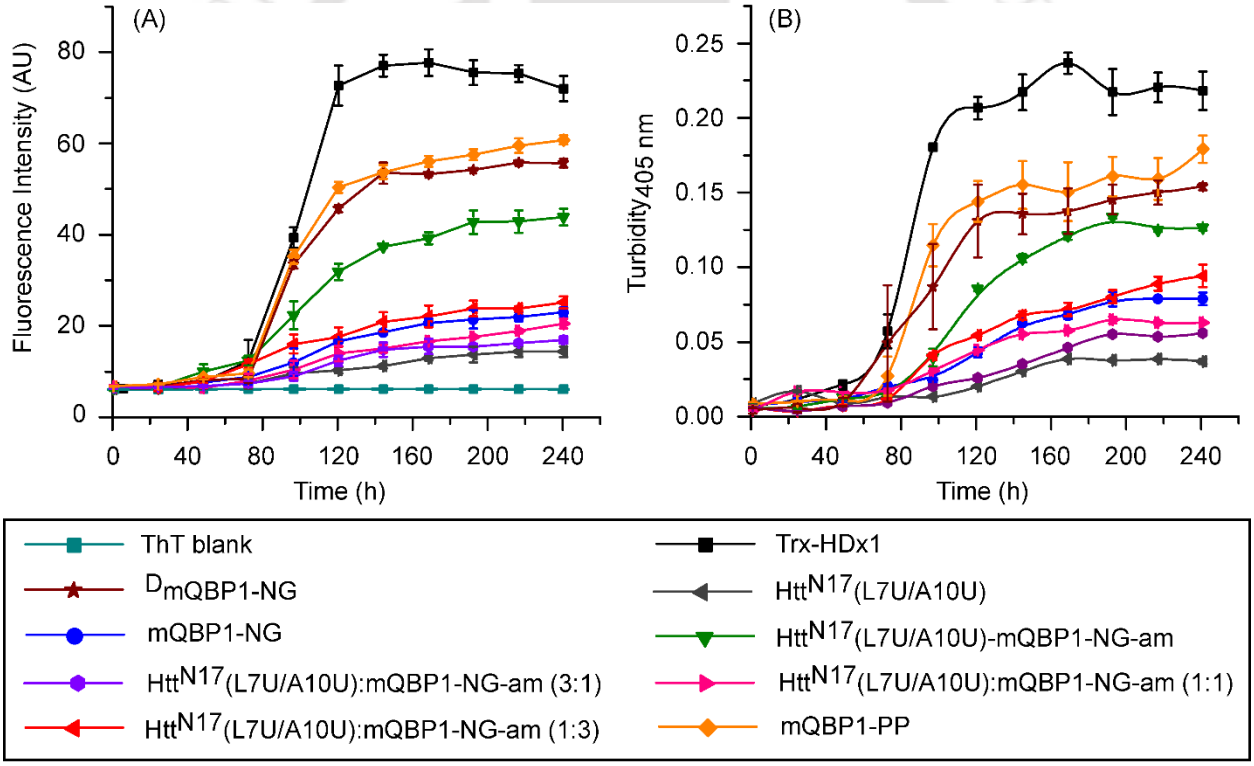

Fig. 5.2. *Aggregation kinetics of Trx-HDx1 in the presence of peptides (A) ThT fluorescence assay (B) Turbidity assay. The error bars represent standard deviation.*

5.3.4. CD spectroscopic analysis of Trx-HDx1 aggregation

The aggregation of Trx-HDx1 and its inhibition by the peptides were further investigated using CD spectroscopy. The freshly prepared Trx-HDx1 shows a negative band around 208 nm and a positive band around 193 nm (dashed line, Fig. 5.3A). The spectrum is very similar to those reported in the literature for Trx-HDx1 [185, 186, 204]. The CD spectrum after 240 h incubation is distinctly different (solid line), with a broad negative band from ~210-230 nm and a weak positive band around 200 nm. The spectrum is similar to that reported in the literature for the aggregated Trx-HDx1 [204]. Very similar spectra were observed in the presence of mQBP1-PP, the peptide used as negative control (Fig. 5.3B) The 0 h and 240 h CD spectra recorded in the presence of equimolar htt^{N17}(L7U/A10U) are more or less overlapping, suggesting strong inhibition of aggregation by the peptide (Fig. 5.3C). Similarly, there is little change in the CD spectrum over time in the presence of mQBP1-NG (Fig. 5.3D). In the presence of the fusion peptide however, the spectral features characteristic of aggregated Trx-HDx1 appear after 240 h incubation (Fig. 5.3E). The fusion peptide, in correlation with the aggregation kinetics data shown in Fig. 5.2, fails to inhibit Trx-HDx1 aggregation. When the Trx-HDx1 is incubated with the mixtures of $httN^{17}$(L7U/A10U) and mQBP1-NG, little change in CD spectrum is observed upon incubation, supporting far better activity compared to the fusion peptide (Fig. 5.3F-H). Large change in CD spectrum, with signatures characteristic of aggregated HDx1, are observed when HDx1 is incubated with the ^{D}mQBP1-NG (Fig. 5.3I). The CD data are in excellent agreement with the ThT fluorescence and turbidimetry aggregation data.

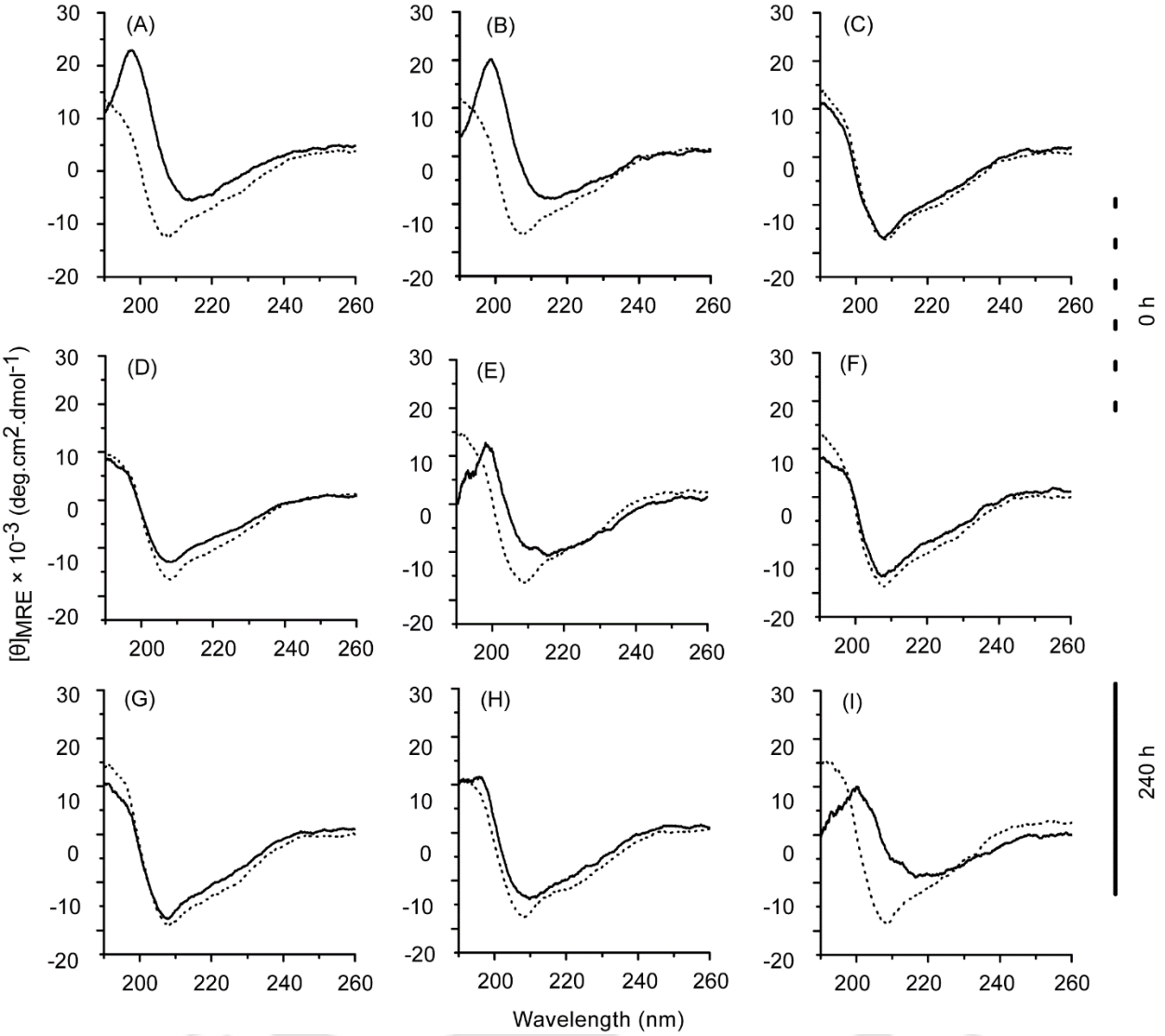

Fig. 5.3. *CD spectra of the Trx-HDx1 in the presence of following peptides. (A) freshly prepared Trx-HDx1 (B) mQBP1-PP (C) htt^{N17}(L7U/A10U)-am (D) mQBP1-NG (E) htt^{N17}(L7U/A10U)-mQBP1-NG (F) httN17(L7U/A10U):mQBP1-NG (3:1) (G) httN17(L7U/A10U):mQBP1-NG (1:1) (H) httN17(L7U/A10U):mQBP1-NG (1:3) (I) ^{D}mQBP1-NG*

5.3.5. AFM imaging

The formation of amyloid fibrils was investigated using AFM imaging of the 240 h-old Trx-HDx1 samples (Fig. 5.4). The Trx-HDx1, when incubated without any peptide, formed distinct fibrillar

structures (Fig. 5.4A). The protein incubated with mQBP1-PP, the peptide used as negative control, shows distinct fibrillar aggregates. No distinct fibrils were obtained in the presence of htt^{N17}(L7U/A10U), the positive control (Fig. 5.4B). In the presence of mQBP1-NG, the other positive control peptide, a few short aggregates were observed (Fig. 5.4C). These data are consistent with the aggregation kinetics data, wherein larger enhancement in ThT fluorescence was observed for the Trx-HDx1 incubated with the mQBP1-NG, compared to when it was incubated with the htt^{N17}(L7U/A10U) (Fig. 5.2A). The fusion protein htt^{N17}(L7U/A10U)-mQBP1-NG failed to inhibit Trx-HDx1 aggregation resulting in distinct fibrillar aggregates (Fig. 4E). The Trx-HDx1 incubated with the 3:1 and 1:1 mixtures of htt^{N17}(L7U/A10U) and mQBP1-NG did not result in any noticeable fibrillar aggregates (Fig. 5.4F and 5.4G, respectively). However, when incubated with the 1:3 htt^{N17}(L7U/A10U) and mQBP1-NG, few fibrillar aggregates were observed (Fig. 5H). The ^{D}mQBP1-NG failed to inhibit Trx-HDx1 aggregation; fibrils were observed for the 240 h-incubated Trx-HDx1 (Fig. 5.4I). The AFM imaging data is in excellent correlation with the aggregation kinetics data.

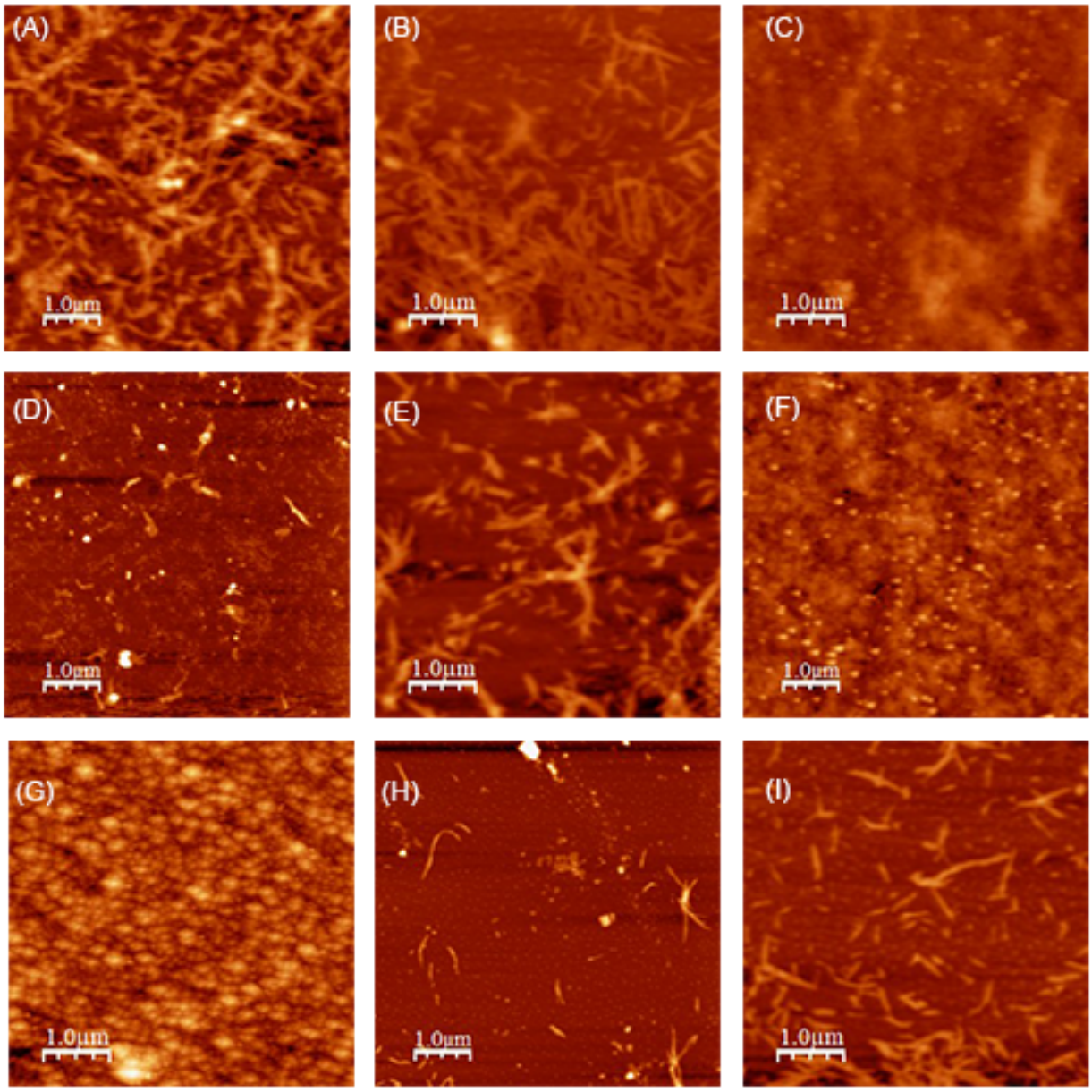

Fig. 5.4. *AFM images of Trx-HDx1 protein samples incubated with following peptides for 240 h (A) Trx-HDx1 (B) mQBP1-PP (C) htt^{N17}(L7U/A10U)-am (D) mQBP1-NG (E) htt^{N17}(L7U/A10U)-mQBP1-NG (F) httN17(L7U/A10U):mQBP1-NG (3:1) (G) httN17(L7U/A10U):mQBP1-NG (1:1) (H) httN17(L7U/A10U):mQBP1-NG (1:3) (I) ^{D}mQBP1-NG. The scale bars represent 1 μm.*

5.4. Conclusions

We investigated the activity of two huntingtin aggregation inhibiting peptides, mQBP1-NG and htt^{N17}(L7U/A10U). The htt^{N17}(L7U/A10U) was found to possess higher activity compared to mQBP1-NG. The activity of the combinations depended on the relative amounts of the two peptides; the higher proportion of htt^{N17}(L7U/A10U) resulted in better activity. The htt^{N17}(L7U/A10U)-mQBP1-NG fusion peptide, however, failed to inhibit the Trx-HDX1 inhibition. The activity of htt^{N17}(L7U/A10U) is attributed to its co-assembly with the N17 region of the huntingtin protein after folding into an α-helix, while that of mQBP1-NG is attributed to its binding with the pathogenic polyQ repeats. Laurents and coworkers have previously shown that the Pro-Gly dipeptide motif in mQBP1 mediates a type II turn while Trp4 and Ile7, together with Lys2, Trp3 and Phe8, form a hydrophobic cluster [156]. The Asn-Gly motif can also mediate a β-turn, which might account for the aggregation inhibition activity of mQBP1-NG. Wetzel and coworkers have previously reported that the htt^{N17} takes up a somewhat compact conformation [168]. When fused with the polyQ stretch, the peptide undergoes a polyQ repeat-dependent unfolding and forming oligomers where the htt^{N17} takes up an α-helical conformation. The CD spectrum of htt^{N17}(L7U/A10U) was found very similar to that reported for htt^{N17}, indicating a similar conformation. However, the fusion peptide htt^{N17}(L7U/A10U)-mQBP1-NG takes up an α-helical conformation. A distinct 3-dimensional structure seems to be essential for mQBP1-NG activity as the ^{D}mQBP1-NG fails to inhibit the activity. It is likely that the α-helical conformation extends into the QBP1-NG region, thereby disrupting its activity. Besides, the longer helix would have different physicochemical properties that could alter its interactions with the N17 region in the huntingtin. As the fusion peptide lacked huntingtin aggregation inhibition activity, further investigations into the reasons behind this loss were not carried out. As QBP1 was identified as a repeat-length sensitive peptide, it is likely that it recognizes some conformation of the polyQ region. Tagging it with the N17 peptide is expected to limit its access to such conformations in the polyQ region. Besides, the tagging with N17 might perturb the N17's structure and physicochemical properties, thereby abolishing its activity. This is further supported by the fact that the mixtures of the two peptides efficiently inhibit the aggregation. It is, therefore, likely that a longer linker in the fusion peptide might have worked better. This is an aspect worth investigating in future.

CHAPTER 6

Conclusion and Future Perspective

6.1. Conclusion and Future Perspective

Peptides happen to be a versatile class of molecules that play highly diverse roles. Living organisms use peptides to combat the pathogens, as the messenger/signaling molecules, and as structural components. This versatility is largely attributed to the chemical diversity conferred by the pool of at least 20 monomers. Besides, certain organisms can incorporate the so called 'non-natural' amino acids through non-ribosomal synthesis, further expanding the monomer diversity. The peptides up to several tens of residues can readily be synthesized using current chemical synthesis protocols. This allows one to incorporate the non-natural amino acids at will, without depending on the biosynthetic pathways.

Peptides have gained considerable interest as far as amyloid research is concerned. Short peptides have been instrumental in understanding the mechanisms underlying peptide self-assembly and amyloid formation. As short peptides can form fibrils very similar to that formed by the disease-related proteins and peptides, an immediate thought would be if they could co-assemble with them. If so, could they be engineered in such a fashion that they recognize the pathogenic protein/peptide, assemble with them, but inhibit the further aggregation? The so called 'β-breaker' peptides work in this fashion. Such peptides would, typically, have a recognition motif that facilitate the assembly with the pathogenic protein/peptide, and another motif, that disfavors the addition of further monomers (Fig. 6.1). Unlike short peptides, the disease-associated amyloidogenic proteins/peptides contain several regions that do not directly initiate/participate in the self-assembly but could have strong modulatory affects. Such regions are also important therapeutic targets. The huntingtin, the subject topic of this thesis, is one such protein. The N-terminal 17-residue peptide, htt^{N17} is critical for aggregation initiation. The peptides that recognize this peptide region and co-assemble with it can interfere with the aggregation process. Wetzel and coworkers have previously reported that when htt^{N17} peptide is added to the model huntingtin exon 1 peptide, the aggregation is inhibited. Thakur and coworkers further investigated the amyloid-inhibiting activity of the N17 peptides from the huntingtin of other organisms. In this thesis, several analogs of the human htt^{N17} were investigated for their aggregation inhibition potential. A highly active htt^{N17} analog was designed by substituting two hydrophobic residues towards the middle of the protein by the helix-promoting residue 2-aminoisobutyric acid.

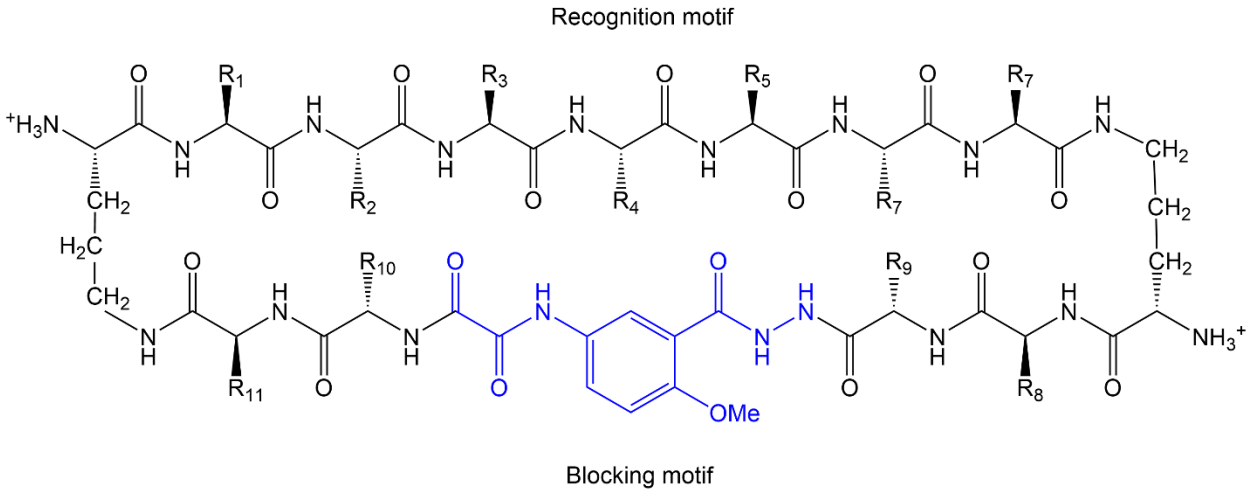

Fig. 6.1 A general structure of a β-sheet macrocycle, a class of β-breaker peptides, designed by Nowick and coworkers [208].

Another strategy to identify the potential amyloid-inhibiting peptides is to screen a library of peptides with random sequences. Peptides against several amyloidogenic proteins have been identified using this strategy. Burke and coworkers, using phage display screening, identified an 11-residue Trp-rich peptide, termed QBP1, that preferentially bind to the pathogenic polyglutamine tract. A minimal region from this peptide (mQBP1) was subsequently identified. Both these peptides contain a Pro-Gly dipeptide motif near their C-termini. As Pro-Gly motifs in proteins are often used as diagnostic of the turn-forming regions, the role of the β-turn supporting motifs was investigated in this thesis. The turn was found to be essential for the peptides' amyloid-inhibiting propensity. Interestingly, however, a fusion peptide obtained by tagging the most active htt^{N17} analog with an active mQBP1 analog was found to be inactive. However, the combinations of the peptides were found to be active.

It is important to note that we have employed the thioredoxin-fused huntingtin exon1 (Trx-HDx1) in this study. The rationale behind using the fused protein was to attain a monomeric protein that displays a reproducible and slow aggregation kinetics. As a change in aggregation kinetics is the standard assay for the aggregation-enhancing or aggregation-inhibition activity of a compound, a highly reproducible kinetics with a lag phase is highly desirable. The free (untagged) HDx1, unfortunately, displays a rapid aggregation without a lag-phase [170] , making it unsuitable for an

aggregation-inhibition assay. For these reasons, even the recent studies of HDx1 aggregation inhibition have been carried out using fused protein; Sanchez-Garcia and coworkers, for example, have used GST-fused HDx1 [131]. Roy and coworkers also used GST-HDx1 [209]. The untagged protein is largely used in the studies wherein the terminal aggregates are being investigated. The free HDx1 is often obtained by removing the tag (thioredoxin or GST) using a protease or simply by expressing the untagged HDx1 and then recovering the protein from the inclusion bodies. Both these methods have pre-formed aggregates that need to be broken by harsh chemical treatments, such as dissolution in TFA and HFIP. HFIP is well-known to introduce secondary structures in the proteins and peptides that can have marked effects on their aggregation behavior [210]. The more number of chemical treatment and drying/freeze-drying steps cause 'lot to lot' variation in the protein preparation. As the proof of principle is now established with these peptides, the study can be extended to the untagged HDx1. Besides, we have not investigated the serum-sensitivity, the cytotoxicity, and the cellular uptake of these peptides in this thesis. As huntingtin largely gets deposited as intracellular aggregates, the cellular uptake happens to be an important attribute of a therapeutic agent that targets HDx1. The peptides that we have investigated do not possess any notable cellular uptake motif. In fact, Nagai and coworkers tagged the QBP1 with cell-penetrating peptides to study its protective effect on the polyQ disease cell and animal models [205]. To further realize the therapeutic potential of QBP1 and htt^{N17}-derived peptides investigated in this study, their cellular uptake needs to be investigated. Further engineering, if required, could very much be required.

The role of htt^{N17} in huntingtin is crucial as it is involved in a variety of cellular functions. Furthermore, its role in the aggregation of the HDx1 makes it a potential target for the therapeutics. Targeting htt^{N17} region, therefore, could be an effective mechanism to combat the HDx1 aggregation. Out of 17 amino acids, the htt^{N17} harbors 3 Lys, 2 Ser, and 1 Thr residues that can undergo PTMs. These modifications have a high impact on the regulation and activity of the huntingtin function and aggregation. Studies on these PTMs show how these modifications modulate the normal and mutant huntingtin. Enzymes involved in these PTMs like kinases, proteases, ubiquitin ligases and hydrolases could turn out to be potential therapeutic targets. Designed molecules like molecular tweezers (CLR01) that specifically bind to the lysine residues in the httN17 region of HDx1, are shown to inhibit the HDx1 aggregation *in vitro* as well as in the living cells. In HDx1, CLR01 disrupts the amphipathic helical nature of httN17 and prevents the

httN17 sequence from self-association [131]. Identification and screening of such molecules, which can interact with htt^{N17} amino acids and modulate the structure of httN17 region, can lead to potential drug molecules to control the HDx1 aggregation.

Huntingtin exon 1 in largely an intrinsically disordered polypeptide, and several intrinsically disordered amyloidogenic proteins have been reported to undergo the liquid-liquid phase separation (LLPS) [211]. Saibil and coworkers have recently reported that the HDx1 undergoes reversible LLPS, a process that is supposedly mediated by the polyQ and the C-terminal Proline-rich region [212]. Using GFP-fused HDx1, Emtage and coworkers showed that the protein-rich phase is somewhat gel-like [213] . Saibil and coworkers found that the huntingtin with the polyQ length of 25 undergoes LLPS in the yeast and mammalian cells. However, only huntingtin with pathogenic polyQ tract undergoes transformation to the solid-like assemblies. The LLPS and the subsequent transformation to the insoluble aggregates could be another therapeutic process. It would be interesting to study how the peptides investigated in this thesis participate in these processes.

Appendix

MALDI-TOF SPECTRA

The MALDI-TOF spectra for all the peptides reported in the thesis.

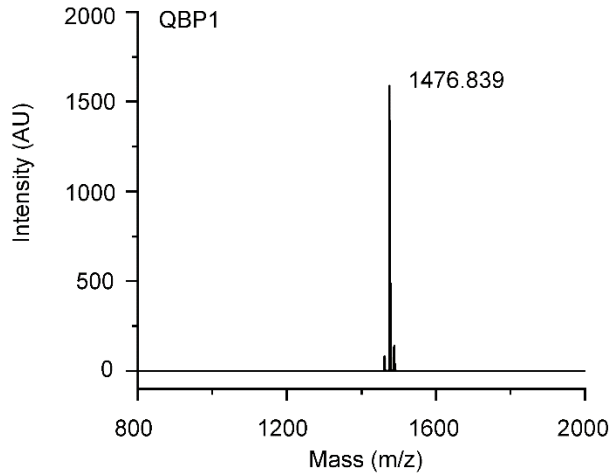

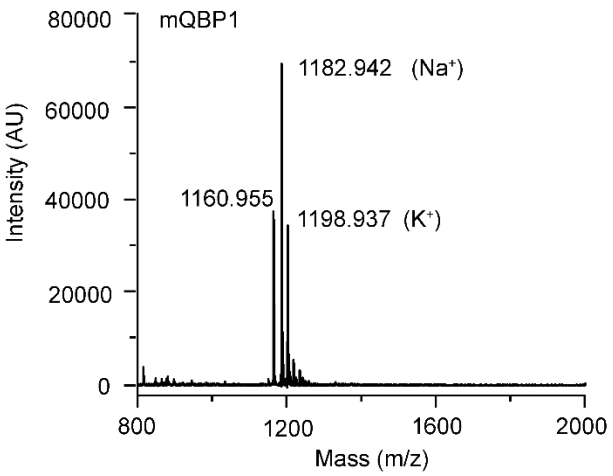

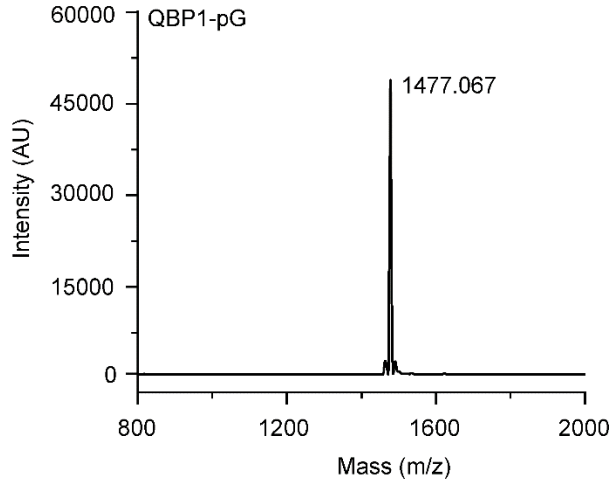

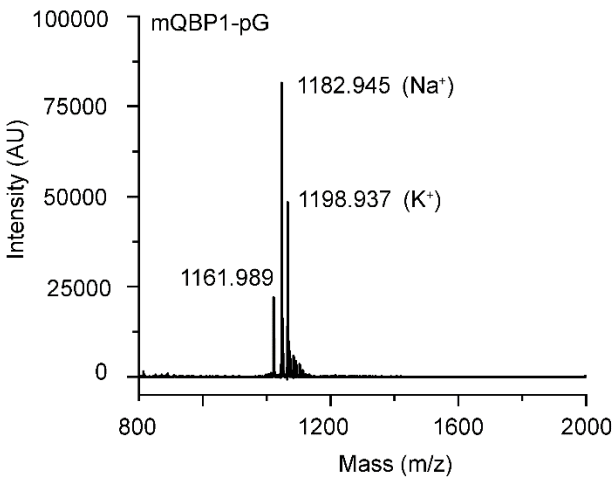

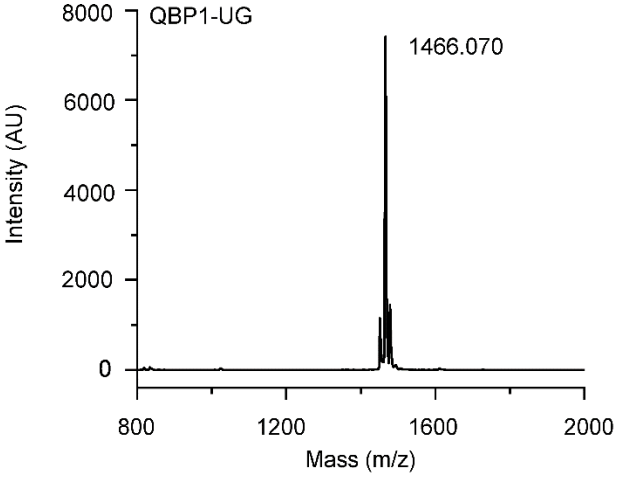

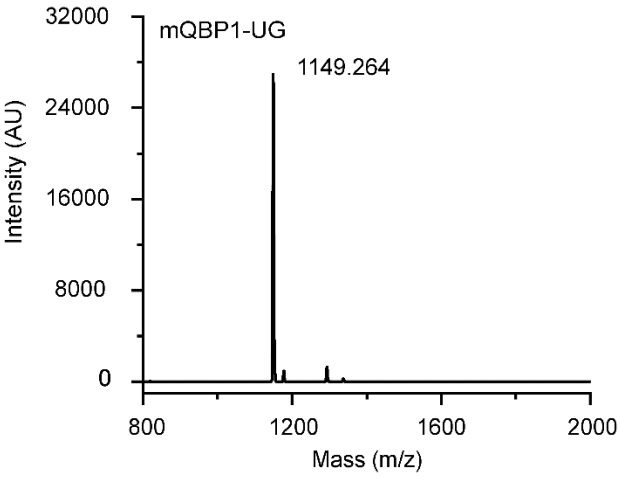

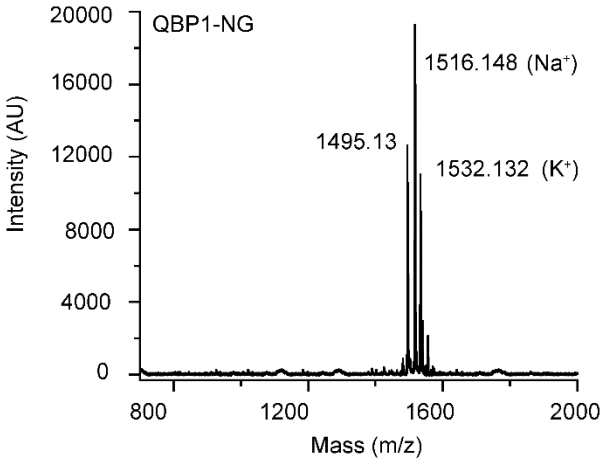

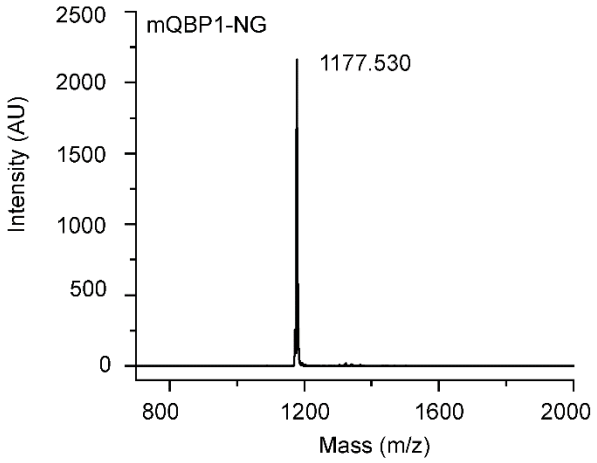

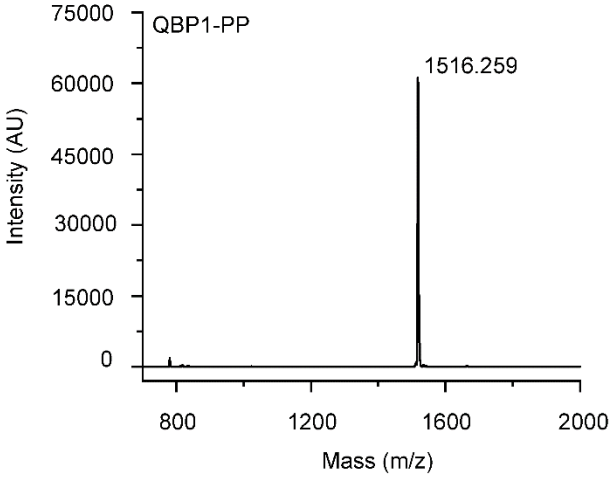

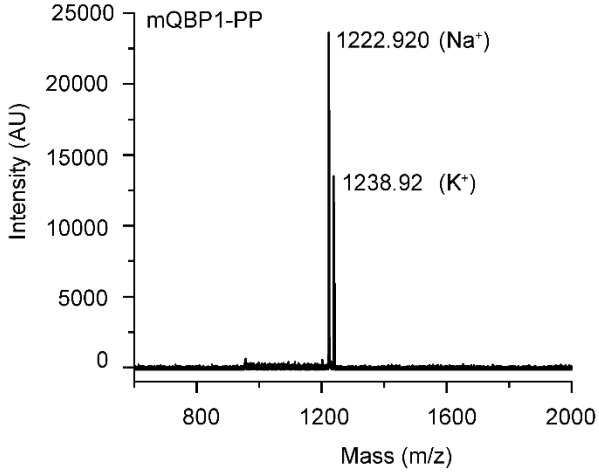

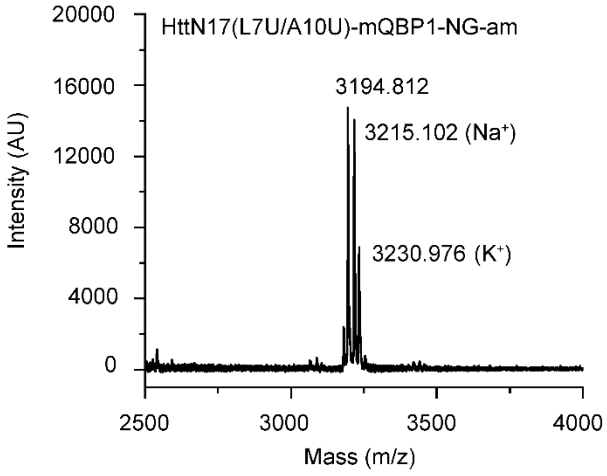

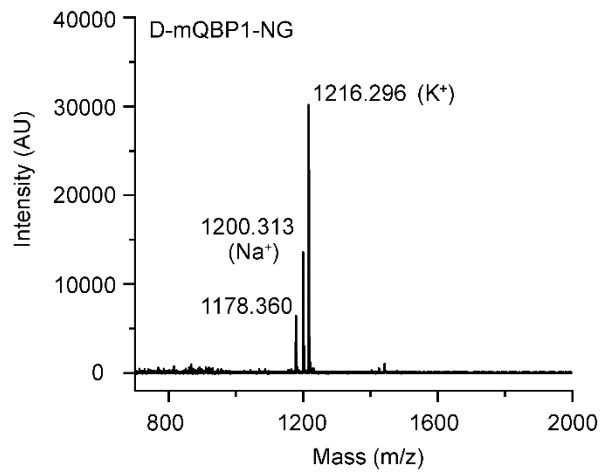

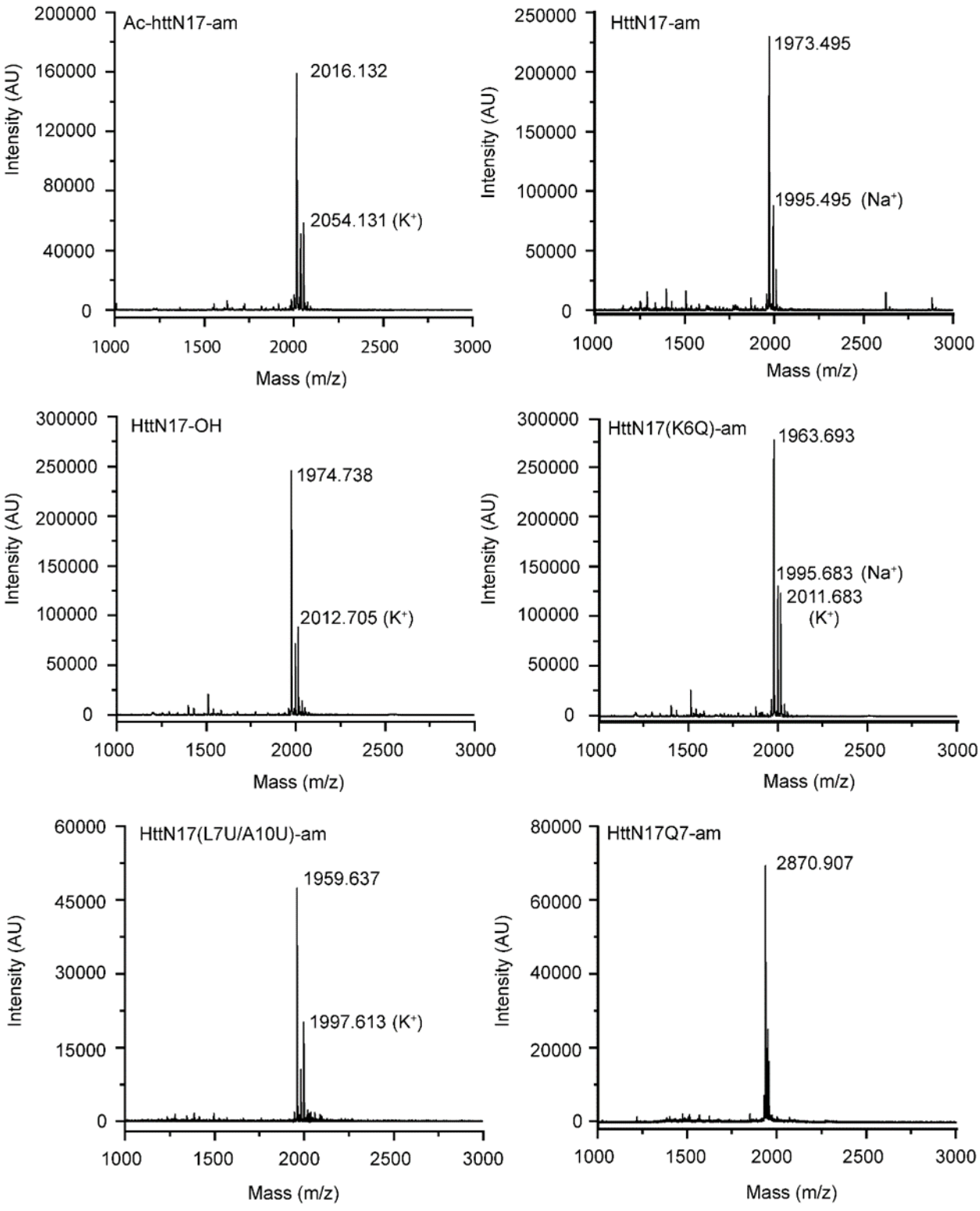

References

1. Ross, C.A. and S.J. Tabrizi, *Huntington's disease: from molecular pathogenesis to clinical treatment.* Lancet Neurol, 2011. **10**(1): p. 83-98.
2. Gusella, J.F. and M.E. MacDonald, *Molecular genetics: Unmasking polyglutamine triggers in neurodegenerative disease.* Nature Reviews Neuroscience, 2000. **1**(2): p. 109-115.
3. Li, S.-H. and X.-J. Li, *Aggregation of N-Terminal Huntingtin is Dependent on the Length of Its Glutamine Repeats.* Human Molecular Genetics, 1998. **7**(5): p. 777-782.
4. *A novel gene containing a trinucleotide repeat that is expanded and unstable on Huntington's disease chromosomes. The Huntington's Disease Collaborative Research Group.* Cell, 1993. **72**(6): p. 971-83.
5. Duff, K., et al., *Psychiatric Symptoms in Huntington's Disease before Diagnosis: The Predict-HD Study.* Biological Psychiatry, 2007. **62**(12): p. 1341-1346.
6. Kirkwood, S.C., et al., *Progression of Symptoms in the Early and Middle Stages of Huntington Disease.* Archives of Neurology, 2001. **58**(2): p. 273-278.
7. Davies, S.W., et al., *Formation of neuronal intranuclear inclusions underlies the neurological dysfunction in mice transgenic for the HD mutation.* Cell, 1997. **90**(3): p. 537-48.
8. Kegel, K.B., et al., *Huntingtin expression stimulates endosomal-lysosomal activity, endosome tubulation, and autophagy.* J Neurosci, 2000. **20**(19): p. 7268-78.
9. Suopanki, J., et al., *Interaction of huntingtin fragments with brain membranes--clues to early dysfunction in Huntington's disease.* J Neurochem, 2006. **96**(3): p. 870-84.
10. Bäuerlein, F.J.B., et al., *In Situ Architecture and Cellular Interactions of PolyQ Inclusions.* Cell, 2017. **171**(1): p. 179-187.e10.
11. Liu, K.Y., et al., *Disruption of the nuclear membrane by perinuclear inclusions of mutant huntingtin causes cell-cycle re-entry and striatal cell death in mouse and cell models of Huntington's disease.* Hum Mol Genet, 2015. **24**(6): p. 1602-16.
12. Ambrose, C.M., et al., *Structure and expression of the Huntington's disease gene: evidence against simple inactivation due to an expanded CAG repeat.* Somat Cell Mol Genet, 1994. **20**(1): p. 27-38.
13. Mangiarini, L., et al., *Exon 1 of the HD gene with an expanded CAG repeat is sufficient to cause a progressive neurological phenotype in transgenic mice.* Cell, 1996. **87**(3): p. 493-506.
14. DiFiglia, M., et al., *Aggregation of huntingtin in neuronal intranuclear inclusions and dystrophic neurites in brain.* Science, 1997. **277**(5334): p. 1990-3.
15. Landles, C., et al., *Proteolysis of mutant huntingtin produces an exon 1 fragment that accumulates as an aggregated protein in neuronal nuclei in Huntington disease.* J Biol Chem, 2010. **285**(12): p. 8808-23.
16. Zheng, Z., et al., *An N-terminal Nuclear Export Signal Regulates Trafficking and Aggregation of Huntingtin (Htt) Protein Exon 1.* Journal of Biological Chemistry, 2013. **288**(9): p. 6063-6071.
17. Tartari, M., et al., *Phylogenetic comparison of huntingtin homologues reveals the appearance of a primitive polyQ in sea urchin.* Mol Biol Evol, 2008. **25**(2): p. 330-8.
18. Darnell, G., et al., *Flanking polyproline sequences inhibit beta-sheet structure in polyglutamine segments by inducing PPII-like helix structure.* J Mol Biol, 2007. **374**(3): p. 688-704.
19. Thakur, A.K., et al., *Polyglutamine disruption of the huntingtin exon 1 N terminus triggers a complex aggregation mechanism.* Nature structural & molecular biology, 2009. **16**(4): p. 380-389.
20. Jayaraman, M., et al., *Slow Amyloid Nucleation via α-Helix-Rich Oligomeric Intermediates in Short Polyglutamine-Containing Huntingtin Fragments.* Journal of Molecular Biology, 2012. **415**(5): p. 881-899.

21. Mishra, R., et al., *Inhibiting the nucleation of amyloid structure in a huntingtin fragment by targeting α-helix-rich oligomeric intermediates.* Journal of molecular biology, 2012. **415**(5): p. 900-917.
22. Bhattacharyya, A.M., A.K. Thakur, and R. Wetzel, *Polyglutamine aggregation nucleation: Thermodynamics of a highly unfavorable protein folding reaction.* Proceedings of the National Academy of Sciences, 2005. **102**(43): p. 15400.
23. Michalek, M., E.S. Salnikov, and B. Bechinger, *Structure and topology of the huntingtin 1-17 membrane anchor by a combined solution and solid-state NMR approach.* Biophysical journal, 2013. **105**(3): p. 699-710.
24. Williamson, T.E., et al., *Modulation of polyglutamine conformations and dimer formation by the N-terminus of huntingtin.* Journal of molecular biology, 2010. **396**(5): p. 1295-1309.
25. Tao, M., et al., *Structure of Membrane-Bound Huntingtin Exon 1 Reveals Membrane Interaction and Aggregation Mechanisms.* Structure, 2019. **27**(10): p. 1570-1580.e4.
26. Burke, K.A., et al., *The interaction of polyglutamine peptides with lipid membranes is regulated by flanking sequences associated with huntingtin.* J Biol Chem, 2013. **288**(21): p. 14993-5005.
27. Ehrnhoefer, D.E., L. Sutton, and M.R. Hayden, *Small changes, big impact: posttranslational modifications and function of huntingtin in Huntington disease.* The Neuroscientist : a review journal bringing neurobiology, neurology and psychiatry, 2011. **17**(5): p. 475-492.
28. Steffan, J.S., et al., *SUMO Modification of Huntingtin and Huntington's Disease Pathology.* Science, 2004. **304**(5667): p. 100.
29. Thompson, L.M., et al., *IKK phosphorylates Huntingtin and targets it for degradation by the proteasome and lysosome.* J Cell Biol, 2009. **187**(7): p. 1083-99.
30. Atwal, R.S., et al., *Huntingtin has a membrane association signal that can modulate huntingtin aggregation, nuclear entry and toxicity.* Human Molecular Genetics, 2007. **16**(21): p. 2600-2615.
31. Rockabrand, E., et al., *The first 17 amino acids of Huntingtin modulate its sub-cellular localization, aggregation and effects on calcium homeostasis.* Human Molecular Genetics, 2006. **16**(1): p. 61-77.
32. Seong, I.S., et al., *Huntingtin facilitates polycomb repressive complex 2.* Human Molecular Genetics, 2009. **19**(4): p. 573-583.
33. Zuccato, C., et al., *Loss of huntingtin-mediated BDNF gene transcription in Huntington's disease.* Science, 2001. **293**(5529): p. 493-8.
34. Lo Sardo, V., et al., *An evolutionary recent neuroepithelial cell adhesion function of huntingtin implicates ADAM10-Ncadherin.* Nat Neurosci, 2012. **15**(5): p. 713-21.
35. Harjes, P. and E.E. Wanker, *The hunt for huntingtin function: interaction partners tell many different stories.* Trends Biochem Sci, 2003. **28**(8): p. 425-33.
36. Caviston, J.P., et al., *Huntingtin facilitates dynein/dynactin-mediated vesicle transport.* Proc Natl Acad Sci U S A, 2007. **104**(24): p. 10045-50.
37. Colin, E., et al., *Huntingtin phosphorylation acts as a molecular switch for anterograde/retrograde transport in neurons.* Embo j, 2008. **27**(15): p. 2124-34.
38. McGuire, J.R., et al., *Interaction of Huntingtin-associated protein-1 with kinesin light chain: implications in intracellular trafficking in neurons.* J Biol Chem, 2006. **281**(6): p. 3552-9.
39. Godin, J.D., et al., *Huntingtin is required for mitotic spindle orientation and mammalian neurogenesis.* Neuron, 2010. **67**(3): p. 392-406.
40. Reiner, A., et al., *Wild-type huntingtin plays a role in brain development and neuronal survival.* Molecular Neurobiology, 2003. **28**(3): p. 259-275.
41. White, J.K., et al., *Huntingtin is required for neurogenesis and is not impaired by the Huntington's disease CAG expansion.* Nat Genet, 1997. **17**(4): p. 404-10.

42. Nasir, J., et al., *Targeted disruption of the Huntington's disease gene results in embryonic lethality and behavioral and morphological changes in heterozygotes.* Cell, 1995. **81**(5): p. 811-23.
43. Dragatsis, I., A. Efstratiadis, and S. Zeitlin, *Mouse mutant embryos lacking huntingtin are rescued from lethality by wild-type extraembryonic tissues.* Development, 1998. **125**(8): p. 1529-1539.
44. Duyao, M.P., et al., *Inactivation of the mouse Huntington's disease gene homolog Hdh.* Science, 1995. **269**(5222): p. 407-10.
45. Arrasate, M., et al., *Inclusion body formation reduces levels of mutant huntingtin and the risk of neuronal death.* Nature, 2004. **431**(7010): p. 805-10.
46. Cattaneo, E., C. Zuccato, and M. Tartari, *Normal huntingtin function: an alternative approach to Huntington's disease.* Nature Reviews Neuroscience, 2005. **6**(12): p. 919-930.
47. Mehler, M.F. and J.R. Petronglo, *Loss-of-Huntingtin in Medial and Lateral Ganglionic Lineages Differentially Disrupts Regional Interneuron and Projection Neuron Subtypes and Promotes Huntington's Disease-Associated Behavioral, Cellular, and Pathological Hallmarks.* 2019. **39**(10): p. 1892-1909.
48. Dragatsis, I., et al., *Effect of early embryonic deletion of huntingtin from pyramidal neurons on the development and long-term survival of neurons in cerebral cortex and striatum.* Neurobiol Dis, 2018. **111**: p. 102-117.
49. McKinstry, S.U., et al., *Huntingtin is required for normal excitatory synapse development in cortical and striatal circuits.* 2014. **34**(28): p. 9455-72.
50. Dragatsis, I., M.S. Levine, and S. Zeitlin, *Inactivation of Hdh in the brain and testis results in progressive neurodegeneration and sterility in mice.* Nat Genet, 2000. **26**(3): p. 300-6.
51. Ismailoglu, I., et al., *Huntingtin protein is essential for mitochondrial metabolism, bioenergetics and structure in murine embryonic stem cells.* Developmental Biology, 2014. **391**(2): p. 230-240.
52. Leavitt, B.R., et al., *Wild-type huntingtin protects neurons from excitotoxicity.* J Neurochem, 2006. **96**(4): p. 1121-9.
53. Burrus, C.J., et al., *Striatal Projection Neurons Require Huntingtin for Synaptic Connectivity and Survival.* Cell Rep, 2020. **30**(3): p. 642-657.e6.
54. Andrade, M.A. and P. Bork, *HEAT repeats in the Huntington's disease protein.* Nature Genetics, 1995. **11**(2): p. 115-116.
55. Takano, H. and J.F. Gusella, *The predominantly HEAT-like motif structure of huntingtin and its association and coincident nuclear entry with dorsal, an NF-kB/Rel/dorsal family transcription factor.* BMC Neurosci, 2002. **3**: p. 15.
56. Li, W., et al., *Expression and characterization of full-length human huntingtin, an elongated HEAT repeat protein.* J Biol Chem, 2006. **281**(23): p. 15916-22.
57. Saudou, F. and S. Humbert, *The Biology of Huntingtin.* Neuron, 2016. **89**(5): p. 910-26.
58. Palidwor, G.A., et al., *Detection of Alpha-Rod Protein Repeats Using a Neural Network and Application to Huntingtin.* PLOS Computational Biology, 2009. **5**(3): p. e1000304.
59. Li, W., et al., *Expression and Characterization of Full-length Human Huntingtin, an Elongated HEAT Repeat Protein *.* Journal of Biological Chemistry, 2006. **281**(23): p. 15916-15922.
60. Warby, S.C., et al., *Activated caspase-6 and caspase-6-cleaved fragments of huntingtin specifically colocalize in the nucleus.* Hum Mol Genet, 2008. **17**(15): p. 2390-404.
61. Sieradzan, K.A., et al., *Huntington's Disease Intranuclear Inclusions Contain Truncated, Ubiquitinated Huntingtin Protein.* Experimental Neurology, 1999. **156**(1): p. 92-99.
62. Ross, C.A. and M.A. Poirier, *Opinion: What is the role of protein aggregation in neurodegeneration?* Nat Rev Mol Cell Biol, 2005. **6**(11): p. 891-8.
63. Wetzel, R., *Physical chemistry of polyglutamine: intriguing tales of a monotonous sequence.* J Mol Biol, 2012. **421**(4-5): p. 466-90.

64. Huang, C.C., et al., *Amyloid formation by mutant huntingtin: threshold, progressivity and recruitment of normal polyglutamine proteins.* Somat Cell Mol Genet, 1998. **24**(4): p. 217-33.
65. Orr, H.T. and H.Y. Zoghbi, *Trinucleotide repeat disorders.* Annu Rev Neurosci, 2007. **30**: p. 575-621.
66. Orr, H.T., *Polyglutamine neurodegeneration: expanded glutamines enhance native functions.* Curr Opin Genet Dev, 2012. **22**(3): p. 251-5.
67. Chen, S., et al., *Polyglutamine aggregation behavior in vitro supports a recruitment mechanism of cytotoxicity.* J Mol Biol, 2001. **311**(1): p. 173-82.
68. Takahashi, Y., et al., *Detection of Polyglutamine Protein Oligomers in Cells by Fluorescence Correlation Spectroscopy.* Journal of Biological Chemistry, 2007. **282**(33): p. 24039-24048.
69. Kim, M.W., et al., *Secondary structure of Huntingtin amino-terminal region.* Structure (London, England : 1993), 2009. **17**(9): p. 1205-1212.
70. Zheng, S., et al., *Deletion of the huntingtin polyglutamine stretch enhances neuronal autophagy and longevity in mice.* PLoS Genet, 2010. **6**(2): p. e1000838.
71. Baxendale, S., et al., *Comparative sequence analysis of the human and pufferfish Huntington's disease genes.* Nature Genetics, 1995. **10**(1): p. 67-76.
72. Bhattacharyya, A., et al., *Oligoproline effects on polyglutamine conformation and aggregation.* J Mol Biol, 2006. **355**(3): p. 524-35.
73. Lakhani, V.V., F. Ding, and N.V. Dokholyan, *Polyglutamine induced misfolding of huntingtin exon1 is modulated by the flanking sequences.* PLoS Comput Biol, 2010. **6**(4): p. e1000772.
74. Hollenbach, B., et al., *Aggregation of truncated GST-HD exon 1 fusion proteins containing normal range and expanded glutamine repeats.* Philosophical transactions of the Royal Society of London. Series B, Biological sciences, 1999. **354**(1386): p. 991-994.
75. Darnell, G.D., et al., *Mechanism of cis-inhibition of polyQ fibrillation by polyP: PPII oligomers and the hydrophobic effect.* Biophysical journal, 2009. **97**(8): p. 2295-2305.
76. Neveklovska, M., et al., *Deletion of the huntingtin proline-rich region does not significantly affect normal huntingtin function in mice.* Journal of Huntington's disease, 2012. **1**(1): p. 71-87.
77. Qin, Z.-H., et al., *Huntingtin Bodies Sequester Vesicle-Associated Proteins by a Polyproline-Dependent Interaction.* The Journal of Neuroscience, 2004. **24**(1): p. 269.
78. Lee, W.-C.M., M. Yoshihara, and J.T. Littleton, *Cytoplasmic aggregates trap polyglutamine-containing proteins and block axonal transport in a Drosophila model of Huntington's disease.* Proceedings of the National Academy of Sciences of the United States of America, 2004. **101**(9): p. 3224-3229.
79. Gunawardena, S., et al., *Disruption of Axonal Transport by Loss of Huntingtin or Expression of Pathogenic PolyQ Proteins in Drosophila.* Neuron, 2003. **40**(1): p. 25-40.
80. Lee, W.-C.M., M. Yoshihara, and J.T. Littleton, *Cytoplasmic aggregates trap polyglutamine-containing proteins and block axonal transport in a Drosophila model of Huntington's disease.* Proceedings of the National Academy of Sciences of the United States of America, 2004. **101**(9): p. 3224-3229.
81. Wheeler, V.C., et al., *Long glutamine tracts cause nuclear localization of a novel form of huntingtin in medium spiny striatal neurons in HdhQ92 and HdhQ111 knock-in mice.* Human Molecular Genetics, 2000. **9**(4): p. 503-513.
82. Chiki, A., et al., *Mutant Exon1 Huntingtin Aggregation is Regulated by T3 Phosphorylation-Induced Structural Changes and Crosstalk between T3 Phosphorylation and Acetylation at K6.* Angewandte Chemie International Edition, 2017. **56**(19): p. 5202-5207.
83. Cariulo, C., et al., *Phosphorylation of huntingtin at residue T3 is decreased in Huntington's disease and modulates mutant huntingtin protein conformation.* Proc Natl Acad Sci U S A, 2017. **114**(50): p. E10809-e10818.

84. Aiken, C.T., et al., *Phosphorylation of threonine 3: implications for Huntingtin aggregation and neurotoxicity.* J Biol Chem, 2009. **284**(43): p. 29427-36.
85. Mishra, R., et al., *Serine phosphorylation suppresses huntingtin amyloid accumulation by altering protein aggregation properties.* J Mol Biol, 2012. **424**(1-2): p. 1-14.
86. Gu, X., et al., *Serines 13 and 16 are critical determinants of full-length human mutant huntingtin induced disease pathogenesis in HD mice.* Neuron, 2009. **64**(6): p. 828-840.
87. Kalchman, M.A., et al., *Huntingtin is ubiquitinated and interacts with a specific ubiquitin-conjugating enzyme.* J Biol Chem, 1996. **271**(32): p. 19385-94.
88. Subramaniam, S., et al., *Rhes, a striatal specific protein, mediates mutant-huntingtin cytotoxicity.* Science, 2009. **324**(5932): p. 1327-30.
89. Subramaniam, S., et al., *Rhes, a physiologic regulator of sumoylation, enhances cross-sumoylation between the basic sumoylation enzymes E1 and Ubc9.* The Journal of biological chemistry, 2010. **285**(27): p. 20428-20432.
90. Jana, N.R., et al., *Co-chaperone CHIP associates with expanded polyglutamine protein and promotes their degradation by proteasomes.* J Biol Chem, 2005. **280**(12): p. 11635-40.
91. Martin, D.D.O., et al., *Autophagy in Huntington disease and huntingtin in autophagy.* Trends in Neurosciences, 2015. **38**(1): p. 26-35.
92. Desterro, J.M., M.S. Rodriguez, and R.T. Hay, *SUMO-1 modification of IkappaBalpha inhibits NF-kappaB activation.* Mol Cell, 1998. **2**(2): p. 233-9.
93. Chaibva, M., et al., *Acetylation within the First 17 Residues of Huntingtin Exon 1 Alters Aggregation and Lipid Binding.* Biophys J, 2016. **111**(2): p. 349-362.
94. Jeong, H., et al., *Acetylation targets mutant huntingtin to autophagosomes for degradation.* Cell, 2009. **137**(1): p. 60-72.
95. Cong, X., et al., *Mass spectrometric identification of novel lysine acetylation sites in huntingtin.* Molecular & cellular proteomics : MCP, 2011. **10**(10): p. M111.009829-M111.009829.
96. Cornett, J., et al., *Polyglutamine expansion of huntingtin impairs its nuclear export.* Nature Genetics, 2005. **37**(2): p. 198-204.
97. Xia, J., et al., *Huntingtin contains a highly conserved nuclear export signal.* Human Molecular Genetics, 2003. **12**(12): p. 1393-1403.
98. Maiuri, T., et al., *The huntingtin N17 domain is a multifunctional CRM1 and Ran-dependent nuclear and cilial export signal.* Human Molecular Genetics, 2013. **22**(7): p. 1383-1394.
99. DiGiovanni, L.F., et al., *Huntingtin N17 domain is a reactive oxygen species sensor regulating huntingtin phosphorylation and localization.* Hum Mol Genet, 2016. **25**(18): p. 3937-3945.
100. Zhang, L., et al., *Molecular Mechanism of Stabilizing the Helical Structure of Huntingtin N17 in a Micellar Environment.* The Journal of Physical Chemistry B, 2017. **121**(18): p. 4713-4721.
101. Michalek, M., et al., *Membrane interactions of the amphipathic amino terminus of huntingtin.* Biochemistry, 2013. **52**(5): p. 847-58.
102. Chaibva, M., K.A. Burke, and J. Legleiter, *Curvature Enhances Binding and Aggregation of Huntingtin at Lipid Membranes.* Biochemistry, 2014. **53**(14): p. 2355-2365.
103. Côté, S., et al., *Probing the Huntingtin 1-17 membrane anchor on a phospholipid bilayer by using all-atom simulations.* Biophysical journal, 2015. **108**(5): p. 1187-1198.
104. Côté, S., G. Wei, and N. Mousseau, *All-Atom Stability and Oligomerization Simulations of Polyglutamine Nanotubes with and without the 17-Amino-Acid N-Terminal Fragment of the Huntingtin Protein.* The Journal of Physical Chemistry B, 2012. **116**(40): p. 12168-12179.
105. Côté, S., G. Wei, and N. Mousseau, *Atomistic mechanisms of huntingtin N-terminal fragment insertion on a phospholipid bilayer revealed by molecular dynamics simulations.* Proteins: Structure, Function, and Bioinformatics, 2014. **82**(7): p. 1409-1427.

106. Nagarajan, A., S. Jawahery, and S. Matysiak, *The Effects of Flanking Sequences in the Interaction of Polyglutamine Peptides with a Membrane Bilayer.* The Journal of Physical Chemistry B, 2014. **118**(24): p. 6368-6379.
107. Kelley, N.W., et al., *The predicted structure of the headpiece of the Huntingtin protein and its implications on Huntingtin aggregation.* Journal of molecular biology, 2009. **388**(5): p. 919-927.
108. Długosz, M. and J. Trylska, *Secondary Structures of Native and Pathogenic Huntingtin N-Terminal Fragments.* The Journal of Physical Chemistry B, 2011. **115**(40): p. 11597-11608.
109. Sivanandam, V.N., et al., *The aggregation-enhancing huntingtin N-terminus is helical in amyloid fibrils.* J Am Chem Soc, 2011. **133**(12): p. 4558-66.
110. Sahoo, B., et al., *Aggregation behavior of chemically synthesized, full-length huntingtin exon1.* Biochemistry, 2014. **53**(24): p. 3897-3907.
111. Poirier, M.A., et al., *Huntingtin spheroids and protofibrils as precursors in polyglutamine fibrilization.* J Biol Chem, 2002. **277**(43): p. 41032-7.
112. Perutz, M.F., et al., *Amyloid fibers are water-filled nanotubes.* Proceedings of the National Academy of Sciences, 2002. **99**(8): p. 5591-5595.
113. Schiefner, A., et al., *A disulfide-free single-domain V(L) intrabody with blocking activity towards huntingtin reveals a novel mode of epitope recognition.* J Mol Biol, 2011. **414**(3): p. 337-55.
114. Kim, M., *Beta conformation of polyglutamine track revealed by a crystal structure of Huntingtin N-terminal region with insertion of three histidine residues.* Prion, 2013. **7**(3): p. 221-8.
115. De Genst, E., et al., *Structure of a single-chain Fv bound to the 17 N-terminal residues of huntingtin provides insights into pathogenic amyloid formation and suppression.* J Mol Biol, 2015. **427**(12): p. 2166-78.
116. Guo, Q., et al., *The cryo-electron microscopy structure of huntingtin.* Nature, 2018. **555**(7694): p. 117-120.
117. Kotler, S.A., et al., *Probing initial transient oligomerization events facilitating Huntingtin fibril nucleation at atomic resolution by relaxation-based NMR.* Proc Natl Acad Sci U S A, 2019. **116**(9): p. 3562-3571.
118. Colby, D.W., et al., *Stochastic kinetics of intracellular huntingtin aggregate formation.* Nature Chemical Biology, 2006. **2**(6): p. 319-323.
119. Chen, S., F.A. Ferrone, and R. Wetzel, *Huntington's disease age-of-onset linked to polyglutamine aggregation nucleation.* Proceedings of the National Academy of Sciences of the United States of America, 2002. **99**(18): p. 11884-11889.
120. Margittai, M. and R. Langen, *Fibrils with parallel in-register structure constitute a major class of amyloid fibrils: molecular insights from electron paramagnetic resonance spectroscopy.* Q Rev Biophys, 2008. **41**(3-4): p. 265-97.
121. Perutz, M.F., et al., *Glutamine repeats as polar zippers: their possible role in inherited neurodegenerative diseases.* Proceedings of the National Academy of Sciences of the United States of America, 1994. **91**(12): p. 5355-5358.
122. Scherzinger, E., et al., *Huntingtin-encoded polyglutamine expansions form amyloid-like protein aggregates in vitro and in vivo.* Cell, 1997. **90**(3): p. 549-58.
123. Sharma, D., et al., *Polyglutamine homopolymers having 8-45 residues form slablike beta-crystallite assemblies.* Proteins, 2005. **61**(2): p. 398-411.
124. Punihaole, D., et al., *Polyglutamine Fibrils: New Insights into Antiparallel β-Sheet Conformational Preference and Side Chain Structure.* J Phys Chem B, 2016. **120**(12): p. 3012-26.
125. Schneider, R., et al., *Structural Characterization of Polyglutamine Fibrils by Solid-State NMR Spectroscopy.* Journal of Molecular Biology, 2011. **412**(1): p. 121-136.
126. Bugg, C.W., et al., *Structural features and domain organization of huntingtin fibrils.* J Biol Chem, 2012. **287**(38): p. 31739-46.

127. Tam, S., et al., *The chaperonin TRiC blocks a huntingtin sequence element that promotes the conformational switch to aggregation.* Nature structural & molecular biology, 2009. **16**(12): p. 1279-1285.
128. Wetzel, R., *Misfolding and Aggregation in Huntington Disease and Other Expanded Polyglutamine Repeat Diseases.* Protein Misfolding Diseases, 2010: p. 305-324.
129. Sivanandam, V.N., et al., *The Aggregation-Enhancing Huntingtin N-Terminus Is Helical in Amyloid Fibrils.* Journal of the American Chemical Society, 2011. **133**(12): p. 4558-4566.
130. Zuccato, C., M. Valenza, and E. Cattaneo, *Molecular mechanisms and potential therapeutical targets in Huntington's disease.* Physiol Rev, 2010. **90**(3): p. 905-81.
131. Vöpel, T., et al., *Inhibition of Huntingtin Exon-1 Aggregation by the Molecular Tweezer CLR01.* Journal of the American Chemical Society, 2017. **139**(16): p. 5640-5643.
132. Lecerf, J.-M., et al., *Human single-chain Fv intrabodies counteract in situ huntingtin aggregation in cellular models of Huntington's disease.* Proceedings of the National Academy of Sciences, 2001. **98**(8): p. 4764-4769.
133. Thakur, A.K., W. Yang, and R. Wetzel, *Inhibition of polyglutamine aggregate cytotoxicity by a structure-based elongation inhibitor.* The FASEB Journal, 2004. **18**(7): p. 923-925.
134. Belwal, V.K., D. Datta, and N. Chaudhary, *The β-turn-supporting motif in the polyglutamine binding peptide QBP1 is essential for inhibiting huntingtin aggregation.* FEBS Letters. **n/a**(n/a).
135. Nagai, Y., et al., *Inhibition of polyglutamine protein aggregation and cell death by novel peptides identified by phage display screening.* J Biol Chem, 2000. **275**(14): p. 10437-42.
136. Kim, Y.J., et al., *Caspase 3-cleaved N-terminal fragments of wild-type and mutant huntingtin are present in normal and Huntington's disease brains, associate with membranes, and undergo calpain-dependent proteolysis.* Proceedings of the National Academy of Sciences of the United States of America, 2001. **98**(22): p. 12784-12789.
137. Burra, G. and A.K. Thakur, *Inhibition of polyglutamine aggregation by SIMILAR huntingtin N-terminal sequences: Prospective molecules for preclinical evaluation in Huntington's disease.* Biopolymers, 2017. **108**(4).
138. Heiser, V., et al., *Identification of benzothiazoles as potential polyglutamine aggregation inhibitors of Huntington's disease by using an automated filter retardation assay.* Proc Natl Acad Sci U S A, 2002. **99 Suppl 4**: p. 16400-6.
139. Atwal, R.S., et al., *Kinase inhibitors modulate huntingtin cell localization and toxicity.* Nature Chemical Biology, 2011. **7**(7): p. 453-460.
140. Bustamante, M.B., et al., *Detection of huntingtin exon 1 phosphorylation by Phos-Tag SDS-PAGE: Predominant phosphorylation on threonine 3 and regulation by IKKbeta.* Biochem Biophys Res Commun, 2015. **463**(4): p. 1317-22.
141. Branco-Santos, J., et al., *Protein phosphatase 1 regulates huntingtin exon 1 aggregation and toxicity.* Human Molecular Genetics, 2017. **26**(19): p. 3763-3775.
142. Gu, X., et al., *N17 Modifies mutant Huntingtin nuclear pathogenesis and severity of disease in HD BAC transgenic mice.* Neuron, 2015. **85**(4): p. 726-41.
143. Stringer, D.K. and R.C. Piper, *Terminating protein ubiquitination: Hasta la vista, ubiquitin.* Cell cycle (Georgetown, Tex.), 2011. **10**(18): p. 3067-3071.
144. Schnell, J.D. and L. Hicke, *Non-traditional functions of ubiquitin and ubiquitin-binding proteins.* J Biol Chem, 2003. **278**(38): p. 35857-60.
145. Mukhopadhyay, D. and H. Riezman, *Proteasome-Independent Functions of Ubiquitin in Endocytosis and Signaling.* Science, 2007. **315**(5809): p. 201.
146. Hay, R.T., *SUMO: A History of Modification.* Molecular Cell, 2005. **18**(1): p. 1-12.

147. Lotz, G.P., et al., *Hsp70 and Hsp40 functionally interact with soluble mutant huntingtin oligomers in a classic ATP-dependent reaction cycle.* The Journal of biological chemistry, 2010. **285**(49): p. 38183-38193.
148. Tam, S., et al., *The chaperonin TRiC controls polyglutamine aggregation and toxicity through subunit-specific interactions.* Nature Cell Biology, 2006. **8**(10): p. 1155-1162.
149. Choudhury, K.R. and N.P. Bhattacharyya, *Chaperone protein HYPK interacts with the first 17 amino acid region of Huntingtin and modulates mutant HTT-mediated aggregation and cytotoxicity.* Biochemical and Biophysical Research Communications, 2015. **456**(1): p. 66-73.
150. Caron, N.S., et al., *Polyglutamine domain flexibility mediates the proximity between flanking sequences in huntingtin.* Proceedings of the National Academy of Sciences, 2013. **110**(36): p. 14610.
151. Sinha, S., et al., *Lysine-specific molecular tweezers are broad-spectrum inhibitors of assembly and toxicity of amyloid proteins.* J Am Chem Soc, 2011. **133**(42): p. 16958-69.
152. Messer, A. and D.C. Butler, *Optimizing intracellular antibodies (intrabodies/nanobodies) to treat neurodegenerative disorders.* Neurobiology of Disease, 2020. **134**: p. 104619.
153. Sheets, M.D., et al., *Efficient construction of a large nonimmune phage antibody library: The production of high-affinity human single-chain antibodies to protein antigens.* Proceedings of the National Academy of Sciences, 1998. **95**(11): p. 6157-6162.
154. Colby, D.W., et al., *Potent inhibition of huntingtin aggregation and cytotoxicity by a disulfide bond-free single-domain intracellular antibody.* Proc Natl Acad Sci U S A, 2004. **101**(51): p. 17616-21.
155. Armen, R.S., et al., *Characterization of a possible amyloidogenic precursor in glutamine-repeat neurodegenerative diseases.* Proceedings of the National Academy of Sciences of the United States of America, 2005. **102**(38): p. 13433-13438.
156. Ramos-Martín, F., et al., *NMR spectroscopy reveals a preferred conformation with a defined hydrophobic cluster for polyglutamine binding peptide 1.* Arch Biochem Biophys, 2014. **558**: p. 104-10.
157. Bennett, M.J., et al., *A linear lattice model for polyglutamine in CAG-expansion diseases.* Proc Natl Acad Sci U S A, 2002. **99**(18): p. 11634-9.
158. Bennett, M.J., et al., *Inaugural Article: A linear lattice model for polyglutamine in CAG-expansion diseases.* Proc Natl Acad Sci U S A, 2002. **99**(18): p. 11634-9.
159. Pronk, S., et al., *GROMACS 4.5: a high-throughput and highly parallel open source molecular simulation toolkit.* Bioinformatics, 2013. **29**(7): p. 845-54.
160. Srinivasan, R., *RIBOSOME—Program to build coordinates for peptides from sequence*. Jenkins Department of Biophysics, Johns Hopkins University, Baltimore, MD, 2013
161. Schmid, N., et al., *Definition and testing of the GROMOS force-field versions 54A7 and 54B7.* Eur Biophys J, 2011. **40**(7): p. 843-56.
162. Castro, T.G. and N.M. Micaêlo, *Modeling of Peptaibol Analogues Incorporating Nonpolar α,α-Dialkyl Glycines Shows Improved α-Helical Preorganization and Spontaneous Membrane Permeation.* The Journal of Physical Chemistry B, 2014. **118**(3): p. 649-658.
163. Datta, D., et al., *Self-assembly of β-turn motif-connected tandem repeats of Aβ16-22 and its aromatic analogs.* Peptide Science, 2018: p. e24099.
164. Chiti, F. and C.M. Dobson, *Protein misfolding, functional amyloid, and human disease.* Annu Rev Biochem, 2006. **75**: p. 333-66.
165. Collaborators, G.B.D.N., *Global, regional, and national burden of neurological disorders, 1990-2016: a systematic analysis for the Global Burden of Disease Study 2016.* The Lancet. Neurology, 2019. **18**(5): p. 459-480.

166. Fan, H.-C., et al., *Polyglutamine (PolyQ) Diseases: Genetics to Treatments.* Cell Transplantation, 2014. **23**(4-5): p. 441-458.
167. Walker, F.O., *Huntington's Disease.* Semin Neurol, 2007. **27**(2): p. 143-50.
168. Thakur, A.K., et al., *Polyglutamine disruption of the huntingtin exon 1 N terminus triggers a complex aggregation mechanism.* Nat Struct Mol Biol, 2009. **16**(4): p. 380-9.
169. Liebman, S.W. and S.C. Meredith, *Protein folding: sticky N17 speeds huntingtin pile-up.* Nat Chem Biol, 2010. **6**(1): p. 7-8.
170. Pandey, N.K., et al., *The 17-residue-long N terminus in huntingtin controls stepwise aggregation in solution and on membranes via different mechanisms.* J Biol Chem, 2018. **293**(7): p. 2597-2605.
171. Armiento, V., A. Spanopoulou, and A. Kapurniotu, *Peptide-Based Molecular Strategies To Interfere with Protein Misfolding, Aggregation, and Cell Degeneration.* Angewandte Chemie (International ed. in English), 2020. **59**(9): p. 3372-3384.
172. Goyal, D., et al., *Rationally Designed Peptides and Peptidomimetics as Inhibitors of Amyloid-β (Aβ) Aggregation: Potential Therapeutics of Alzheimer's Disease.* ACS Comb Sci, 2017. **19**(2): p. 55-80.
173. Ryan, P., et al., *Peptides, Peptidomimetics, and Carbohydrate–Peptide Conjugates as Amyloidogenic Aggregation Inhibitors for Alzheimer's Disease.* ACS Chemical Neuroscience, 2018. **9**(7): p. 1530-1551.
174. Eisele, Y.S., et al., *Targeting protein aggregation for the treatment of degenerative diseases.* Nature reviews. Drug discovery, 2015. **14**(11): p. 759-780.
175. Ren, H., et al., *Amino Acid Sequence Requirements of Peptides That Inhibit Polyglutamine-Protein Aggregation and Cell Death.* Biochemical and Biophysical Research Communications, 2001. **288**(3): p. 703-710.
176. Tomita, K., et al., *Structure–activity relationship study on polyglutamine binding peptide QBP1.* Bioorganic & Medicinal Chemistry, 2009. **17**(3): p. 1259-1263.
177. Awasthi, S.K., S. Raghothama, and P. Balaram, *A designed beta-hairpin peptide.* Biochem Biophys Res Commun, 1995. **216**(1): p. 375-81.
178. Crisma, M., et al., *Peptide models for β-turns.* International Journal of Peptide and Protein Research, 1984. **23**(4): p. 411-419.
179. Awasthi, S.K., et al., *Solvent-induced β-hairpin to helix conformational transition in a designed peptide.* Biopolymers, 2001. **58**(5): p. 465-476.
180. Kang, Y.K. and I.K. Yoo, *Propensities of peptides containing the Asn-Gly segment to form beta-turn and beta-hairpin structures.* Biopolymers, 2016. **105**(9): p. 653-64.
181. Cochran, A.G., N.J. Skelton, and M.A. Starovasnik, *Tryptophan zippers: stable, monomeric beta -hairpins.* Proc Natl Acad Sci U S A, 2001. **98**(10): p. 5578-83.
182. Diez-García, F., et al., *Structure of a simplified β-hairpin and its ATP complex.* Archives of Biochemistry and Biophysics, 2013. **537**(1): p. 62-71.
183. Perczel, A., et al., *Synthesis and conformational analysis of N-glycopeptides. II. CD, molecular dynamics, and NMR spectroscopic studies on linear N-glycopeptides.* Biopolymers, 1993. **33**(4): p. 665-85.
184. Creighton, T.E., *Proteins: Structures and Molecular Properties*. 2 ed. 1993: W. H. Freeman.
185. Fodale, V., et al., *Polyglutamine- and Temperature-Dependent Conformational Rigidity in Mutant Huntingtin Revealed by Immunoassays and Circular Dichroism Spectroscopy.* PLOS ONE, 2014. **9**(12): p. e112262.
186. Bravo-Arredondo, J.M., et al., *The folding equilibrium of huntingtin exon 1 monomer depends on its polyglutamine tract.* Journal of Biological Chemistry, 2018. **293**(51): p. 19613-19623.
187. Whitmore, L. and B.A. Wallace, *DICHROWEB, an online server for protein secondary structure analyses from circular dichroism spectroscopic data.* Nucleic Acids Research, 2004. **32**(suppl_2): p. W668-W673.

188. Lopes, J.L.S., et al., *Distinct circular dichroism spectroscopic signatures of polyproline II and unordered secondary structures: Applications in secondary structure analyses.* Protein Science, 2014. **23**(12): p. 1765-1772.
189. Nagai, Y., et al., *Inhibition of Polyglutamine Protein Aggregation and Cell Death by Novel Peptides Identified by Phage Display Screening.* Journal of Biological Chemistry, 2000. **275**(14): p. 10437-10442.
190. Mompeán, M., et al., *Molecular mechanism of the inhibition of TDP-43 amyloidogenesis by QBP1.* Archives of Biochemistry and Biophysics, 2019. **675**: p. 108113.
191. Hervás, R., et al., *Molecular Basis of Orb2 Amyloidogenesis and Blockade of Memory Consolidation.* PLOS Biology, 2016. **14**(1): p. e1002361.
192. Ramos-Martín, F., et al., *NMR spectroscopy reveals a preferred conformation with a defined hydrophobic cluster for polyglutamine binding peptide 1.* Archives of Biochemistry and Biophysics, 2014. **558**: p. 104-110.
193. Takahashi, K., et al., *Low-energy conformations of two lysine-containing tetrapeptides of collagen: Implications for posttranslational lysine hydroxylation.* Biopolymers, 1987. **26**(10): p. 1781-1788.
194. Rose, G.D., L.M. Glerasch, and J.A. Smith, *Turns in Peptides and Proteins*, in *Advances in Protein Chemistry*, C.B. Anfinsen, J.T. Edsall, and F.M. Richards, Editors. 1985, Academic Press. p. 1-109.
195. Lieberman, A.P., V.G. Shakkottai, and R.L. Albin, *Polyglutamine Repeats in Neurodegenerative Diseases.* Annual Review of Pathology: Mechanisms of Disease, 2019. **14**(1): p. 1-27.
196. Yushchenko, T., E. Deuerling, and K. Hauser, *Insights into the Aggregation Mechanism of PolyQ Proteins with Different Glutamine Repeat Lengths.* Biophys J, 2018. **114**(8): p. 1847-1857.
197. Gruber, A., et al., *Molecular and structural architecture of polyQ aggregates in yeast.* Proceedings of the National Academy of Sciences, 2018. **115**(15): p. E3446-E3453.
198. Thakur, A.K., et al., *Polyglutamine disruption of the huntingtin exon 1 N terminus triggers a complex aggregation mechanism.* Nature Structural & Molecular Biology, 2009. **16**(4): p. 380-389.
199. Nagai, Y., et al., *A toxic monomeric conformer of the polyglutamine protein.* Nat Struct Mol Biol, 2007. **14**(4): p. 332-40.
200. Hoop, C.L., et al., *Polyglutamine Amyloid Core Boundaries and Flanking Domain Dynamics in Huntingtin Fragment Fibrils Determined by Solid-State Nuclear Magnetic Resonance.* Biochemistry, 2014. **53**(42): p. 6653-6666.
201. Isas, J.M., R. Langen, and A.B. Siemer, *Solid-State Nuclear Magnetic Resonance on the Static and Dynamic Domains of Huntingtin Exon-1 Fibrils.* Biochemistry, 2015. **54**(25): p. 3942-3949.
202. Tossi, A., L. Sandri, and A. Giangaspero, *New consensus hydrophobicity scale extended to non-proteinogenic amino acids*, in *Peptides 2002: Proceedings of the 27th European Peptide Symposium*, E. Benedetti and C. Pedone, Editors. 2002, Napoli: Edizioni Ziino: Italy. p. 416-417.
203. Burra, G. and A.K. Thakur, *Inhibition of polyglutamine aggregation by SIMILAR huntingtin N-terminal sequences: Prospective molecules for preclinical evaluation in Huntington's disease.* Peptide Science, 2017. **108**(4): p. e23021.
204. Belwal, V.K., D. Datta, and N. Chaudhary, *The β-turn-supporting motif in the polyglutamine binding peptide QBP1 is essential for inhibiting huntingtin aggregation.* FEBS Letters, 2020. **594**(17): p. 2894-2903.
205. Popiel, H.A., et al., *The Aggregation Inhibitor Peptide QBP1 as a Therapeutic Molecule for the Polyglutamine Neurodegenerative Diseases.* Journal of Amino Acids, 2011. **2011**: p. 10.
206. Martin, E.B., et al., *Evaluation of the effect of d-amino acid incorporation into amyloid-reactive peptides.* Journal of Translational Medicine, 2017. **15**(1): p. 247.
207. Garton, M., et al., *Method to generate highly stable D-amino acid analogs of bioactive helical peptides using a mirror image of the entire PDB.* Proceedings of the National Academy of Sciences, 2018. **115**(7): p. 1505-1510.

208. Cheng, P.N., et al., *Amyloid β-sheet mimics that antagonize protein aggregation and reduce amyloid toxicity.* Nat Chem, 2012. **4**(11): p. 927-33.
209. Chaudhary, R.K., et al., *Inhibition of Aggregation of Mutant Huntingtin by Nucleic Acid Aptamers In Vitro and in a Yeast Model of Huntington's Disease.* Molecular therapy : the journal of the American Society of Gene Therapy, 2015. **23**(12): p. 1912-1926.
210. Pachahara, S.K., et al., *Hexafluoroisopropanol induces self-assembly of β-amyloid peptides into highly ordered nanostructures.* Journal of Peptide Science, 2012. **18**(4): p. 233-241.
211. Belwal, V.K. and N. Chaudhary, *Amyloids and their untapped potential as hydrogelators.* Soft Matter, 2020.
212. Peskett, T.R., et al., *A Liquid to Solid Phase Transition Underlying Pathological Huntingtin Exon1 Aggregation.* Mol Cell, 2018. **70**(4): p. 588-601.e6.
213. Aktar, F., et al., *The huntingtin inclusion is a dynamic phase-separated compartment.* Life science alliance, 2019. **2**(5): p. e201900489.